Lappeenrannan teknillinen yliopisto
Lappeenranta University of Technology

Janne Kovanen

IMPROVING DYNAMIC CHARACTERISTICS OF OPEN-LOOP CONTROLLED LOG CRANE

Thesis for the degree of Doctor of Science (Technology) to be presented with due permission for public examination and criticism in the auditorium 1382 at Lappeenranta University of Technology, Lappeenranta, Finland on the 3th of October, 2003, at noon.

Acta Universitatis
Lappeenrantaensis
163

Supervisor Professor Heikki Handroos
Institute of Mechatronics and Virtual Engineering
Department of Mechanical Engineering
Lappeenranta University of Technology
Finland

Reviewers Associate Professor Peder Pedersen
Institute of Energy Technology
Aalborg University
Denmark

Professor Matti Pietola
Department of Machine Design
Helsinki University of Technology
Finland

Opponents Associate Professor Peder Pedersen
Institute of Energy Technology
Aalborg University
Denmark

Associate Professor Takao Nishiumi
Department of Mechanical Systems Engineering
National Defense Academy
Japan

ISBN 951-764-798-0
ISSN 1456-4491

Lappeenrannan teknillinen yliopisto
Digipaino 2003

Abstract

Janne Kovanen

IMPROVING DYNAMIC CHARACTERISTICS OF OPEN-LOOP CONTROLLED LOG CRANE

Lappeenranta, 2003
97 p.
Acta Universitatis Lappeenrantaensis 163
Diss. Lappeenranta University of Technology

ISBN 951-764-798-0
ISSN 1456-4491

The improvement of the dynamics of flexible manipulators like log cranes often requires advanced control methods. This thesis discusses the vibration problems in the cranes used in commercial forestry machines. Two control methods, adaptive filtering and semi-active damping, are presented. The adaptive filter uses a part of the lowest natural frequency of the crane as a filtering frequency. The payload estimation algorithm, filtering of control signal and algorithm for calculation of the lowest natural frequency of the crane are presented. The semi-active damping method is based on pressure feedback. The pressure vibration, scaled with suitable gain, is added to the control signal of the valve of the lift cylinder to suppress vibrations.

The adaptive filter cuts off high frequency impulses coming from the operator and semi-active damping suppresses the crane's oscillation, which is often caused by some external disturbance. In field tests performed on the crane, a correctly tuned (25 % tuning) adaptive filter reduced pressure vibration by 14-17 % and semi-active damping correspondingly by 21-43%. Applying of these methods require auxiliary transducers, installed in specific points in the crane, and electronically controlled directional control valves.

Keywords: Vibration, suppression, open-loop, control, flexible, log crane
UDC 62-82 : 681.587.34 : 534.83

8.10.2003

JANNE KOVANEN: "IMPROVING DYNAMIC CHARACTERISTICS OF OPEN-LOOP CONTROLLED LOG CRANE, LIST OF MISTAKES FOUND AFTER PRINTING

Page 13:
"… results according to which 19.3% of the trees left standing are damaged during the thinning process and about 30% of these trees are left standing".
Correction:
"… results according to which 19.3% of the trees left standing are exposed to hit during the thinning process and about 3.6% of these trees are damaged".

Page 24:
Equation 3.3. Pressure is marked with capital letter *P*, should be small letter *p*.

Page 29:
Equation 3.11: $H(s) = \frac{1}{s + \omega}$. Should be $H(s) = \frac{\omega}{s + \omega}$.

Page 30:
Equation 3.13: $\omega = \sqrt{\frac{m}{k_s}}$. Should be $\omega = \sqrt{\frac{k_s}{m}}$.

Page 33:
"The crane specific matrix **M**…". Should be: "The crane specific matrix **a**…".

Page 39:
"To calculate the coordinates of the load mass, matrix $\mathbf{J}_{p4}$ has to be defined". Should be: matrix $\mathbf{J}_{p5}$.

Page 43:
$\mathbf{G}_1$ is scalar, not matrix. Should be: G_1.

Page 62:
"The damping signal moves a spool of the control valve, which increases vibration".

To avoid misunderstanding, the sentence should be: "The damping signal moves a spool of the control valve when pressure vibration increases".

Page 67:
"…measurement data from point three… ". Should be: "measurement data from point marked by letter i".

Page 90, Appendix C:
"Chapter 4 presents…" Should be: "Chapter 3.2.4.1. presents…".

In Lappeenranta, 8th October 2003

Janne Kovanen

Preface

The work presented in this thesis was carried out in the Institute of Mechatronics and Virtual Engineering at Lappeenranta University of Technology, Finland, during the period between 1999 and 2003. The work was done as a part of the LiikkuVÄRE research project, financed by TEKES (the Finnish Technology Development Centre), and with the support of John Deere Timberjack.

My supervisor, Professor Heikki Handroos, who provided me with valuable guidance throughout the research, deserves a lot of the credit for the successful work. I would also like to thank all my colleagues who assisted to the best of their abilities. I offer special thanks to Doctor Asko Rouvinen, who gave me many tools for building the simulation model of the log crane. Mr Jussi Sopanen gave me good advice on modeling problems, Mr Mikko Liukkula made a base work in modeling of flexible extension boom, and Mr Juha Koivisto helped me in carrying out the laboratory tests.

John Deere Timberjack supported my research greatly by kindly offering me the possibility to test control methods in a real log forwarder. Mr Arto Vento, Mr Pertti Sirainen and Mr Tatu Westerholm of John Deere Timberjack helped greatly during the field test-drives.

I would like to thank the reviewers of my thesis, Assosiate Professor Peder Pedersen from Aalborg University, Denmark, and Professor Matti Pietola from Helsinki University of Technology, Finland.

The financial support provided by the Graduate School of Concurrent Mechanical Engineering (GSCME), the Jenny and Antti Wihuri Foundation, the Henry Ford Foundation and the Lahja and Lauri Hotinen Foundation is gratefully acknowledged.

Finally, I would like to give a big hug to my wife, Janika, for her support and make a small request of our 3-month old daughter, Veera: Read through this book some day; hopefully you will give me a big smile, just as you did when I asked you for your opinion on the manuscript.

Janne Kovanen
September, 2003
Lappeenranta, Finland

Table of Contents

1 Introduction 11
1.1 Motivation- Demands from Forestry 13
1.2 Advanced Manipulator Control in the Forest Machinery Technology of Tomorrow or Just a Future Scenario 14
1.3 Aim of the Research 14
1.4 Research Methods 15
1.5 Scope of the Work 16
1.6 Contribution of the Dissertation 16
1.7 Outline of the Dissertation 17

2 Vibration Suppression Methods 18
2.1 General overview 18
2.2 Vibration Suppression in Hydraulic Manipulators 20
2.2.1 Suppression by Hydraulic Accumulator 21
2.2.2 Methods Employed in Excavator Boom Control 22

3 Applied Vibration Reduction Methods for Log Cranes 23
3.1 Simulation Models for Log Cranes 23
3.1.1 Linearization as a Tool for Monitoring Dynamic Behaviour of a Mechanism 26
3.1.2 The Simulator in the MATLAB/Simulink-ADAMS Interface 28
3.2 Adaptive Filter 28
3.2.1 The Basis for Filtering the Control Signal 28
3.2.2 Natural Frequency Surface Fitting 31
3.2.3 An Adaptive Algorithm for Filtering the Control Signal 34
3.2.4 Determination of Payload 35
3.2.4.1 Kinematics of the crane 36
3.2.4.2 Weights of the Components and Inertia Tensors 40
3.2.4.3 Velocities and Acceleration of the Link 41
3.2.4.4 Cylinder Force 44
3.3 Semi-Active Damping 45

4 The Simulations and Test Drives 49
4.1 General Information on the Testing of the Controllers 49
4.1.1 Arrangements 49
4.1.2 Control Hardware 50
4.2 Adaptive Filter 50
4.3 Determination of the Payload and Vibration Recognition 54
4.4 Semi-Active Damping 62
4.5 Field Tests 64
4.5.1 Step Response Tests 64
4.5.2 The Loading of Logs to the Carriage 70
4.6 Notes on the Field Measurements 71
4.7 Discussion and Future Suggestions 74

5 Conclusions 77

REFERENCES 79
Appendix A Lowest Natural Frequencies of the Different Cranes 84
Appendix B Transformation Matrixes 88
Appendix C Four Bar Mechanism 90
Appendix D Outward and Inward Iteration 93

Abbreviations and Symbols

Abbreviation

ADAMS	Automatic Dynamic Analysis of Mechanical Systems
CM	Centre of Mass
DOF	Degree of Freedom
FFT	Fast Fourier Transform
IMVE	Institute of Mechatronics and Virtual Engineering
LUT	Lappeenranta University of Technology
PWM	Pulse Width Modulated
RMS	Root Mean Square

Symbols

$\mathbf{A}$	Matrix defining $\partial \mathbf{g} / \partial y$ at operating point y^*
$\mathbf{A}^{\mathrm{i}}$	Rotation matrix of i
$\mathbf{A}_{\mathrm{i,i}}$	Rotation matrix
A^*	Help variable
$A_{1,2}$	Area on piston side and on the rod side
$\mathbf{a}$	Coefficient matrix in surface fitting
a	Restrictor area, coefficient in surface fitting
a_{m}	Coefficient for input m in discrete controller
$\mathbf{B}$	Matrix defining $\partial \mathbf{g} / \partial \dot{y}$ at operating point y^*
B^*	Help variable
b_{n}	Coefficient for output n in discrete controller
$\boldsymbol{C}$	Vector that contains different $\boldsymbol{c}_{\mathrm{i}}$ vectors
$\mathbf{C}_{\mathrm{q}}$	Jacobian matrix
C_{q}	Flow coefficient
c	Coefficient in surface fitting
c_{a}	Help variable
$\boldsymbol{c}_{\mathrm{i}}$	Vector that includes coefficients c for mass i
D^*	Help variable
E^*	Help variable
$E(\mathrm{z})$	Input of controller (discrete)
e_{k}	Current input value
$e_{\mathrm{k-m}}$	Old input value
F	Calculated frequency
$\boldsymbol{F}_{\mathrm{i,i}}$	Force acting on the link i
F_{c}	Lift cylinder force
F_{h}	High-pass filtered cylinder force
F_{hpmax}	Maximum amplitude of high-pass filtered cylinder force
F_{l}	Static load of the cylinder
F_{μ}	Friction force
$\boldsymbol{f}_{\mathrm{i,i}}$	Force acting on the link i, inward iteration
$\mathbf{f}_{\mathrm{i}}$	Frequency matrix
$\mathbf{G}_{1\ldots3}$	Help variable

$\mathbf{g}$	Mixed system of second-order differential and algebraic equations
g	Gravity
H(s)	Transfer function
H(z)	Transfer function (discrete)
h	Step size
$\mathbf{I}_{\mathrm{i}}$	Eigenvalues of the inertia tensor I (Principal moments)
i	Running index number
$\mathbf{J}_{\mathrm{pi}}$	4x4 matrix, 4th column gives the location of the joint i
$\mathbf{J}_{\mathrm{cmi}}$	4x4 matrix, 4th column gives the location of the CM of the link i
j	Running index number
$K_{\mathrm{v,f}}$	Factors that depend on static force
k	Time unit
k_s	Spring constant
L_{ij}	Length of vector i-j
$\mathrm{M_f}$	Polynomial that uses mass to calculate the frequency
$\mathbf{M}$	Matrix form of $\mathrm{M_f}$
m	Mass, index number
m_{i}	Mass of link i
m_{avg}	Avarage load
N	Number of samples
$\boldsymbol{N}_{\mathrm{i,i}}$	Torque vector
$\boldsymbol{N}_{\mathrm{tot}}$	Sum of torque vectors
n	Number of links, index number
$\boldsymbol{n}_{\mathrm{i,i}}$	Torque acting on the link i
$\boldsymbol{P}_{\mathrm{i,i+1}}$	Position vector (from joint i to i+1)
$\boldsymbol{P}_{\mathrm{i,i,cm}}$	Position vector of the centre of mass
$p_{1,2}$	Pressure in chambers one and two
$\mathrm{p_f}$	Polynomial that uses cylinder strokes to define frequency
$\boldsymbol{p}_{\mathrm{i}}$	Vector form of $\mathrm{p_f}$
Q	Volymetric flow rate
$Q_{\mathrm{i,o}}$	Input and output flow rate
$\boldsymbol{Q}_e^{\,j}$	Generalized forces acting on body j
$\boldsymbol{Q}_0$	Generalized forces acting at linearisation time
q_0	Flow rate
$\boldsymbol{q}$	Generalized coordinates
$\mathbf{R_i}$	5x9 frequency matrix for mass i
$\boldsymbol{R}^{\mathbf{i}}$	Position of the local coordinate system of i in global coordinate system
$\mathbf{R_{i,i+1}}$	Rotation matrix defining rotation of i+1 respect to i
R_{sum}	Running sum
$\boldsymbol{r}^{\mathrm{i}}$	Global translation and rotation of the frame in point i
s	Laplace variable
s_{i}	Cylinder i stroke
s_{E}	Extension (length)
$\mathbf{T}$	Systems kinetic energy
$\mathbf{T}_{\mathrm{ij}}$	Transformation matrix from link i to j
$\mathbf{T}_{\mathrm{mi}}$	Transformation matrix from joint i to the location of the centre of mass i

t	Time
t_0	Time at state of equilibrium
U(z)	Output
U_{damp}	Damping signal
$\bar{\boldsymbol{u}}^{\text{i}}$	Location vector in local frame *i*
$\bar{\text{u}}_{\text{j}}^{\text{i}}$	Component *j* in location vector in local frame *i*
u_{k}	Next output value
$u_{\text{k-n}}$	Old output
V	Volume
v	Velocity of the cylinder stroke
v_{max}	Maximum velocity of the cylinder stroke
v_{h}	Velocity, high passed value
$\mathbf{v}_{\text{i}}$	Eigenvector matrix of inertia tensor *i* (Principal axes), velocity of the link
$\boldsymbol{v}_{\text{i,i,cm}}$	Velocity of the centre of mass, link *i*
X	Lift cylinder stroke, X coordinate
$X_{\text{n,n-1}}$	Current and previous lift cylinder stroke value
x_{i}	X-coordinate of the centre of mass of the link *i*
x_{a}	Moment arm of the lift cylinder
Y	Jib cylinder stroke, Y coordinate
$\boldsymbol{y}$	Vector of generalized coordinates, derivate of generalized coordinates and Lagrange mulipliers
$\boldsymbol{y}_0$	$\boldsymbol{y}$ at linearisation time
$\boldsymbol{y}^*$	Operating point
Z	Z coordinate
$\hat{\boldsymbol{Z}}_{i,i}$	Direction vector in joint *i*
$\boldsymbol{z}$	Complex constant vector
z^{-k}	Delay of *k* time unit
α_{J}	Angle between the pillar and the lift
α_{L}	Angle between the jib boom and the lift boom
β	Force transmission angle
β_{e}	Effective bulk modulus of the fluid
ε_{i}	Angle
η	Cylinder efficiency
$\boldsymbol{\lambda}$	Vector of Lagrange coefficients
ω	Natural frequency
$\boldsymbol{\omega}_{\text{i,i}}$	Rotational velocity of the link *i*
$\theta_{\text{i,i}}$	Rotational angle
σ	Complex constant scalar
ρ	Fluid mass density
$\boldsymbol{\tau}_{\text{i}}$	Torque in joint *i*
ς	Damping factor

1 Introduction

Serial manipulator structures are widely used in many mobile applications such as excavators, log cranes, harvesters and log trucks. Traditionally, these manipulators are controlled using a mechanical joystick that controls proportional directional valves mechanically or electrically. The proportional directional valves control the velocities of actuators and thus have a direct effect on the dynamic behaviour of the crane. The control system is of the open-loop type, which means that position or velocity of the crane is not measured and controlled in closed-loop manner. Figure 1.1 shows a common log crane that is used in a log forwarder and Figure 1.2 presents basic difference of the open-loop and closed-loop control. In the closed-loop control controlled quantity is measured and used in controller to better control result. In common the hydraulic manipulators, as log crane, are utilizing open-loop control and all feedback operations are “in the hands of the operator”. This means that the operator follows movements of the crane and changes his control actions depending on state of the crane. Disturbances in Figure 1.2, in the case of the log crane, can be for example collisions to trees, carriage or soil, or sway of the mass load.

Figure 1.1 A 1010B log forwarder working in a logging area (John Deere Timberjack).

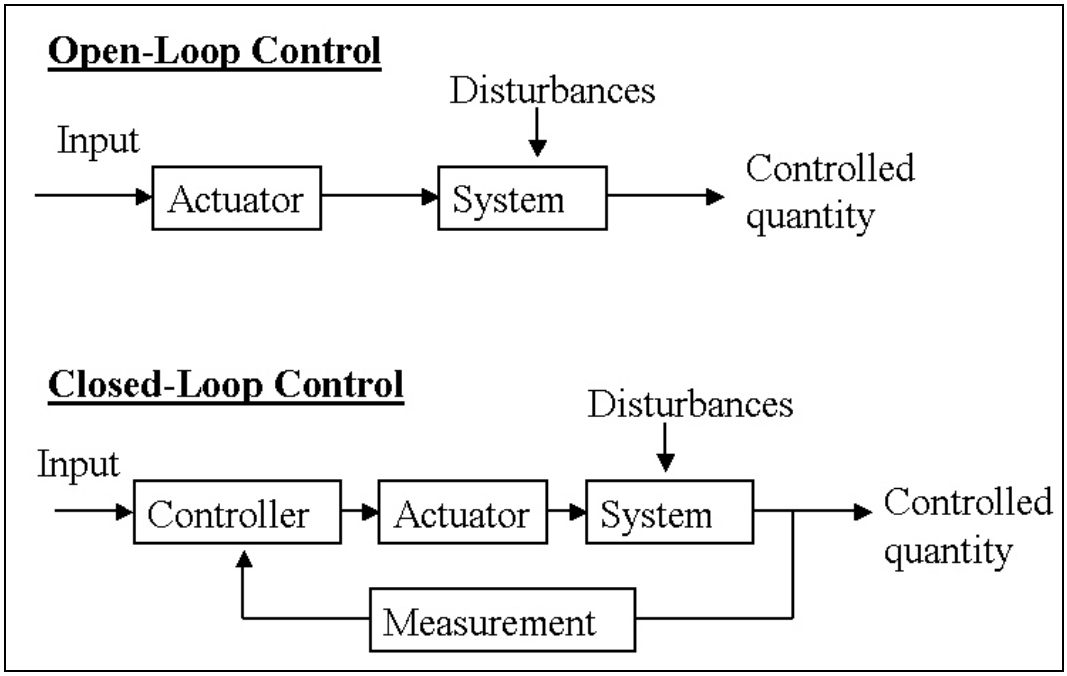

Figure 1.2 Open-loop and closed-loop control

With the increase of the electronics during the last 15-20 years, electronic control systems have been taken into use in mobile machines. So-called ramp functions are widely used with electrically controlled directional valves to smoothen the control signals of the valves and, in this way, protect the manipulator against harmful inputs from the operator. These harmful inputs can include, for example, excessively the rapid movement of the joystick or rapid changes in the direction of movement, which results in excitation on the structural frequencies of the manipulator. A commonly used method for tuning the open-loop control of a log crane is to use the maximum load at the end tip and tune the ramp functions to be so slow that only small amplitude vibrations arise during accelerations and decelerations. This kind of adjustment reduces the working capacity of the empty boom because the ramp functions with constant parameters do not take into account large variations in the dynamics of the flexible boom. Tuning the ramp functions to be faster leads to many more vibrations arise.

Work cycles, in which accurate load handling is required, suffer when the manipulator is too flexible and is able to sway and shake. The lack of stiffness and high velocities both contribute to the excitation of vibration. An experienced operator can minimize the harmful movements of a manipulator and damp out undesired oscillation, although in especially fast working situations and long work shifts this is not always easy for a human to perform in the same way that robots do. In the long term, vibration cycles decrease the fatigue lifetime of the manipulator and the components.

A traditional solution for stiffness problem is to design the manipulator to be structurally sufficiently stiff. The links and joints of the manipulator cannot be made infinitely stiff in mobile machines, because this increases the mass and,

therefore, limits the velocity of the manipulator and requires high levels of drive power. Similar problems exist in industry where traditional robot structures and controllers did not satisfy the increasing specifications for speed, acceleration and accuracy. New control strategies together with the reduction of weight and inertia were required and will be required to meet these specifications. A decrease in weight leads to larger link and joint deformations and thereby reduces structural resonance frequencies.

One possibility to improve the stiffness and accuracy of a manipulator is to change a serial kinematic structure to a parallel kinematic manipulator. Parallel manipulators consist of multiple actuators that are acting in parallel to the end-effector. Parallel actuators decrease the workspace required and are, therefore, not suitable for applications in which a large workspace is compulsory.

1.1 Motivation- Demands from Forestry

During the last ten years, the development of computer-controlled power transmission, measurement systems, failure diagnosis systems and satellite GPS systems for the forestry machines has attracted a lot of research interest. The manipulator itself has seen main changes in its overall size, reach and kinematics. Manipulator control systems have developed and incorporated CAN bush. (Konttinen 1997).

Ecological thinking has come to the design of log forwarders. The trend in Northern European log harvesting is to avoid damages to the forest surface and to care for the forest after the actual harvesting has taken place. The use of bio-oil in forest machines is one example how ecological thinking has steered design.

Thinning forests wounds the bark of the trees that are left standing and, in this way, makes these trees susceptible to tree illnesses. Thinning forests, especially during the summer, is more risky for the trees left standing, because the warm weather facilitates tree illnesses. Siren (1999, p.78-79) has obtained results according to which 19.3 % of the trees left standing are damaged during the thinning process and about 30 % of these trees are left standing. Damages to trees lead to quality losses, and it is well known that particularly spruce is prone to rot once its bark is damaged. It is difficult to estimate the financial losses due to tree damages during harvesting and thinning operations, but Siren has calculated that the total losses in a test forest after two thinning operations were about 200 euros per hectare, of which one third originated from log handling. (Siren 1999, p.102.)

In 1999, about 200 new log forwarders were sold in Finland and almost the same number of harvesters was sold (MTT Vakola 2003). In 2003, the total number of harvesters and log forwarders in use in Finland is about 1650 and 1800, respectively. Depending on their size, manufacturer and service programs, new harvesters cost between approximately 200 and 500 thousand euros and log forwarders correspondingly between approximately 200 and 300 thousand euros. It is obvious that profitability demands influence the driver who is, in many cases, also the owner of the forestry machine. It would be easy to assume that profitability demands result in a fast working pace, which leads to the standing

trees sustaining many hits. According to Metsälehti magazine (7/2002), most complaints from forest owners in the wood trade concerned the damages caused by harvesting in their forests.

Siren's results demonstrate the opposite: A highly profitable operator causes less damage to the trees that remain standing. This result can be explained, largely, by the fact that about 40 % of the harvesting time goes to the operation of the crane, which requires good experience. Smooth log handling enables high-quality work, which results in high profits. Therefore, a lot of effort should be made in training and selecting operators. The operation of a harvesting machine requires the attainment to handle heavy machinery and the awareness of the importance of using the correct harvesting technique. (Siren 1999, p. 133, 145)

Not only are the standing trees damaged by the crane. The biggest single factor behind harvest damage is the weight of forest machines. Heavy machines leave deep trails in the forest and damage the roots of trees. Regardless of their small effect on the total weight of a loaded log forwarder, lighter manipulator structures could save money through the smaller components and actuators required.

1.2 Advanced Manipulator Control in the Forest Machinery Technology of Tomorrow or Just a Future Scenario

In addition to operator training, the improvement of the control of the forest machine manipulators can be seen as a promising task in the protection of the trees left standing after thinning. Increased velocities together with an accurate control system help achieve the desired level of work efficiency. One key factor that influences the use of advanced control methods is the cost competition between manufacturers. New control systems cannot significantly raise the costs of a machine, and this is one reason why extra transducers are seen as being a big question mark among manufacturers. The lack of sensors is, therefore, one main bottleneck in the application of new control methods. Another reason is the reliability of transducers. A difficult environment makes high demands on electronics, and there is also the risk of mechanical damages. On the other hand, competition can provide opportunities to make strides forward with advanced solutions and high performance.

Because of the open-loop control in log cranes, new methods cannot directly apply closed-loop control methods. Closed-loop systems often suffer from problems related to achieving stability. In mobile working machines, all forms of instability are banned. Safe working also has to be guaranteed in transducer malfunction situations.

1.3 Aim of the Research

Many characteristics of the flexible hydraulic manipulators are mentioned above. These characteristics have direct or indirect effect on the dynamic behavior of the manipulator. In addition to manipulator itself, the operator and the control system have direct effect to the behavior of the manipulator. It is a well known fact that

impulses with the same frequencies as the nominal frequencies of a mechanical system produce vibrations in the mechanism. The excitation of undesired oscillation can be prevented by avoiding impulses near the structural natural frequencies of a mechanism (Rao 1990, p.454). In long term, the most important natural frequencies of a manipulator are the lowest ones and, in particular, the first one. The professional user of a manipulator tries to avoid producing the first vibration mode through their operational habits. If vibrations are produced, a professional user attempts to suppress them by stopping all movement or by producing small damping movements in the manipulator using the joystick.

To improve dynamics of the flexible hydraulic manipulator one has to own knowledge from used technology and skill to see all interactions between different factors affecting to this mechatronic system. The aim of this dissertation is to find new vibration reduction methods for flexible hydraulic manipulators. These methods are based on shaping of the operator's control signal in such a way that open-loop control is still applied. The vibration reduction methods are designed mainly for forestry machines fitted with electronic control systems.

The control methods have been developed through the study of the dynamics of manipulators. The natural frequencies for the adaptive vibration reduction method have been collected using the dynamic simulation model of a manipulator. An algorithm that takes into account the dynamics of a manipulator is developed here. In second part of the dissertation, a semi-active vibration reduction method is developed based on known pressure feedback applications. The semi-active controller does not require an additional actuator and is implemented by coding a damper into the control system of the manipulator. This dissertation attempts to provide the knowledge of the professional operator in the written form.

1.4 Research Methods

The main steps in the development of a controller for a flexible manipulator are:

1) The identification and modeling of the dynamics
2) The choice and development of the control algorithm, the calculation of the control parameters
3) The implementation of the controller

The dynamic simulation model and controller simulators are constructed by using commercial and generally available software applications. The dynamic simulation models are verified using existing manipulators in both laboratory and field conditions. The verified models are used to collect information on the dynamics of the manipulator. The calculation and tuning of control parameters is performed using the simulation models. The controller models developed here are compiled for a simulator that applies real-time software and hardware. Real manipulators are equipped with transducers for testing. The controllers are tested in real time hardware-in-the-loop simulations.

1.5 Scope of the Work

This research is limited to the field of serial manipulators. The proposed methods use transducers, and it is assumed that in the near future reliable, reasonably priced transducers will be available for these methods. The transducers measure the stroke of the cylinder (linear measurement) and the pressure in cylinder chambers. It would be possible to use acceleration transducers in the place of the pressure transducers and joint angle measurement instead of linear position measurement. Even though load measurement transducers are available, such transducers were not applied in this study. The common problem of these transducers is that they are suitable only for static measurement. The proposed controller requires load information without a long time delay and, therefore, the tests were driven with a known constant load or the load was calculated using the kinematics of the manipulator and the pressure information. It was observed that the calculation performed accurately only in simple work cycles where the pressure vibration was small. Nevertheless, load calculation was in use in some field tests.

The performance of the developed controllers was studied by comparing the new controllers with widely used ramp control functions in simple step tests and long field tests. In the field of control systems, it is common practice to compare new controllers with traditional PID controllers. Because of the nature of the studied manipulators, their comparison with ramp functions was assumed to be appropriate. Because of the lack of a suitable key figure, the RMS value (Root Mean Square) is used as such. The RMS results are comparable only when calculated in a similar manner.

The results of the field tests are machine-dependent: The manipulators used were old and exhibited backslashes. The measurement temperature influences the strain gauge results.

The parameters of the ramp function have not been measured on real cranes. The parameters were tuned to the amplifier cards according to factory instructions and with the help of the professional operator.

1.6 Contribution of the Dissertation

The dissertation presents control methods that improve dynamic characteristics of the open-loop controlled log crane. The work puts forward vibration suppression methods that have been developed for a modern hydraulically driven manipulator control system. The proposed methods are independent of the experience of the operator. The aim is to provide better control for the manipulator. Two vibration suppression methods for the open-loop control of a flexible manipulator are presented here. The first of these, the adaptive filter, takes into consideration the changing dynamics of the manipulator when shaping the valve input. The adaptive filter is based on the calculation of the natural frequencies of the crane. The calculation of the natural frequencies requires a dynamic simulation model in

which most important parts are modeled as flexible. In addition, load information is needed and this thesis presents a method for calculating the load using information provided by the transducer. The natural frequencies are collected at separate points in the work area with different loads by linearising the equations of motion of the simulation model. A surface fitting algorithm that calculates the lowest natural frequency of the manipulator is presented here. The lowest natural frequency is used in a low pass type of filter that smoothens the control signal. The presented adaptive filter was patented during the course of this research (Pat. FI 109349B) and the real-time model of the controller was implemented in a test algorithm. The test results show the algorithm to be feasible.

The second method presented here is a semi-active vibration suppression method that is based on pressure feedback. Pressure feedback is widely used in closed-loop control techniques in order to improve, for instance, trajectory tracking. In this dissertation, pressure feedback is applied in a common open-loop control system as an auxiliary damper. The implementation of the proposed method does not require the addition of additional damper actuators to the machine. Traditionally, additional dampers are used.

1.7 Outline of the Dissertation

This dissertation presents the development of the two vibration suppression methods and tests carried out on them and finally offers ideas on how to utilize the results. Chapter 2 presents vibration suppression methods and applications used in mobile machines and flexible structures. This study does not attempt to be complete because there are numerous methods, for instance, in the area of control systems. This study focuses on the area of flexible manipulators. Chapter 3 concentrates on the development of vibration suppression methods; the theories and simulation models behind the controllers are given. The dynamic simulation model of a flexible manipulator and the process of linearising the equations of motion are presented. The linearising process gives the natural frequencies of the manipulator and, in this work; only the lowest natural frequencies are required. An algorithm that calculates the lowest natural frequency of the manipulator is also presented. Part of the lowest natural frequency is used as the filter frequency in an adaptive filter. Furthermore, information on the load being lifted is required for the calculation of the natural frequencies, and an algorithm that calculates the mass load from the measured pressure and position information is presented. Later on, semi-active damping is developed based on literature. Chapter 4 presents the testing of controllers and the results of field tests performed on real log forwarder cranes. The experimental arrangement, hardware settings and some notification for future measurements are given. This chapter also discusses the usability and benefits of the proposed methods. Finally, chapter 5 presents the conclusions of this study.

2 Vibration Suppression Methods

2.1 General overview

Flexibility presents a great challenge to the control systems of different kind of mechanical systems. If mechanical components deflect during movement, there exists the risk that vibration will occur at the structural frequencies. Deflections also weaken the trajectory-tracking ability that is an essential requirement for some systems. The control system can also include its own flexibility, which is harmful to the performance of the system. Vibration suppression methods can be classified as passive, semi-active and active vibration suppression methods. Passive vibration suppression methods are tuned to work only in some operation point and the vibration suppression achieved outside of the operation points is often weak. Active or semi-active vibration suppression methods can adapt to different situations and operation points. In the active vibration suppression methods auxiliary energy is imported to the system. In many applications, a closed-loop control system is used with these suppression methods.

Most vibration suppression methods exploit transducer signals that indicate the state of the point under study. The point can be in any sensitive part of the mechanism, or the measurement signal can indicate only the state of the actuator. In the case of flexible manipulators, the end-effector position can be measured directly or indirectly. Direct end-effector pose measurement is often possible only in laboratory conditions, since it is often carried out using, for instance, 3D laser tracking systems. In some excavators, direct pose measurement is used in special situations such as in construction sites or ditch excavation where the excavator moves in a limited area. Also, in some space applications, machine vision systems have been successfully used. End-effector acceleration measurement is one method that has been used, but it encounters difficulties when the acceleration has to be divided into separate components. Otherwise, direct pose measurement involves many difficulties that arise from the working conditions, visual and other obstructions or sometimes from large global rotations and translations of the machine.

The indirect measurement method measures the position or rotations of different links or joints and uses a kinematic model of the mechanism to calculate the position and orientation of the manipulator. Position data obtained from the use of this method applies to an absolutely rigid system, and the flexibility of the links or joints has to be measured with auxiliary sensors. These can be based on the measurement of stress in a certain point and on the calculation of deformations. Another method involves the use of optical transducers for deflection measurement. The measurement methods and sensor types used depend on the application, actuators and source of the flexibility.

Unlike the addition of extra dampers to a machine, the control of the main actuators is an attractive option for engineers. In industrial robot applications, continuous path control plays an important role, for example, in welding, grinding and painting operations. Accurate vibration-free path control is often reached by using different polynomials or mathematical functions that give smooth trajectories. Craig (1986, Chapter 7) gives some basic functions that result in

smooth velocity profiles. These can also be applied in point-to-point control. The velocity profiles are normally not based on the natural frequencies of a system, so the amount of vibration reduction obtained with the profiles varies from system to system; furthermore, the vibration reduction capability may vary as a function of the distance. By taking into account the lowest mode of vibration and the distance between the actual and desired position, different Trapezoidal, S-Curve, and parabolic velocity profiles can be tuned for improved and predictable vibration reduction. (Craig 1986, Chapter 7).

Kwon (1995) presents the feedforward method to improve the tracking control of a hydraulically driven long-reach manipulator. The load-compensated velocity feedforward loop is used in parallel with a pressure feedback loop to increase the bandwidth of the controller. The controller compensates for dynamics of the hydraulic actuator and, according to Kwon, increases the stability of the feedback controller.

Vibration control methods, which are based on the shaping of the input signal, are extensively discussed in Singhose's doctoral thesis (1997). Singhose presents an extensive variety of methods for designing command generators for flexible systems. The aim is to find a shape for the reference command that would produce the desired trajectory and dynamic behaviour. The methods are based on the calculation of the optimal control signal according to constraint equations. Singhose's thesis continues the work of Singer (Pat. US 4916635), Meckl and Seering (1985, 1988) who presented similar research results earlier on. Some research results have been reached in co-operation (Pat.US 5638267). Singer et al. (Pat. US 4916635) patented a method in which the shaping of the input signal is used to minimize the vibration of the dynamic system at its natural frequencies. The input signal is calculated from two constraint equations that bound the available solution input to the system characteristics. Meckl and Seering (1985) describe a shaped forcing function for moving a dynamic system over an incremental distance with a minimum of residual vibration. The function is constructed by combining the harmonics of a ramped sinusoid function so that a minimum amount of energy is introduced into the system at its resonant frequencies. Another article (Meckl & Seering 1988) presents an experimental system where a Cartesian robot was used to test shaped reference inputs and to compare their responses with step responses. The results indicated a noticeable reduction in residual vibration for the shaped inputs.

A common problem that arises when input-shaping methods are considered is that perfect or good knowledge of the plant modal parameters is required in order to reduce residual vibration to zero. Therefore, input-shaping methods have often been used in applications where the modal parameters remain fixed and the working conditions are well known. If the controller is tuned on the basis of a finite dimensional model (the number of modelled natural frequencies is small), the presence of neglected dynamics may drive the controlled plant to instability. This is the so-called spillover phenomenon (Cavallo et. al. 1996).

Sidman et al. (Pat. US 5459383) measured the vibrations near the actuator motor of a mechanical head used for positioning in a disc drive and used an extra feedback loop parallel to position and velocity loops in order to damp the

vibration of the head. The measured vibrations were fed back into the servo system using a high-gain feedback loop.

Filtering is a widely used method for smoothening control signals. Deniard et al. (1993, p.170-187) used a first-order filter with interpolation to build velocity trajectory profiles for controlling industrial robots. The used cut-off frequency was 3.3 Hz when the lowest vibration mode of the robot had been measured at 5.1 Hz. Scaramuzzo (Pat. US 5465035) has presented a method that uses piecewise trigonometric input signals. A pre-shaped input signal is bandwidth-limited in such a way that its energy is concentrated below the frequency of the lowest system resonance.

It is widely known that passive suspensions have limitations when it comes to the isolation of vibration. The vehicle industry has researched different kinds of active dampers for use as vehicle engine suspension systems. Best at al. (Pat. US 4869474) have patented a vehicle engine suspension system where electrically actuated engine mounts are fed power from a control system that is responsive to the acceleration of the vehicle body. The engine mounts generate forces that are of such an amplitude and phase that they reduce the vibration of the vehicle body. The proposed method that uses acceleration measurement, servo valves and a hydraulic actuator is a common way of building an active damper.

Nagai (1993, 161-170) has also introduced different semi-active and active dampers for use in vehicles. The semi-active suspension introduced uses the on-off control law to switch or change the parameters of the damper. In the active suspension system, conventional suspension elements are replaced with hydraulic actuators, servo valves and transducers that measure the vertical acceleration of the vehicle body.

Many limits imposed by the size of the damper, the force capacity and available room in vehicle have guaranteed that vehicle engine systems have been the focus of wide research. Gossman et al. (Pat. US 5423523) have developed a mount that has improved efficiency of force transmission. The force losses are minimized by minimizing of the mass and velocity of the fluid used in the damper and by using passageways with short and large cross-sectional areas.

2.2 Vibration Suppression in Hydraulic Manipulators

The most common and natural way of protecting any machine or structure is to recognize the correct work conditions and boundaries in advance. The operator can reduce the velocity of the manipulator or lift reasonable loads with it. Putkonen (Pat. US 4815614) patented a static method for independently reducing the velocity of a log crane. The crane is equipped with a load sensor, on the basis of which the velocity of the crane is controlled. When the load is heavy, the velocity is forced to remain low in order to protect the crane. Yamagata (Pat. JP5157101) has presented a similar method. Pressure transducers are used to detect the load of the manipulator, and the velocity of the lift cylinder is limited in accordance with the load on hydraulic actuator.

Krus & Gunnarsson (1995) used accelometers in the control of hydraulic cranes. They measured the load acceleration at the end tip of the crane and used acceleration instead of load pressure, which has traditionally been used in many control algorithms, in the control of the crane. The position feedback used the acceleration signal to damp vibration. Also, impact detection based on the use of acceleration information was presented.

In the field of forestry machines, perhaps the most traditional vibration suppression methods utilize hydraulic accumulators and so-called ramp functions in electronic control systems. Ramp functions and hydraulic accumulators without active control can be classified as passive vibration reduction methods. Some other semi-active vibration suppression methods have been tested in forestry machines, for example, in cabin seat isolation.

2.2.1 Suppression by Hydraulic Accumulator

Hydraulic accumulators are used in hydraulic circuits to store energy, suppress vibration and act as an energy source. Manufacturers of manipulators have added hydraulic accumulators to their machines to protect the boom structure and to provide better dynamics. The weak point in the use of passive vibration reduction methods is that they can only be tuned to operate under certain conditions. Tuning settings that function well in certain situations may not necessarily function in others; in other work situations, the behaviour of the manipulator may be too "jerky", as operators describe its behaviour. Manufacturers also often explain that, for basic machines, the cost of the accumulator excessively increases the total price of the manipulator.

Määttälä (2002) carried out a study into the effects of a hydraulic damper unit on a full-length log crane. In the lift movement, the pressure peaks were reduced, on average, by 15 % when the hydraulic accumulator was in use. The pressure shocks were better damped out at low pre-charge pressures, and at high pre-charge pressures, the stress measured in the strain gauge measurement points was lower. The benefits obtained through the use of a hydraulic accumulator depend on the volume of the accumulator, the pre-charge pressure of the accumulator and the tune of the valve that controls the flow in and out of the accumulator.

The settings of the throttle valve of a hydraulic accumulator change the stiffness of the accumulator and, therefore, influence the benefits obtained. When the valve is more open, the hydraulic natural frequency of the accumulator is lower and the number and amplitude of the pressure peaks is reduced; however, the amplitude of the stress peaks in the critical points is higher. On the contrary, when the valve is more closed, the natural frequency of the accumulator is higher, the number and amplitude of the pressure peaks increases and the amplitude of stress peaks is reduced. (Määttälä 2002).

2.2.2 Methods Employed in Excavator Boom Control

In the construction industry, excavators are often used in construction sites that are surrounded by traffic, people, electric cables and buildings. The operator has to use the excavator carefully and keep in mind that any lapses can lead to severe accidents. Because the excavator's manipulator is often much heavier than in forest machines and the loads are loaded into the bucket near the undercarriage, a lower velocity is required from the manipulator. Nonetheless, vibrations in the manipulator reduce the work quality and are not permitted in accurate position tasks.

During last five years, one main area in excavator research has been the development of different digging control systems. In automatic depth control systems, the controller calculates the motion speed and direction of the bucket in order for the pre-set digging depth to be achieved (Masakazu 2000).

In the early 90's, the Japanese excavator manufacturer, Hitachi, patented many vibration suppressing and control devices for hydraulic working machines (Pat. JP5321297, Pat. JP5157101, Pat. JP5060104, Pat. JP6185501). In most of its inventions, the company used an extra directional valve to suppress vibration and also proposed a calculation method for improving the behaviour of the system. The above-mentioned extra valve feeds oil into the lift cylinder, the main actuator of the excavator boom and suppresses vibrations. The valve's control signal is calculated using the pressures and velocity of the lift cylinder. The disadvantage of this solution is that an additional hydraulic circuit is needed with the directional valve.

3 Applied Vibration Reduction Methods for Log Cranes

3.1 Simulation Models for Log Cranes

The construction of an analytical simulation model for a flexible manipulator, which contains actuators, is usually a challenging and time-consuming job. For this reason, it is convenient to apply suitable dynamic simulation software, such as ADAMS (Automatic Dynamic Analysis of Mechanical Systems). In this case, ADAMS was available and experience from previous research projects had shown it to be an efficient tool in modelling multibody systems.

The simulation model used for the hydraulically driven log crane consists of the model of the flexible boom mechanism and the equations that describe the hydraulics and interactions between the mechanism and the hydraulics. The methods for modelling flexible multibody systems (Shabana 1998, Chapnik 1993, Linjama 1998) and rigid systems (Papadopoulos 1996) are presented in many references and are not discussed in detail in this thesis. The equations of motion with the constraining equations can be presented in Lagrangian form as follows:

$$\frac{d}{dt}\left(\frac{\partial \mathbf{T}}{\partial \dot{\boldsymbol{q}}}\right) - \left(\frac{\partial \mathbf{T}}{\partial \boldsymbol{q}}\right) - \mathbf{C}_q \boldsymbol{\lambda} = \boldsymbol{Q}_e{}^j, \tag{3.1}$$

where $\mathbf{T}$ is the kinetic energy of the system, $\mathbf{C}_q$ a Jacobian matrix of rigid body generalized coordinates $\boldsymbol{q}$, $\boldsymbol{\lambda}$ a vector of Lagrangian coefficients and $\boldsymbol{Q}_e{}^j$ a general force vector. ADAMS is based on the Lagrangian method that relies upon this Lagrangian equation.

A flexible body has to be modelled using a suitable, specific approximation method. Finite element and assumed modes methods are commonly used approximation methods (Mikkola 1997). In the ADAMS software, a flexible boom can be built using the ADAMS/Flex toolbox, or the description of part of the geometry and flexibility can be imported from some other application. Depending on the software in which the flexibility is modelled, there are different ways of describing flexibility. A flexible part can be constructed from rigid parts and springs that connect the rigid parts together. In this case, the spring coefficients are obtained from the stiffness matrix and the mass properties, similarly, from the mass matrix.

The stiffness matrixes of the pillar and the lift boom (calculated using the ANSYS software) were imported to ADAMS; furthermore, the crane has a jib boom with an extension. There are usually two, sometimes three, beams in the extension boom and prismatic slide bearings between these beams. When the extension actuator pushes the inner beam out from outer beam, the sliding contact point changes. Because a sliding contacts between flexible bodies modelled using nodes are difficult to model, the jib and the extension boom were modelled using six DOF beam elements from ADAMS/Flex.

The hydraulic system of the log crane consists of slew, lift, jib and extension cylinders, proportional directional valves, hoses, a pump and a tank. The hydraulic cylinders act as an interface between the mechanism and the hydraulic system. The pressure in the cylinder chambers is converted to the cylinder force that is applied to the mechanism. The cylinders are connected to the directional valves by hoses that are modelled as flexible fluid volumes. The pump is modelled to be a constant pressure source, and there is small (1-bar) pressure acting in the tank.

The hydraulic system was modelled using the hydraulic model generator, developed at LUT (Rouvinen 1995) and modified for the components in question. The models and methods employed in their postulation are discussed in more detail in references (Handroos 1990, Käppi & Ellman 1999). Basically, the hydraulic system is based on two main equations, the equations of flow resistance and continuity. The commonly used flow resistance equation (Merrit 1967) is written as

$$Q = C_q a \sqrt{\frac{2\Delta p}{\rho}}, \tag{3.2}$$

where Q is volymetric flow rate, a restrictor area, Δp pressure differential, ρ fluid mass density and C_q is a flow coefficient that depends on the geometry of the valve orifice and the Reynolds number.

The flow continuity equation for the control volume can be written as (Merrit 1967)

$$Q_i - Q_0 = \frac{dV}{dt} + \frac{V}{\beta_e}\frac{dP}{dt}, \tag{3.3}$$

where Q_i is input flow rate, Q_o output flow rate, V volume and β_e is a effective bulk modulus of the fluid.

The boundary deformation term, $\frac{dV}{dt}$, describes the effect of the varying cylinder chamber volume as the piston moves. From equation (3.3), the pressure derivative can be solved as follows:

$$\frac{dP}{dt} = \frac{\beta_e}{V}\left(Q_i - Q_0 - \frac{dV}{dt}\right) \tag{3.4}$$

Equation (3.4) is used in the hydraulic model generator to describe the pressure dynamics in fluid volumes.

The smaller of the cranes studied in this research, namely the PATU 655, was equipped with high-bandwidth proportional valves, so-called Regel-valves that are manufactured by Rexroth-Bosch. The hydraulic circuit was kept as simple as

possible, which for example, meant that counter-balance valves were not used. High-bandwidth proportional valves were used at the beginning of the testing to minimize the effect of the valve properties and especially the effect of the so-called dead zone.

Usually, proportional directional valves that have inferior dynamic characteristics are used in mobile machines. The Timberjack crane, the TJ71F72, was controlled by VOAC K170LS proportional valves (a model of the valve is presented by Käppi & Ellman 1999). The features of low bandwidth valves include pressure compensation, nonlinear flow gain and a large dead band. The load sensing line was not connected in the laboratory because it would have led to problems with long hose lines. The same valve block was applied in log forwarders with load sensing lines. The valve solenoids require a PWM current. Therefore, special amplifiers (PARKER PWD 00A-400) between the control computer and valve were used so that ± 10 V DC voltages could be used to control the valve.

Figure 3.1 present the main parts of the crane under study and Table 3.1 lists the features of the parts and programs used in modelling them.

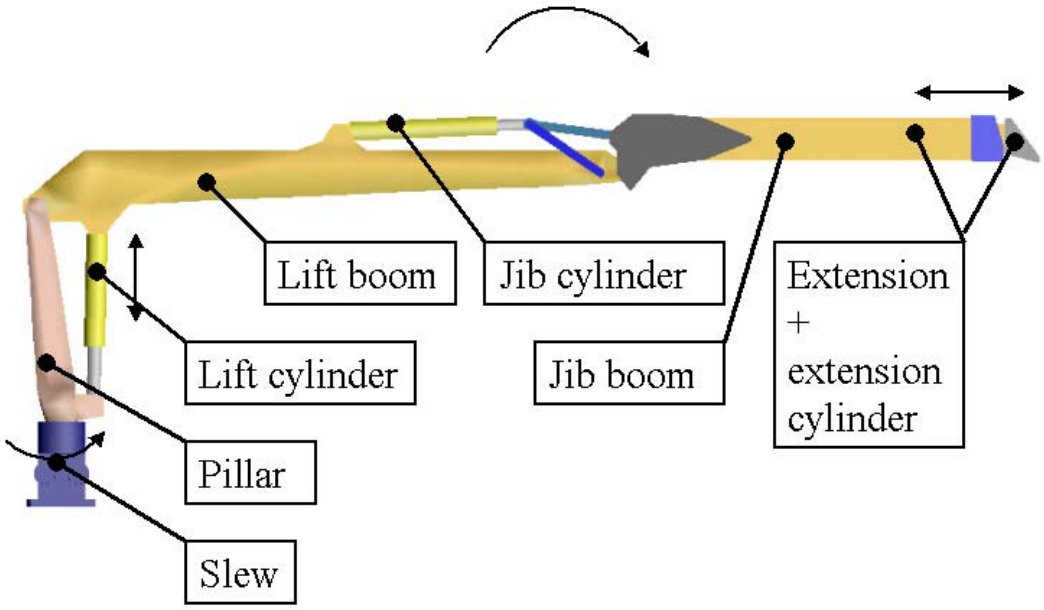

Figure 3.1 The simulation model of the crane

Table 3.1 The features of the main members of the crane

PART	FEATURES	PROGRAM
Slew	Rigid, two cylinders, coupler	ADAMS
Pillar	Flexible	ANSYS
Lift boom	Flexible	ANSYS
Jib boom	Flexible	ADAMS/Flex
Extension	Flexible, contact forces with the jib boom	ADAMS/Flex

Three crane models were used in the development work: PATU 655, manufactured by Kesla Oy, TJ71F72, and TJ71F100 made by John Deere Timberjack. The first crane, PATU 655, is designed for mid-weight tractor applications while the latter two are used in Timberjack log forwarders. All the simulation models have a pillar and a lift boom modelled using the ANSYS finite element software. The PATU 655 crane model, without the gripper, rotator and mass load, is shown in Figure 3.2. TJ71F72 is shown in Figure 3.1 and TJ71F100 later on in Chapter 4 (Figure 4.1).

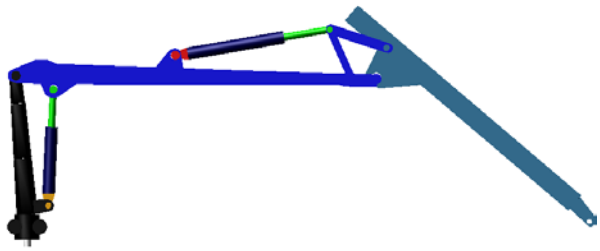

Figure 3.2 The simulation model of the PATU 655 crane

3.1.1 Linearization as a Tool for Monitoring Dynamic Behaviour of a Mechanism

ADAMS automatically formulates the equations of motion that are in Lagrangian form. Each body has a centre of mass (CM) to which the local reference frame is usually attached. The body has three translational and three rotational degrees of freedom. If the kinetic energy, **T**, in equation (3.1) is written in terms of generalized coordinates, $\boldsymbol{q}$, and their derivatives, the amount of second-order differential and algebraic equations can be written as

$$\mathbf{g}(\ddot{\boldsymbol{q}},\dot{\boldsymbol{q}},\boldsymbol{q},\boldsymbol{\lambda},\boldsymbol{Q}_e^j,t)=0\,. \tag{3.5}$$

In order to utilize standard numerical integration methods, these second-order differential equations are transformed to first-order equations, which can be done by introducing velocities as solution variables.

$$\mathbf{g}(\dot{\boldsymbol{y}}, \boldsymbol{y}, \boldsymbol{Q}_e^{\,j}, t) = 0\,, \tag{3.6}$$

where $\boldsymbol{y} = \begin{bmatrix} \boldsymbol{q} \\ \dot{\boldsymbol{q}} \\ \boldsymbol{\lambda} \end{bmatrix}$.

The system equations, as given by (3.6), can be linearised at the operating point $\boldsymbol{y}^* = (\dot{\boldsymbol{y}}_0, \dot{\boldsymbol{y}}_0, \boldsymbol{Q}_0, t_0)$ as

$$\delta\mathbf{g} = \mathbf{A}\big|_{\mathbf{y}^*} \cdot \delta\boldsymbol{y} - \mathbf{B}\big|_{\mathbf{y}^*} \cdot \delta\dot{\boldsymbol{y}} + \partial\mathbf{g}/\partial\boldsymbol{Q}_e^{\,j}\,\big|_{\mathbf{y}^*} \cdot \delta\boldsymbol{Q}_e^{\,j} + \partial\mathbf{g}/\partial t\big|_{\mathbf{y}^*} \cdot \delta t = 0 \tag{3.7}$$

where $\delta\boldsymbol{y}, \delta\dot{\boldsymbol{y}}, \delta\boldsymbol{Q}_e^{\,j}$ and δt are variations about $\boldsymbol{y}^* = (\dot{\boldsymbol{y}}_0, \boldsymbol{y}_0, \boldsymbol{Q}_0, t_0)$ and

$$\mathbf{A} \equiv \partial\mathbf{g}/\partial\,\boldsymbol{y}\big|_{\mathbf{y}^*}$$
$$\mathbf{B} \equiv -\partial\mathbf{g}/\partial\,\dot{\boldsymbol{y}}\big|_{\mathbf{y}^*}\,.$$

Assuming that the mechanical system, represented by **g**, is in a state of static equilibrium or in another state at $\boldsymbol{y}^*$ such that matrices **A** and **B** are time-invariant, $\partial\mathbf{g}/\partial t = 0$. Furthermore, if we assume the general forces in equation (3.7) to be zero ($\delta\boldsymbol{Q}_e^{\,j} = 0$), we can express $\delta\boldsymbol{y}$ as (Sohoni 1986)

$$\delta\boldsymbol{y} = e^{\sigma t}\boldsymbol{z}\,, \tag{3.8}$$

where $\boldsymbol{z}$ is a complex constant vector and σ a complex constant scalar.

Equation (3.8) can be differentiated with respect to time, which gives

$$\delta\dot{\boldsymbol{y}} = \sigma e^{\sigma t}\boldsymbol{z}\,. \tag{3.9}$$

Substituting (3.8) and (3.9) into (3.7) leads to the generalized eigenvalue problem

$$\mathbf{A}\boldsymbol{z} = \sigma\mathbf{B}\boldsymbol{z}\,. \tag{3.10}$$

To be able to solve (3.10), matrices **A** and **B** have to be constructed. Matrices **A** and **B** are constructed for the corrector formula of the numerical integration procedure in ADAMS, and thereby, sufficient information for the solution can be gathered. (Sohoni 1986, ADAMS 2002).

3.1.2 The Simulator in the MATLAB/Simulink-ADAMS Interface

In the first phase, the control algorithm was tested, tuned and verified by applying a crane simulator in the MATLAB/Simulink-ADAMS interface. The crane simulator was constructed by linking the ADAMS model of the log crane to the MATLAB/Simulink control simulation program via the ADAMS/Controls module. In the ADAMS/ Controls module, the control signals and mass loads were defined as the input and the cylinder strokes as the output variables. The ADAMS/Controls module builds an "Adams_sub" subroutine block for Simulink (see Figure 3.3). This subroutine block starts the ADAMS/ Solver when the simulation is started in the Simulink model and handles the change of input and output variables. The subroutine block enables the interactive simulation of dynamics. Both programs use their own integrators (ADAMS 2002).

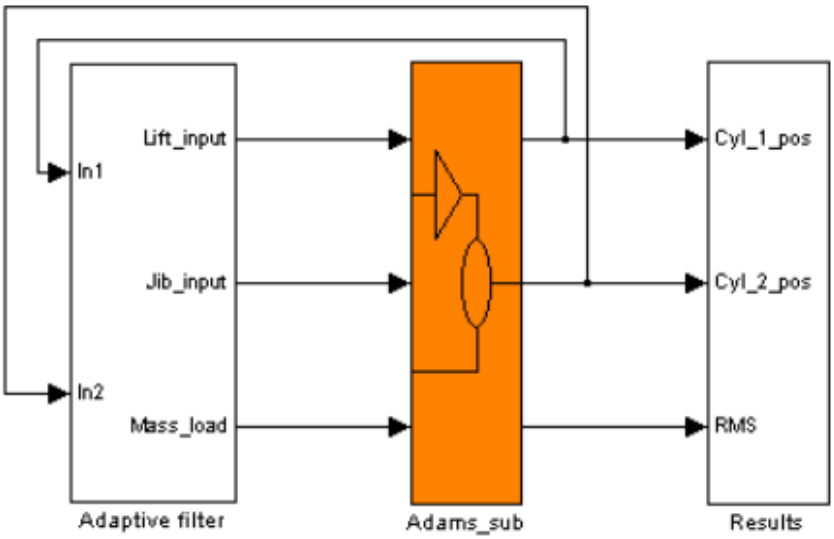

Figure 3.3 An example of the crane simulators used in MATLAB/Simulink

3.2 Adaptive Filter

3.2.1 The Basis for Filtering the Control Signal

It is well known that an external force excites vibrations in a mechanical system more easily if the frequency of the external force coincides with one of the natural frequencies of the system. Under these conditions, resonance occurs and the systems start to oscillate. The impulses, possibly coming from the system's own actuator, should not be near the lowest natural frequency of the system or any of its multiples. It is also known that the jerk, the second derivative of velocity, is strongly coupled with the excitement of structural vibrations. Therefore, in industrial applications, for example, it is important that the jerk be limited because

this results in improved path tracking and reduces the wear of the components. In order to minimize the effects of jerk, it is important to use a control function that allows for the adjustment of jerk. Because jerk is a first derivative of acceleration and a second derivative of velocity, it is obvious that we need a second- or higher-order function between the user's velocity reference and final control signal of the valve. Macfarlane & Croft (2001) used a method in which the concatenation of fifth-order polynomials provided a smooth trajectory between two points. The polynomial coefficients were calculated in such way that they handle the transition from zero acceleration to non-zero acceleration and, in this way, limit jerk.

In the following, the transfer functions are named as the first- and the second-order filters. First- and second-order filters have the following transfer functions:

1-order: $$H(s) = \frac{1}{s + \omega} \tag{3.11}$$

2-order: $$H(s) = \frac{\omega^2}{s^2 + 2\varsigma\omega s + \omega^2} \tag{3.12}$$

Figure 3.4 and 3.5 illustrate the velocity step response and jerk of the ramp function, the first- (3.11) and the second-order transfer function (3.12).

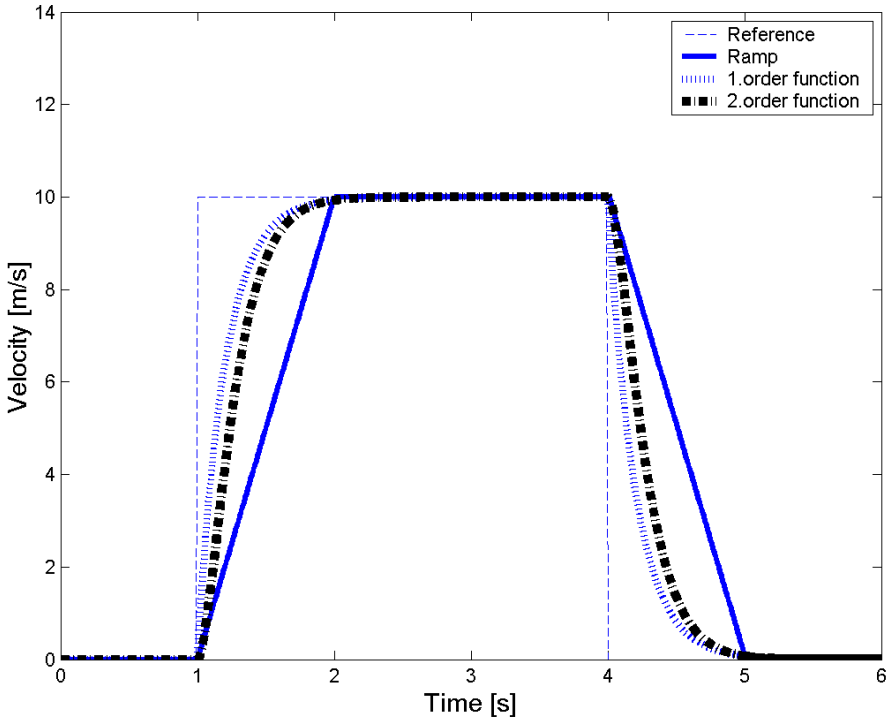

Figure 3.4 Step response (velocity input)

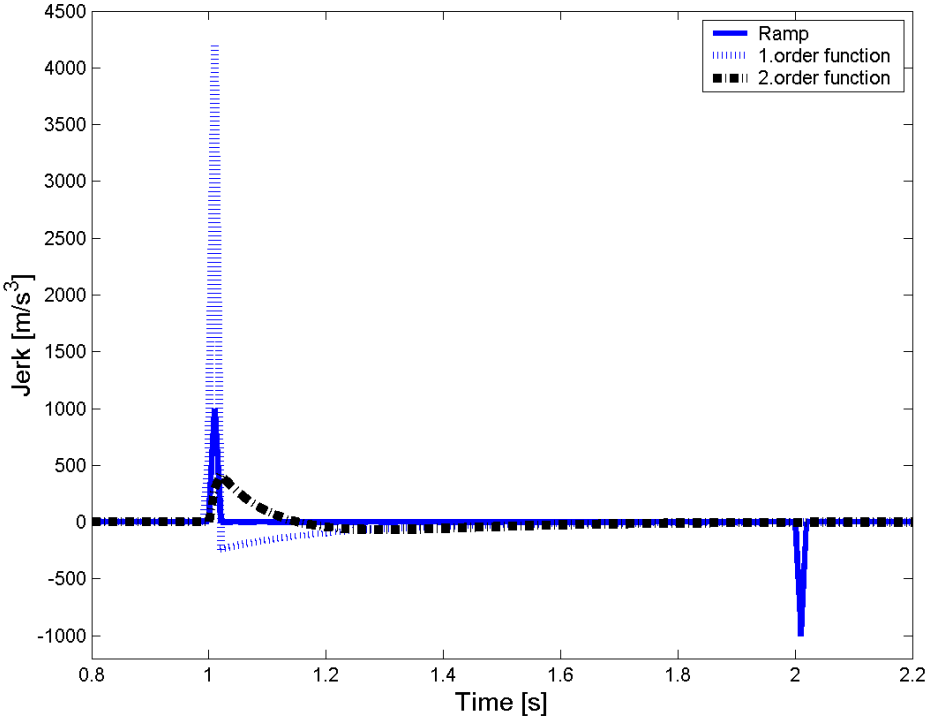

Figure 3.5 Jerk of step response (velocity input).

The first-order filter has already been tested in some modern mobile hydraulics controllers. Figure 3.5 shows that first-order filter has bigger jerk at the starting point with a similar response to that of the second-order filter. If the frequency of the first-order filter were to be decreased, the response time would become too long to achieve effective control properties. On the other hand, the second order filter can reduce jerk without a significant increase in the response time. If we use a critical damping factor, ζ (0.9…1.0), and force the filter frequency, ω, to follow the lowest natural frequency of the manipulator below its critical value, we can construct an adaptive filter for open-loop control. The problem is how to calculate the filter frequency. The manipulator changes its position and inclination during the work cycle and handles different loads. The calculation of the natural frequencies of the manipulator is analogical to the calculation of the natural frequencies of a spring-damper system, as shown in Equation (3.13):

$$\omega = \sqrt{\frac{m}{k_s}} \tag{3.13}$$

In the case of the manipulator, mass m is the complete mass of the manipulator with the load and the spring constant, k_s, is the stiffness of the manipulator which depends on the operation point of the manipulator. Thus, the dynamics of the manipulator can be determined by studying the natural frequencies of the dynamic simulation model. The equations of motion form a dynamic system model that can be linearised to obtain so-called eigendata. Another possibility is to compute step responses using the model and to study, for instance, pressure data and calculate

the natural frequencies using this information. The simulation model can be forced to different positions and inclinations and the natural frequencies can be computed using the steady state conditions. Because the load is unknown, the natural frequencies have to be calculated for many different mass loads in a specific position and inclination. After the whole workspace has been covered, the correlation of the natural frequencies with the position, inclination and the load of the manipulator have to be defined. (Kovanen & Handroos 2001 A,B)

The solution of the eigenvalue problem equation (3.10) results complex valued eigendata (eigenvalues, mode shapes) from which the lowest natural frequency can be selected. In practice, ADAMS/Linear computes this process after the user has decided the operating point. The gathering of eigendata was automated with the use of an ADAMS macro. The macro varied the position and load mass of the crane, computed the static analysis, used the ADAMS/ linear module to linearize the system model after static analysis and saved the eigendata to a text file. The eigendata was gathered for three different mass loads for PATU 655 and for four mass loads for TJ71F72. In the case of PATU 655, the simulation model, the lift cylinder stroke, was divided into nine points and the jib cylinder stroke into five points. For TJ71F72, the number of stroke points of the lift cylinder was reduced to five because the results of latter simulations proved that such a reduction was possible. The lowest natural frequency in each position had to be selected "by hand" from the result file. The natural frequencies collected are presented in Appendix A.

From the results, it can be seen that the frequencies increase as a function of the jib cylinder stroke and decrease as a function of the mass load. The reason for the discontinuities in the surface (the "hills and craters" in Figure 3.7 (a)) is the fact that at some points, ADAMS did not find a solution for the static analysis. If the static analysis did not succeed, the macro performed a short dynamic analysis in the operating point. In this analysis, the crane model just oscillated about the same position and after the oscillation was damped, the linearization was performed. In some points, where the dynamic analysis was computed, the oscillation was not damped enough prior to linearization, and this increased the error.

3.2.2 Natural Frequency Surface Fitting

The verified simulation model of PATU 655 and some preliminary tests on the real crane guaranteed that the simulated eigendata was good enough for surface fitting. A function for the lowest natural frequency had to be constructed next. It had to be simple enough for real-time calculation, and it was, therefore, natural to take only three variables for curve fitting: the measured strokes of the jib and lift cylinder and the load mass. The surface fitting process was divided into two parts. Firstly, the orientation of the boom, i.e. the cylinder strokes, was fitted to correlate. Secondly separate natural frequency surfaces were connected together by fitting the results of the first fitting process. In this step, the mass load, m, was set as a variable in the second order function. Figure 3.6 shows the outline of the fitting process:

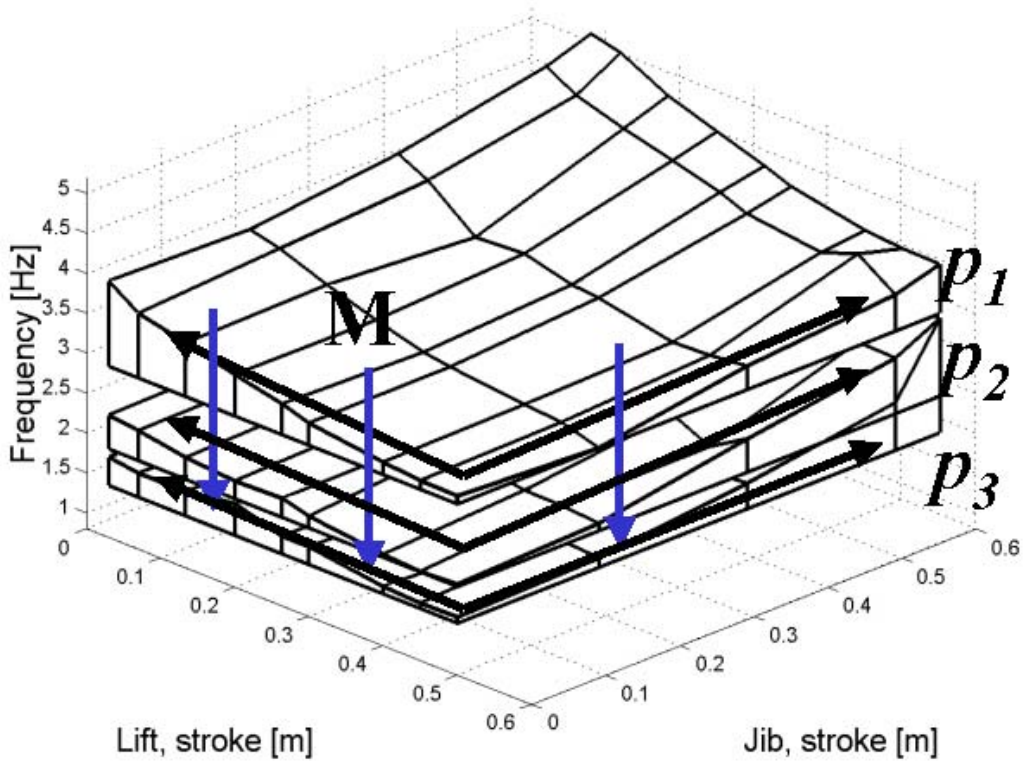

Figure 3.6 Surface fitting.

Polynomials with two variables were chosen for the first part of the surface fitting.

$$p_f(X,Y) = c(i,1) + c(i,2)X + c(i,3)Y + c(i,4)X^2 + c(i,5)XY + c(i,6)Y^2 \tag{3.14}$$

$$\boldsymbol{p}_i = c(i,j)\cdot \boldsymbol{p} \tag{3.15}$$

where

$$\boldsymbol{p} = \left[ones(size(X)) \quad X \quad Y \quad X^2 \quad XY \quad Y^2\right] \tag{3.16}$$

Different c(i,j) coefficients for every mass i define how the frequency varies as a function of the cylinder strokes, X (lift) and Y (jib). A vector, $\boldsymbol{c}_i$, can be defined using MATLAB's left division, "\", operator that utilizes the least mean squares method (MATLAB 1999):

$$\boldsymbol{c}_i = \boldsymbol{p}_i \setminus \mathbf{R}_i \tag{3.17}$$

where $\mathbf{R}_i$ is a 5x9 matrix of the frequencies at mass i.

In the next step, the separate natural frequency surfaces were connected together by fitting the ***c*** coefficient vectors. In this step, the mass load *m* was set as a variable into the second order function

$$\mathrm{M}_f(m) = a(1) + a(2)m^{-1} + a(3)m^2 \ . \tag{3.18}$$

This can be expressed in the following matrix form:

$$\mathbf{M}(m) = \begin{bmatrix} a(1) & a(2)m^{-1} & a(3)m^2 \end{bmatrix}. \tag{3.19}$$

For different masses, *m*, the coefficient matrix, **a**, is defined as

$$\mathbf{a}=\mathbf{M} \setminus \boldsymbol{C}' \tag{3.20}$$

where vector $\boldsymbol{C}$ contains $\boldsymbol{c}_i$ vectors for the different masses.

$$\boldsymbol{C}=[\boldsymbol{c}_1\ \boldsymbol{c}_2\ \boldsymbol{c}_3]. \tag{3.21}$$

Finally, the frequency is a result of matrix multiplication:

$$F(X,Y,m) = \mathbf{p} \cdot \mathbf{M} \tag{3.22}$$

The polynomials used, p_f and M_f, were empirically selected, but nevertheless, the obtained correlation was good. The selected polynomials can define the change of a requested variable with a reasonable error ranging between a minimum of -0.28 Hz and a maximum of 0.36 Hz. The error is so small that there was no need to test any other polynomials or functions for surface fitting. Using a commercial surface fitting software application, it would be possible to search for the optimal functions from among thousands of functions. The crane-specific result matrix, **M**, can be saved and used in an algorithm that calculates the lowest natural frequency by using the cylinder strokes and the mass load as the input data. Figure 3.7 shows a comparison of the simulated frequency surface and the results of surface fitting in one case.

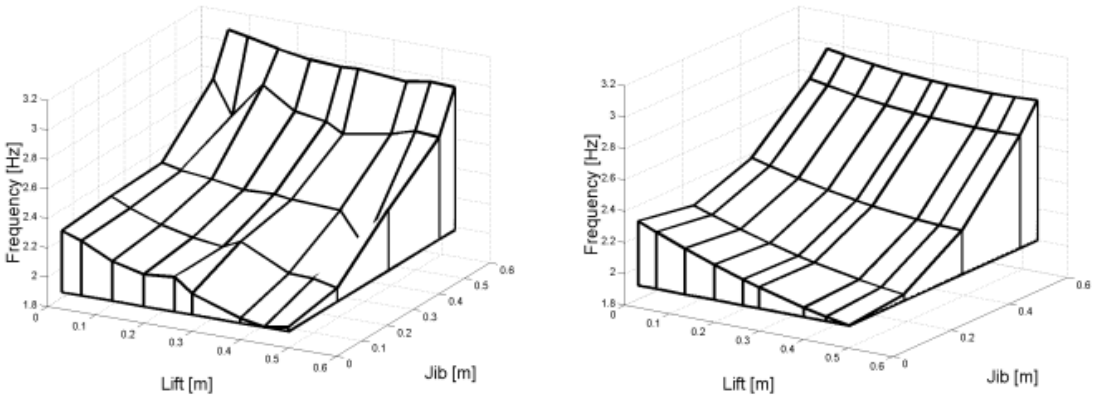

Figure 3.7 A comparison of the frequency surfaces, (a) simulated frequencies and (b) results of surface fitting for a mass load of 200 kg for the PATU 655 crane.

The effect of the extension cylinder on the natural frequencies is noticeable. If the load is far away from the forest machine, the extension is used to reach the load, and in such a situation, the efficient length of the manipulator changes. The effect of the extension length on the lowest natural frequency of the crane has to be studied case by case, but for the TJ71F100 crane, the behaviour was noticed to be almost linear. The lowest natural frequency falls according to Equation 3.23:

$$F = F - 0.15 \cdot s_E \tag{3.23}$$

where s_E is the transition of the extension.

This is true only when the jib angle remains within the range 0…-90º. Long extensions are not used beyond -90º, because otherwise the crane will hit itself. This has to be taken into account when reading the natural frequency matrices in Appendix A. The effect of the extension on the lowest natural frequency is also presented in Appendix A in the form of figures.

3.2.3 An Adaptive Algorithm for Filtering the Control Signal

A second-order filter with the transfer function (3.12) is of an adequate degree for controlling the jerk. The lowest natural frequency can be calculated as presented in previous chapter. To be able to use a changing filter frequency in the second-order filter, a filtering algorithm has to be constructed. For digital controllers, the filter has to be discrete, i.e. transfer function (3.12) is transformed from H(s) to H(z). This transform is also called the z-transform. The digital control algorithm uses the previous values of the input and output with the present value of the input to calculate the output. This can be presented as

$$u_k = a_0 e_k + a_1 e_{k-1} + ... + a_m e_{k-m} - b_1 u_{k-1} - b_2 u_{k-2} - ... - b_n u_{k-n} \tag{3.24}$$

where a_0, $a_1 ... a_m$, b_0, $b_1 ... b_n$ are constants and e_{i-m} , u_{i-n} the previous inputs and outputs. This can be written in transfer function form as follows:

$$H(z) = \frac{U(z)}{E(z)} = \frac{a_0 + a_1 z^{-1} + a_2 z^{-2} + ... a_m z^{-m}}{1 + b_1 z^{-1} + b_2 z^{-2} + b_3 z^{-3} + ... + b_n z^{-n}} \tag{3.25}$$

where z^{-k} is the delay of the time unit k.

We can obtain discrete transfer functions from the continuous time transfer function (3.12) by the substitution of an approximation for the Laplace variable, s. Different approximation terms exist (Proakis 1988), but we found that the following Tustin approximation satisfied our needs.

$$s = \frac{2}{h}\left(\frac{1 - z^{-1}}{1 + z^{-1}} \right) \tag{3.26}$$

Substituting (3.26) into (3.25) yields

$$H(z) = \frac{U(z)}{E(z)} = \frac{\frac{A^*}{B^*} \cdot \left(1 + 2z^{-1} + z^{-2}\right)}{1 + \frac{D^*}{B^*} z^{-1} + \frac{E^*}{B^*} z^{-2}} \tag{3.27}$$

where

$$A^* = \omega^2$$
$$B^* = c_a{}^2 + \omega^2 + 2\varsigma\omega c_a$$
$$D^* = 2\left(\omega^2 - c_a{}^2\right)$$
$$E^* = c_a{}^2 + \omega^2 - 2\varsigma\omega c_a$$
$$c_a = \frac{2}{h}$$

and h is a step size.

Equation (3.27) can be written in the form of Equation (3.24) and used as a digital filter

$$U(z) = \frac{A^*}{B^*} e_i + \frac{2A^*}{B^*} e_{i-1} + \frac{A^*}{B^*} e_{i-2} - \left(\frac{D^*}{B^*} u_{i-1} + \frac{E^*}{B^*} u_{i-2} \right) \tag{3.28}$$

While the lowest natural frequency can be counted one key question is still remaining: What part of the frequency can be used in filter? Is there a risk to excite the lowest mode by using some part of the lowest natural frequency? Among the rotating machines so-called sub harmonics are seen harmful, especially half and third critical frequencies. In the test simulations the filtering frequency of the adaptive filter ω was varied and most effective results were achieved using 30 % of the lowest natural frequency as filtering frequency. Over 50 % tunings raised vibrations easier than traditional ramp function and these were left outside testing. Also aim was to avoid possible sub harmonics of the lowest natural frequency and therefore tunings near 50 % (half critical sub harmonic) were left out. On the other hand the filter tuning must not affect too slow movements of the crane. Tunings under 20 % result harmful slowness of manipulator.

3.2.4 Determination of Payload

The calculation of the mass of the load from the pressure of the lift cylinder is based on force balance. Every link of the manipulator that moves around the joint between the pillar and the lift boom has a centre of mass (CM) and moment arm in reference to joint J_{p1}. The positions of the CM move with the crane when the lift, jib and extension cylinder extends or retracts. At the same time, the pressure

in the chambers of the lift cylinder changes to produce a force and moment that raises the crane. The principle of static force balance is shown in Figure 3.8

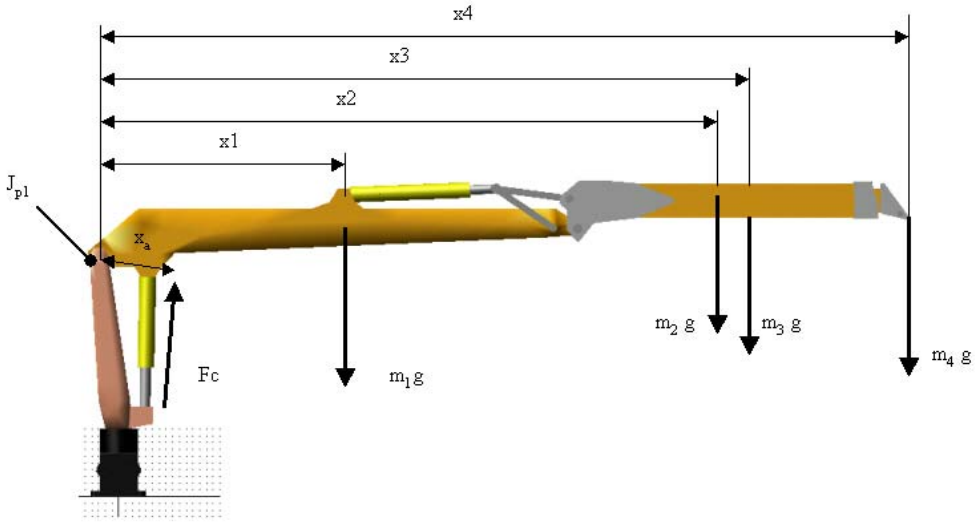

Figure 3.8 The static force balance of the crane and the labels of the masses and moment arms.

In the case of the crane, the static force balance can be written as

$$\sum M_{J1} = F_c \cdot x_a - m_1 \cdot g \cdot x_1 - m_2 \cdot g \cdot x_2 - m_3 \cdot g \cdot x_3 - m_4 \cdot g \cdot x_4 = 0 \tag{3.29}$$

where x_1, x_2, x_3 and x_4 are x-coordinates of the centers of mass m_1, m_2, m_3, m_4 and x_a is moment arm of the lift cylinder. The load mass m_4 can be solved from equation (3.29):

$$m_4 = \frac{F_c \cdot x_a}{g \cdot x_4} - \frac{x_1}{x_4} \cdot m_1 - \frac{x_2}{x_4} \cdot m_2 - \frac{x_3}{x_4} \cdot m_3 . \tag{3.30}$$

The kinematic model of the crane is required in order to obtain the x-coordinates. Dimensions of the crane are known and the cylinder strokes can be measured, and thus, the kinematic model can be constructed. However, static force balance does not work well when the crane is in motion, and therefore, the dynamics of the crane have to be taken into account.

3.2.4.1 Kinematics of the crane

Each member of the manipulator can be described in space by using three Cartesian and three rotational coordinates. If the global origin is located at the base of the manipulator and the manipulator's geometry is known, the joints can be defined with the use of position vectors and rotation matrixes.

Any single point in a rigid body in a global space can be defined using a 3x1 position vector, $\boldsymbol{R}^i$. If vector $\boldsymbol{R}^i$ defines the local coordinate system of the body

and we know the location vector, $\bar{\boldsymbol{u}}^i$, of point *i* in relation to the local coordinate system, we can calculate the location of point *i* in the global coordinate system by summing the position vectors. This gives the correct solution only if the global and local coordinate systems have the same orientation, which is not always the case. The orientation of the body relative to some other coordinate system can be defined with a 3x3 rotation matrix, $\mathbf{A}^i$. This yields

$$\boldsymbol{r}^i = \boldsymbol{R}^i + \mathbf{A}^i \, \bar{\boldsymbol{u}}^i \tag{3.31}$$

where

$$\boldsymbol{R}^i = \begin{bmatrix} X & Y & Z \end{bmatrix}'$$

$$\mathbf{A}^i = \begin{bmatrix} \cos(\theta_i) & \sin(\theta_i) & 0 \\ -\sin(\theta_i) & \cos(\theta_i) & 0 \\ 0 & 0 & 1 \end{bmatrix} \tag{3.32}$$

$$\bar{\boldsymbol{u}}^i = \begin{bmatrix} \bar{u}^i_2 & \bar{u}^i_2 & \bar{u}^i_3 \end{bmatrix}$$

Equation (3.31) describes a general transformation of the position vector in one coordinate system to another. Translation and rotation can be presented together in a 4x4 transformation matrix $\mathbf{T}_{ij}$ (Craig 1986):

$$\mathbf{T}_{ij} = \begin{bmatrix} \mathbf{A}^i & \boldsymbol{R}^i \\ 0 & 1 \end{bmatrix} \tag{3.33}$$

where the running subscripts *i* and *j* define from what point to what point the transformation is performed. Using this transformation matrix, the mapping is

$$\boldsymbol{r}^i_4 = \mathbf{T}_{ij} \, \bar{\boldsymbol{u}}^i_4 \tag{3.34}$$

where the trailing subscript 4 defines the size of the vector.

$$\bar{\boldsymbol{u}}^i_4 = \begin{bmatrix} \bar{u}^i_1 & \bar{u}^i_2 & \bar{u}^i_3 & 1 \end{bmatrix}$$

$$\boldsymbol{r}^i_4 = \begin{bmatrix} r^i_1 & r^i_2 & r^i_3 & 1 \end{bmatrix}$$

Figure 3.9 shows the numbering of the joints and CMs of the studied booms. Table 3.2 gives the lengths of the vectors in the x- and y-directions, and the zero stroke length of the cylinders can be found in Table 3.3.

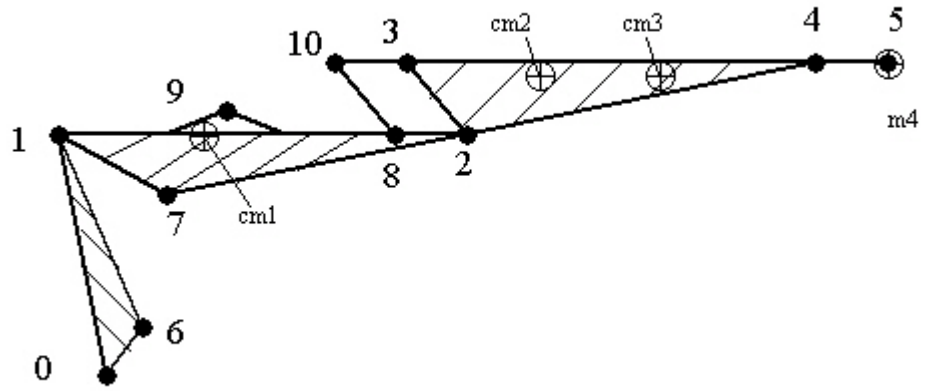

Figure 3.9 The numbering of the joints.

Table 3.2 The Lengths of the vectors

Vector	Length [m]	Vector	Length [m]
$0\text{-}1_x$	0.148	$0\text{-}6_x$	0.192
$0\text{-}1_y$	1.785	$0\text{-}6_y$	0.6
$1\text{-}2_x$	3.55	$1\text{-}7_x$	0.365
$1\text{-}2_y$	0.2	$1\text{-}7_y$	-0.085
$2\text{-}3_x$	-0.06	$9\text{-}8_x$	1.558
$2\text{-}3_y$	0.222	$9\text{-}8_y$	-0.245
$3\text{-}4_x$	2.3	$8\text{-}2_x$	0.180
$3\text{-}4_y$	-0.012	$8\text{-}2_y$	-0.005
$4\text{-}5_x$	0.17	8-10	0.515
$4\text{-}5_y$	0.0	10-3	0.550
$1\text{-}6_x$	0.34	3-2	0.23
$1\text{-}6_y$	1.185		

Table 3.3 The minimum length of the cylinder

Cylinder	Minimum length at zero stroke
Lift (6-7)	0.918
Jib (9-10)	1.134
Extension (4-5)*	0.17

*) The extra transition that comes from the dimensions of the part, the cylinder is situated inside the jib boom.

The transformation matrixes for crane under interest are presented in Appendix B. The lift and jib angles can be calculated from the cylinder stroke measurements and crane geometry. The jib cylinder transfers force to the jib boom through a four-bar mechanism. Solving the four-bar mechanism gives the jib angle that is used in the calculation of the rotation terms in the transformation matrix. The calculations for the four-bar mechanism are given in Appendix C.

The position of the different joints and point masses are calculated by multiplying the transformation matrices. The position of joint J_{p1} between the pillar and the lift boom is fixed relative to the global coordinate system and can be obtained from the transformation matrix, $\mathbf{T}_{01}$:

$$(x, y, z) = (\mathbf{T}_{01}(1,4), \mathbf{T}_{01}(2,4), \mathbf{T}_{01}(3,4)). \tag{3.35}$$

The locations of the other joints can be calculated through compound transformations:

$$\mathbf{J}_{p2} = \mathbf{T}_{01} \cdot \mathbf{T}_{12} \tag{3.36}$$

$$\mathbf{J}_{p3} = \mathbf{T}_{01} \cdot \mathbf{T}_{12} \cdot \mathbf{T}_{23} \tag{3.37}$$

$$\mathbf{J}_{p4} = \mathbf{T}_{01} \cdot \mathbf{T}_{12} \cdot \mathbf{T}_{23} \cdot \mathbf{T}_{34} \tag{3.38}$$

In each $\mathbf{J}_{pi}$ matrix, the fourth column gives the global coordinates of the point. The location of the center of mass is calculated in a similar way:

$$\mathbf{J}_{cm1} = \mathbf{T}_{01} \cdot \mathbf{T}_{m1} \tag{3.39}$$

$$\mathbf{J}_{cm2} = \mathbf{T}_{01} \cdot \mathbf{T}_{12} \cdot \mathbf{T}_{23} \cdot \mathbf{T}_{m2} \tag{3.40}$$

$$\mathbf{J}_{cm3} = \mathbf{T}_{01} \cdot \mathbf{T}_{12} \cdot \mathbf{T}_{23} \cdot \mathbf{T}_{34} \cdot \mathbf{T}_{m3} \tag{3.41}$$

To calculate the coordinates of the load mass, matrix $\mathbf{J}_{p4}$ has to be defined:

$$\mathbf{J}_{p5} = \mathbf{T}_{01} \cdot \mathbf{T}_{12} \cdot \mathbf{T}_{23} \cdot \mathbf{T}_{34} \cdot \mathbf{T}_{45} \tag{3.42}$$

In addition to the moment arms (the x-coordinates) of the different masses, the kinematic model gives position of lift cylinder's rod joint in the global reference coordinate system.

$$\mathbf{J}_{p7} = \mathbf{T}_{01} \cdot \mathbf{T}_{17} \tag{3.43}$$

By using this location, the moment arm of the lift cylinder can be solved. The geometry of the crane causes the force transmission angle between the lift cylinder and lift boom to remain near the optimal value of 90 degrees. However, the effect of this angle, β, are taken into account by multiplying the cylinder force by $\sin(\beta)$. The force transmission angle, β, is shown in Figure 3.10 .

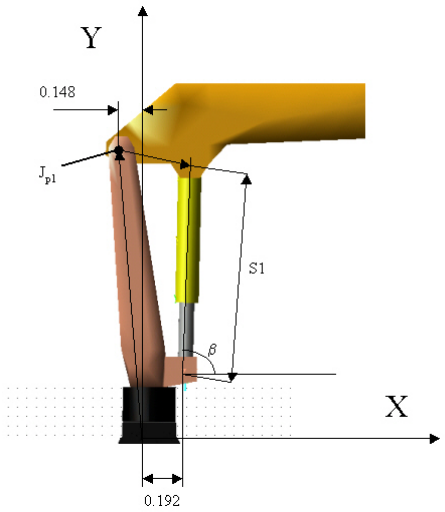

Figure 3.10 The moment arm of the lift cylinder

3.2.4.2 Weights of the Components and Inertia Tensors

The weights of the different components were estimated. Manufacturing drawings did not provide this information for every component, but because all the main components were modeled in the ADAMS software, their masses could be calculated in ADAMS that can also provide the coordinates of the CM in the local reference coordinate system. The distances to the nearest joint can be calculated from this data. Table 3.4 gives the weights of the main components of the crane.

Table 3.4 Component weights and centres of mass relative to the nearest joint on the left

Component	Mass [kg]	Distance to nearest joint (x,y) [m] in initial position, CM
Lift boom m_1	352 (*)	Cm1=(1.813, - 0.241)
Jib boom m_2	226 (**)	Cm2=(0.805, -0.023)
Extension m_3	80 (***)	Cm3=(1.436, -0.012)
Gripper +rotator +m_4	225 (Gripper +rotator)	(2.45, -0.112)

(*) Including the jib cylinder and four-bar mechanism (total +80 kg)

(**) Including the plates in the jib boom, the extension cylinder tube and the hoses (+100 kg)

(***) Including the estimation of the weights of some plates, the extension cylinder rod and the hoses (+20 kg)

The accurate inertia tensors of the different members can be obtained from the ANSYS or ADAMS software or can be calculated by making simplifications to

the link geometries. Following the inertia tensors ($\mathbf{I}_i$) and the main axes ($\mathbf{v}_i$), the matrices for the sub assemblies of the lift boom, jib boom and extension, were calculated from the ADAMS model. Weights of the sub assemblies are presented in Table 3.4.

$$\mathbf{I}_1 = \begin{bmatrix} 10.37 & 0 & 0 \\ 0 & 442.65 & 0 \\ 0 & 0 & 447.50 \end{bmatrix} \qquad \mathbf{v}_1 = \begin{bmatrix} 0.0000 & 0.0000 & 1.0000 \\ -0.9967 & -0.0810 & 0.0000 \\ -0.0810 & 0.9967 & 0.0000 \end{bmatrix}$$

$$\mathbf{I}_2 = \begin{bmatrix} 3.46 & 0 & 0 \\ 0 & 95.51 & 0 \\ 0 & 0 & 93.97 \end{bmatrix} \qquad \mathbf{v}_2 = \begin{bmatrix} 0.0043 & -0.0448 & -0.9990 \\ 0.9998 & -0.0193 & 0.0052 \\ 0.0195 & 0.9988 & -0.0448 \end{bmatrix}$$

$$\mathbf{I}_3 = \begin{bmatrix} 0.4 & 0 & 0 \\ 0 & 25.64 & 0 \\ 0 & 0 & 25.73 \end{bmatrix} \qquad \mathbf{v}_3 = \begin{bmatrix} 0.0001 & -0.0021 & -1.0000 \\ 0.9999 & 0.0142 & 0.0001 \\ -0.0142 & 0.9999 & -0.0021 \end{bmatrix}$$

Assuming that the kinematics and mass distribution are known, the joint torques can be calculated. The positions, velocities and accelerations of the joints can be obtained from the kinematic model of the crane using the cylinder stroke measurement. For the calculation of the inertial forces acting on the each member of the crane, the rotational velocities, rotational and linear accelerations are required for each member. Because the members, or links, are connected to a chain, the calculation is done in an iterative nature. The calculation starts from the base member, proceeds to the end tip and returns to the base. By using this technique, the joint torques are given in “return” phase.

3.2.4.3 Velocities and Acceleration of the Link

Outward iteration means that the inertial forces acting on the links are calculated in an iterative manner: first, the rotational velocity and rotational acceleration of a link one are calculated and then the calculations proceed to the next link until the last link is reached. In outward and inward iteration, the numbering of the joints and links is changed to maintain the logical number sequence in the following equations. Figure 3.11 shows a new numbering and iteration route.

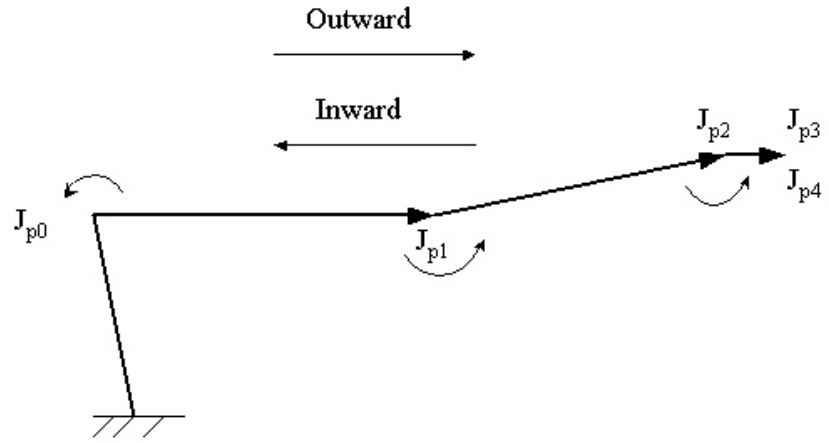

Figure 3.11 The outward and inward iteration for computing the forces and torques acting on the crane

In the outward iteration, index *i* starts from 0 and runs to *n*-1, where *n* is the number of links. The rotational velocity of link *i* can be given as

$$\boldsymbol{\omega}_{i+1,i+1} = \mathbf{A}_{i+1,i}\boldsymbol{\omega}_{i,i} + \dot{\theta}_{i+1}\hat{\boldsymbol{Z}}_{i+1,i+1} \tag{3.44}$$

The transformation of angular acceleration from one link to the next is obtained from the following equation:

$$\dot{\boldsymbol{\omega}}_{i+1,i+1} = \mathbf{A}_{i+1,i}\dot{\boldsymbol{\omega}}_{i,i} + \mathbf{A}_{i+1,i}\boldsymbol{\omega}_{i,i} \times \dot{\theta}_{i+1}\hat{\boldsymbol{Z}}_{i+1} + \ddot{\theta}_{i+1}\hat{\boldsymbol{Z}}_{i+1,i+1} \tag{3.45}$$

If the local origin of each link is situated in the joint point, the linear acceleration of frame origin of the link can be calculated as follows:

$$\dot{\boldsymbol{v}}_{i+1,i+1} = \mathbf{A}_{i+1,i}\,(\dot{\boldsymbol{\omega}}_{i,i} \times \boldsymbol{P}_{i,i+1} + \boldsymbol{\omega}_{i,i} \times (\boldsymbol{\omega}_{i,i} \times \boldsymbol{P}_{i,i+1}) + \dot{\boldsymbol{v}}_{i,i}) \tag{3.46}$$

Also, the linear acceleration of the CM of each body is required and can be obtained from

$$\dot{\boldsymbol{v}}_{i+1,i+1,cm} = \dot{\boldsymbol{\omega}}_{i+1,i+1} \times \boldsymbol{P}_{i+1,i+1,cm} + \boldsymbol{\omega}_{i+1,i+1} \times (\boldsymbol{\omega}_{i+1,i+1} \times \boldsymbol{P}_{i+1,i+1,cm}) + \dot{\boldsymbol{v}}_{i+1,i+1}) \tag{3.47}$$

After obtaining the rotational velocity and rotational acceleration of a link, the force and torque that cause movement can be calculated from Newton's law:

$$\boldsymbol{F}_{i+1,i+1} = m_{i+1}\dot{\boldsymbol{v}}_{i+1,i+1,cm} \tag{3.48}$$

$$\boldsymbol{N}_{i+1,i+1} = \mathbf{I}_{i+1}\dot{\boldsymbol{\omega}}_{i+1,i+1} + \boldsymbol{\omega}_{i+1,i+1} \times \mathbf{I}_{i+1}\boldsymbol{\omega}_{i+1,i+1} \tag{3.49}$$

The inertia tensor, $\mathbf{I}_{i+1}$, is written in a frame that is situated in the CM.

The inward iteration from link 3 to link 1 gives the forces that affect on each link and the torque in the joints. First, the forces are calculated based on the outward iteration:

$$\boldsymbol{f}_{i,i} = \mathbf{A}_{i,i+1}\boldsymbol{f}_{i+1,i+1} + \boldsymbol{F}_{i,i} \tag{3.50}$$

$$\text{where } \mathbf{A}_{i,i+1} = \begin{bmatrix} \cos(\theta_i) & -\sin(\theta_i) & 0 \\ \sin(\theta_i) & \cos(\theta_i) & 0 \\ 0 & 0 & 1 \end{bmatrix}$$

The torque acting on link i can be obtained from

$$\boldsymbol{n}_{i,i} = \boldsymbol{N}_{i,i} + \mathbf{A}_{i,i+1}\boldsymbol{n}_{i+1,i+1} + \boldsymbol{P}_{i,i,cm} \times \boldsymbol{F}_{i,i} + \boldsymbol{P}_{i,i+1} \times \mathbf{A}_{i,i+1}\boldsymbol{f}_{i+1,i+1}. \tag{3.51}$$

The torque that is needed in a joint is given as

$$\boldsymbol{\tau}_i = \boldsymbol{n}_{i,i}^{\,T}\widehat{\mathbf{Z}}_{i,i} \ . \tag{3.52}$$

All the required equations are collected to calculate the torque in the joints. (Craig 1986, Chapter 6).

The outward and the inward iterations are presented in Appendix D. The final results of the iterations give the torque in the first joint of the manipulator. The lift cylinder produces the required torque in the joint 1. The lift cylinder force can be calculated using the measured pressures. The moment arm and force transmission angle are calculated using the global coordinates from $\mathbf{J}_{p7}$. The negative x-axis value of joint J_{p0} has to be taken into account by adding an x-value (0.148) to the value of the x-coordinate of $\mathbf{J}_{p7}$. The product of the moment arm and the cylinder force is a torque vector $\boldsymbol{\tau}_1$.

$$\boldsymbol{\tau}_1 = \begin{bmatrix} 0 & 0 & F_c \sin(\beta)\left(\mathbf{J}_{p7}(1,4) + 0.148\right) \end{bmatrix} \tag{3.53}$$

By setting the values of the torque equations (3.52) and (3.53) to be equal and making certain simplifications, the mass load can be solved; the mass load takes the following form:

$$\boldsymbol{f}_{4,4} = \mathbf{G}_1 \cdot \left(\boldsymbol{N}_{\text{tot}} + \mathbf{G}_2 + \mathbf{G}_3 - \boldsymbol{\tau}_1\right) \tag{3.54}$$

$$\text{where } \boldsymbol{N}_{tot} = \boldsymbol{N}_{1,1} + \mathbf{A}_{1,2}\boldsymbol{N}_{2,2} + \mathbf{A}_{1,2}\mathbf{A}_{2,3}\boldsymbol{N}_{3,3}$$

$$\mathbf{G}_1 = -\left(9.81 \cdot \left(\mathbf{J}_{p4}(1,4) - \mathbf{J}_{p1}(1,4)\right)\right)^{-1}$$

$$\mathbf{G}_2 = \mathbf{A}_{1,2}\mathbf{A}_{2,3}\boldsymbol{P}_{3,3,cm} \times \boldsymbol{F}_{3,3} + \mathbf{A}_{1,2}\boldsymbol{P}_{2,2,cm} \times \boldsymbol{F}_{2,2} + \boldsymbol{P}_{1,1,cm} \times \boldsymbol{F}_{1,1}$$

$$\mathbf{G}_3 = \mathbf{A}_{1,2}\left(\boldsymbol{P}_{2,3} \times \mathbf{A}_{2,3}\boldsymbol{F}_{3,3}\right) + \boldsymbol{P}_{1,2} \times \mathbf{A}_{1,2}\left(\boldsymbol{F}_{3,3} + \boldsymbol{F}_{2,2}\right)$$

3.2.4.4 Cylinder Force

The cylinder force F_c is essential for the calculation of the load. The theoretic lift cylinder force can be expressed as

$$F_c = \left(A_1 \cdot p_1 - A_2 \cdot p_2\right) \cdot \eta - F_\mu \tag{3.55}$$

The friction force, F_μ, normally consists of coulomb and viscous friction. Coulomb friction has a large effect on the cylinder forces at small velocities, but a small effect on the calculation of the load. The modeling of coulomb friction would require the use of highly nonlinear functions, so only a linear viscous friction model was used:

$$F_\mu = \left(A_1 \cdot p_1 - A_2 \cdot p_2\right) \cdot \left(1 - \eta\right) \cdot \frac{v}{v_{\max}} \tag{3.56}$$

where v the velocity of the cylinder and $v_{\max}$ the maximum velocity of the cylinder. The efficiency of the cylinder, η, is needed here because the friction force comprises of a part of the losses of the cylinder. In crane applications, the velocity of the lift cylinder, v, rarely reaches a value of one, and so the friction force cannot exceed the total losses.

Using equations (3.55) and (3.56), the cylinder force can be written as

$$F_c = \left(A_1 \cdot p_1 - A_2 \cdot p_2\right) \cdot \left(1 - \frac{v}{v_{\max}} \cdot \left(\frac{1}{\eta} - 1\right)\right)\eta \tag{3.57}$$

The cylinder force changes a lot when the mass load changes or the crane oscillates, and it is the biggest single factor in the calculation of the mass load in Equation (3.54). The problem is to recognize when the crane is oscillating and when the load is changing. In the former case, the calculation algorithm produces the largest errors in the same phase as that in which the force vibrates, and it is necessary to use the previous load value in the adaptive filter. The fast recognition of the release and picking up of the load helps the adaptive filter in providing the best control signal. Chapter 4.2 presents a proposal for resolving the problem of force vibrations.

3.3 Semi-Active Damping

Contrary to the addition of extra dampers to a machine, the control of the main actuators is an attractive option for engineers. Hydraulic accumulators have been tested in crane applications, but often their inferior reliability, price competitiveness and performance have been obstacles to their widespread use.

The general overview of vibration suppression methods in chapter 2 mentioned an application (Pat. JP5321297), in which an extra directional valve had been added to a hydraulic circuit, was mentioned. This valve feeds oil to the lift cylinder, the main actuator of the boom of the excavator and suppresses vibrations. The control signal of the valve is calculated from the pressures and velocity of the lift cylinder. The disadvantage of this solution is that an additional hydraulic circuit is needed for the directional valve.

Although application (Pat. JP5321297) uses additional components, it employs a simple and effective algorithm for the calculation of the damping signal. This algorithm is based on so-called pressure feedback; the pressure in the cylinder chambers is measured and used in a feedback loop in order to suppress vibrations. At the same time, the vibration of the cylinder force is reduced, which leads to better dynamic behavior. The lift cylinder force of the excavator, F_c, was calculated from the pressures:

$$F_c = A_1 \cdot p_1 - A_2 \cdot p_2 \tag{3.58}$$

where A_1, A_2 are areas of the piston and p_1, p_2 the pressures in the different chambers of the cylinder.

The velocity of the lift cylinder, v, was calculated from the measured stroke values, X_n and X_{n-1}:

$$v = \frac{\left(X_n - X_{n-1}\right)}{\Delta t} \tag{3.59}$$

The obtained values were passed through a high-pass filter to cut off the static part below a certain frequency. The high-passed velocity, v_h, and force, F_h, were multiplied by the gains, K_v and K_f, that were dependent on the static force of the cylinder, F_l. The flow rate command value, Δq_o, was generated for the extra damping valve that supplies or exhausts a rate of the extra flow that corresponds to this value.

$$\Delta q_o = -K_v\left(F_l\right)\cdot v_h - K_f\left(F_l\right)\cdot F_h \tag{3.60}$$

References (Pat. JP5321297, Pat. US 5459383) offer the basis for the development of an electronic semi-active damper. When pressure transducers are used, the cylinder force can be calculated from Equation (3.57). Later on in this thesis, the cylinder force and velocity (derived from the measured stroke) can be filtered with a second-order high-pass filter to obtain the oscillation.

The high-passed velocity, v_h, and force, F_h, are summed and multiplied by minus one to obtain the analogous presentation for equation (3.60). As reference (Pat. JP5321297) did not give exact values for gains K_v and K_f, they are set to one. Originally, equation (3.60) gives the flow rate of the damping flow, but because the aim was to eliminate the extra valve, it has to be transformed into a suitable form for the existing electronically controlled valve.

The flow rate and velocity input to the electronically controlled proportional valve analogously influence this kind of hydraulic system. Using this analogy, we can calculate what kind of velocity input we should provide to the valve in order to obtain the same behavior that the extra valve gives. The gains of equation (3.60) were empirically tuned and the same method was used in this work during the tuning of the semi-active controller.

The gains were defined in the following test drives: a heavily loaded crane was driven up and down vigorously in order to obtain the maximum value of the high-passed force. In reference (Pat. JP5321297), the gains were dependent on the static force of the cylinder. In order to obtain a simple tuning process, only one gain that comes from the maximum value of the cylinder force is used. This maximum value, F_{hpmax}, is used as the denominator of the equation of the new damp signal, U_{damp}:

$$U_{damp} = \frac{-(v_h + F_h)}{F_{hpmax}} \tag{3.61}$$

In this form, without the gain K_v, the high-passed velocity, v_h, has very little influence on damping. Still, the simulations and test-drives show that the calculated damp signal works in the form presented here. Much more interest had to be focused on the tuning and selection of the maximum vibration value, F_{hpmax}. The denominator value, F_{hpmax}, has to be large enough for the damping signal not to grow too large in comparison with the original range of the input signals and also in order for the control valve to be able to execute it. In the test drives, different values of F_{hpmax} were tested, but most tests were driven using the preset value, 2.2e5. One option is to multiply the damping signal, U_{damp}, by some gain to increase the damping effect. In Chapter 4, where the test drives are discussed, the gain is switched between one and two. Figure 3.12 and Figure 3.13 present the function of the semi-active damper.

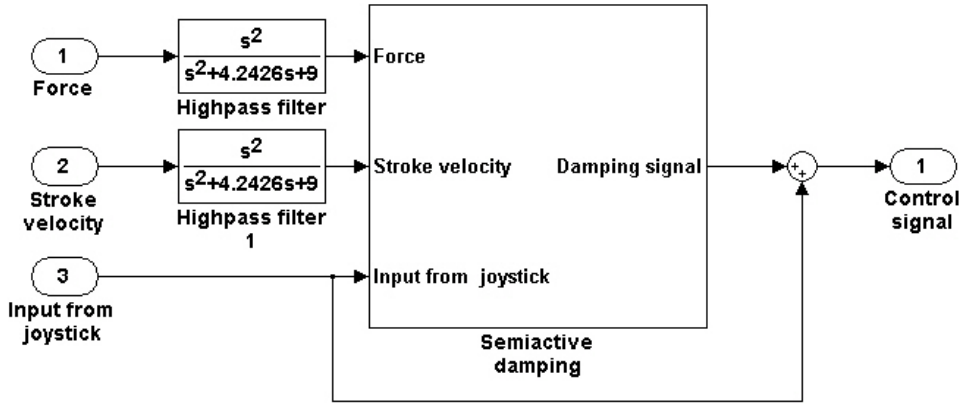

Figure 3.12 The inputs and outputs of semi-active damping.

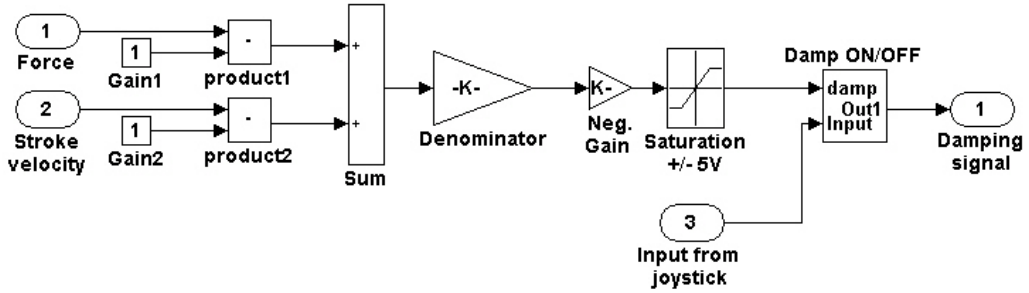

Figure 3.13 Semi-active damping. The high-passed cylinder force and velocity are summed up and divided by the maximum force magnitude. The saturation- and "Damp ON/OFF"–blocks restrict damping to certain range and situations.

For better usability and safety, the damping signal can be limited to a certain range with the use of a saturation function, or it can be added to the original input signal only under certain situations. At the beginning of the tests, the damping signal was limited to 50 % of valve's maximum input scale so that the signal always remained within the range of ±5 volts. Also, the damping signal was used only when the operator decelerated the boom and when the joystick signal went below a preset value. The preset values of ±2 volts were observed to guarantee a natural driving touch. When the operator's joystick signal fell within the range of– 2…2 volts, the crane was able to move slowly with precision, decelerating or harmful vibration was raised and the operator tried to suppress them. When the damper was in use, the operator could leave it to handle the damping and just keep the joystick near the middle position, which corresponds to the preset value area (Kovanen & Handroos, 2002).

The effect of semi-active damping on the control signal is shown in Figure 3.14. The original control signal is on the left side, the calculated damping signal in the middle and the sum of these on the right side of the Figure 3.14.

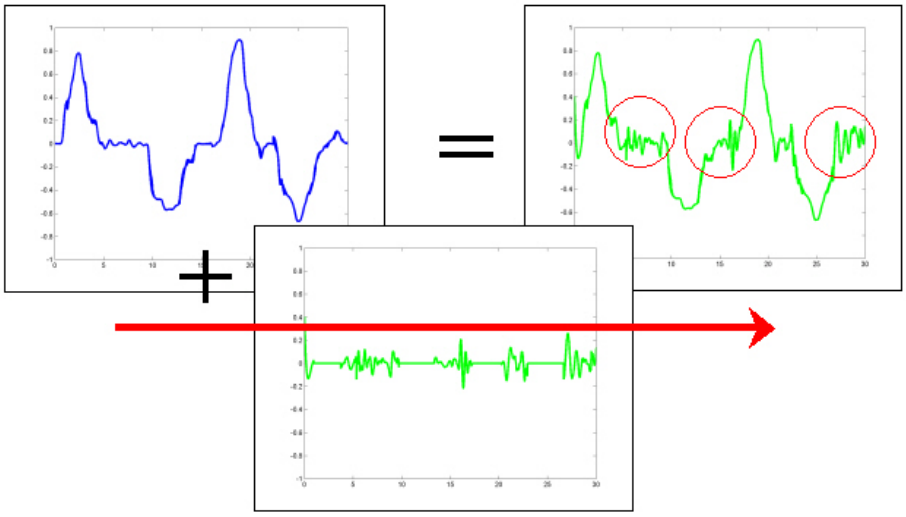

Figure 3.14 The control signal after the damping part is added.

4 The Simulations and Test Drives

4.1 General Information on the Testing of the Controllers

To evaluate the proposed controllers and compare them with a traditional ramp function, some test-drives were performed. The basic test work cycle was a step response test that was carried out both upwards and downwards. Using both main operation directions provided a wider view of the vibration suppression capabilities of the proposed methods. Most test drives were carried out using real cranes, although simulation models were available. This was done because the simulation times were long and the testing of the different controller tunings was, hence, made faster. On the other hand, using different commercial cranes within a limited time frame forced the test program to be executed quickly and the result could only be analyzed after the tests.

4.1.1 Arrangements

Several test drives were carried out under laboratory conditions in order to verify the simulation models, test the adaptive filter and tune the semi-active damping. The very first simple step tests were driven to verify the analogy of the simulation model with the real boom. The pressures in the cylinder chambers and the cylinder strokes were measured and compared with the simulation results. The pressure transducer used gave an analog output of 0…10 V that was suitable for the control hardware. The lift, jib, extension and slew cylinder strokes were measured using linear cable analog transducers. In some field tests, strain gauges were used to measure the stresses in the most critical points of the crane. The positioning and naming of the transducers and strain gauges is shown in Figure 4.1.

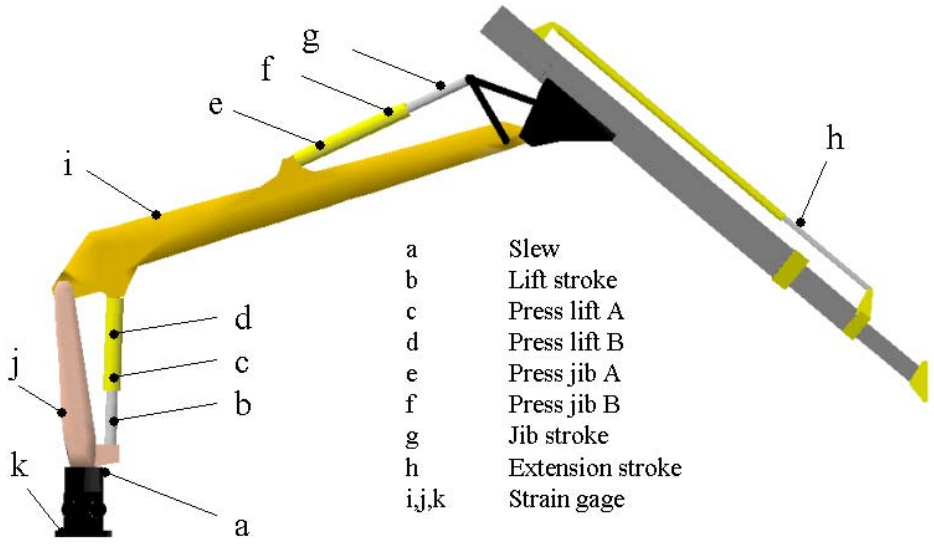

Figure 4.1 The positioning of the transducers and strain gauges in TJ71F100

The first tests were performed using a middleweight log crane, a PATU 655. In year 2000, Timberjack delivered a TJ71F72 log forwarder crane to LUT and

arranged the possibility for an experienced test operator to operate it. The test operator tuned the velocities and traditional ramp control of the crane in order for the controllers to be adequately compared. Very soon, the crane in question was observed to be too stiff for the laboratory tests. This meant that the lowest natural frequencies were not excited with small loads, and with big loads, the crane almost decoupled from the floor. Furthermore, the roof of the laboratory restricted the safe working area below what it would normally have been. For these reasons and due to the promising test results that were obtained using the PATU 655, a field test was organized in the winter of 2001 in Tampere. John Deere Timberjack provided a log forwarder with a more flexible and longer crane, a TJ71F100, for the tests. For the adaptive filter, the natural frequencies of this crane were calculated from the simulation model.

4.1.2 Control Hardware

In a traditional test process, the controller prototype is usually inserted into the system to be controlled and carefully tested during field tests. This process involves many problems, because the system being controlled can be expensive and complex, as is the case with aircrafts, locomotives or plants. The long time needed for development increases the costs, and safety requirements inhibit tests with applications during the use of a real machine. The solution is to perform system tests in a virtual environment.

Real-time simulations of controllers require suitable real-time interfaces. Nowadays, there are many software manufacturers on the markets; Real-Time Linux, dSPACE (dSPACE GmbH) and Opal-RT (Opal-RT Technologies Inc), to mention a few software applications. IMVE had used the commercial real-time simulation software application, dSPACE, with hardware solutions provided by the same manufacturer. A strong feature of dSPACE is its compilation of real-time c file code MATLAB/Simulink models, which enables the fast simulation of different controllers without time-consuming code writing. The real-time code is transferred from the master computer to a separate processor card of dSPACE. The processor card handles the calculation and communicates with the I/O cards, which are connected via a bush cable to a connector panel to which all the transducer signal cables are connected. Physically, dSPACE cards can be placed inside the master computer or in an extension box. In the field tests, the processor and I/O card were placed in an Autobox extension box (dSPACE 2001) and a notebook was used as the master computer. In addition to the cards and the notebook, some power supplies and connection panels were needed. All these electronic devices were placed inside the cabin of the log forwarder and the power was taken from the machine accumulator.

4.2 Adaptive Filter

The basic work cycle in both the laboratory and the field was step response. In the beginning, the adaptive filter was tested using a PATU 655 crane in the simulator and on the real crane. Ramp times of 0.4 s (normal) and 0.8 s (disadvantageously

slow) were chosen for the purpose of comparison. At this point, it has to be mentioned that the ramp times in real joysticks are smaller because of the slowness of human control; i.e. users cannot and do not want to move a joystick from zero to the maximum position at infinite acceleration when the normal settings of the control system of the log crane are applied. On the other hand, a ramp time of 0.8 s is too slow for normal operation but it was used here to have a reference for the smooth movement of the crane.

The velocity and acceleration of the end tip of the crane were monitored, and the RMS value was calculated from these measurements. The RMS value defines the efficient value of vibration and is widely used, especially for rotating machines (Nohynek 1996, Doebelin 1990).

In the test simulations (Chapter 3.2.3), it was observed that the use of 70 % tuning as the filter frequency resulted in vibrations that were almost as large vibrations as those for the 0.4-s ramp time, and for this reason, this tuning was excluded from the tests. The input signals for the different valves before and after filtering (30% tuning) can be seen in Figure 4.2.

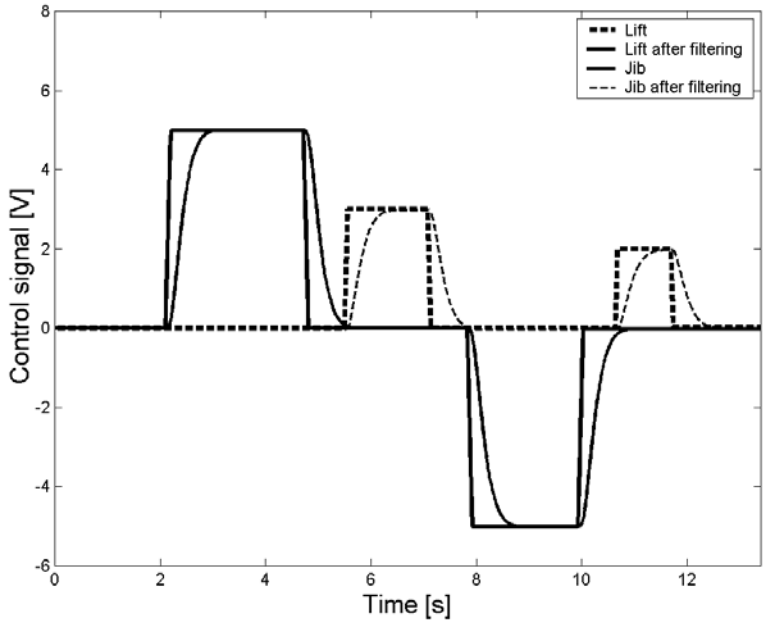

Figure 4.2 A comparison of the input signal before and after the adaptive filter.

We can take a closer look at the input for the lift cylinders and compare the jerk of the different control signals, as shown in Figure 3.5. The difference between the different control signals in Figure 4.3 is noticeable; the ramp functions result in a transient peak every time the velocity input changes, while the filtered control signal results in the smooth alteration of the jerk.

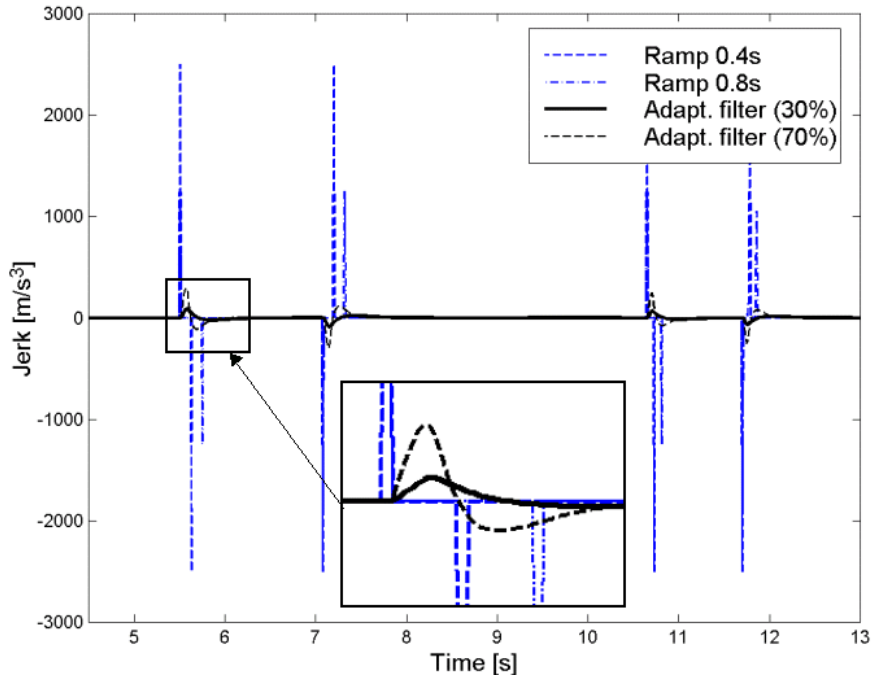

Figure 4.3 The jerk profiles of the different velocity instructions of the lift cylinder.

The effect of the larger jerk can also be seen from the pressure and acceleration curves in Figure 4.4 and 4.5 as well as from the Y-position curves of the boom end tips in Figure 4.6. Figures 4.4 and 4.5 show that the oscillation at the end tip of the crane is proportional to the pressure vibration in the chambers of the lift cylinders. The transient peaks in the jerk raise vibration at the end tip of the crane.

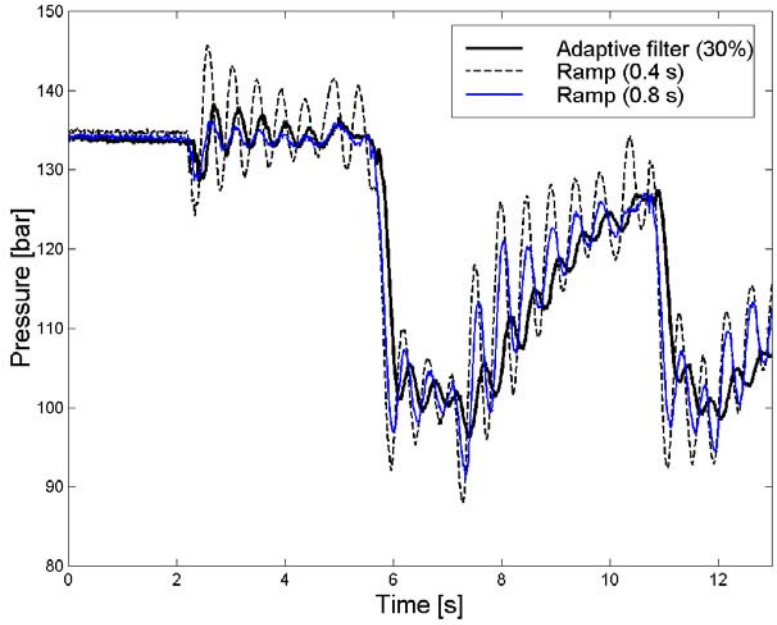

Figure 4.4 The pressure in the A chamber of the lift cylinder for different controllers.

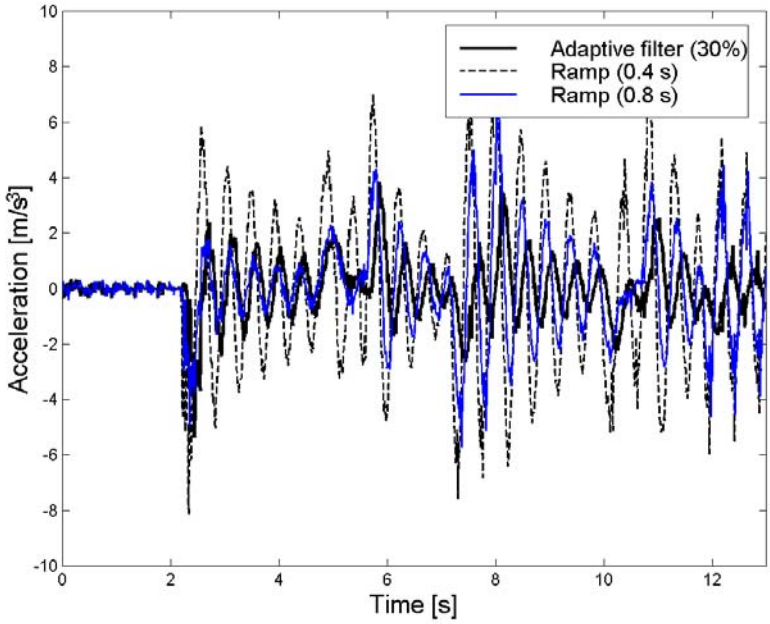

Figure 4.5 The acceleration at the end tip of the boom

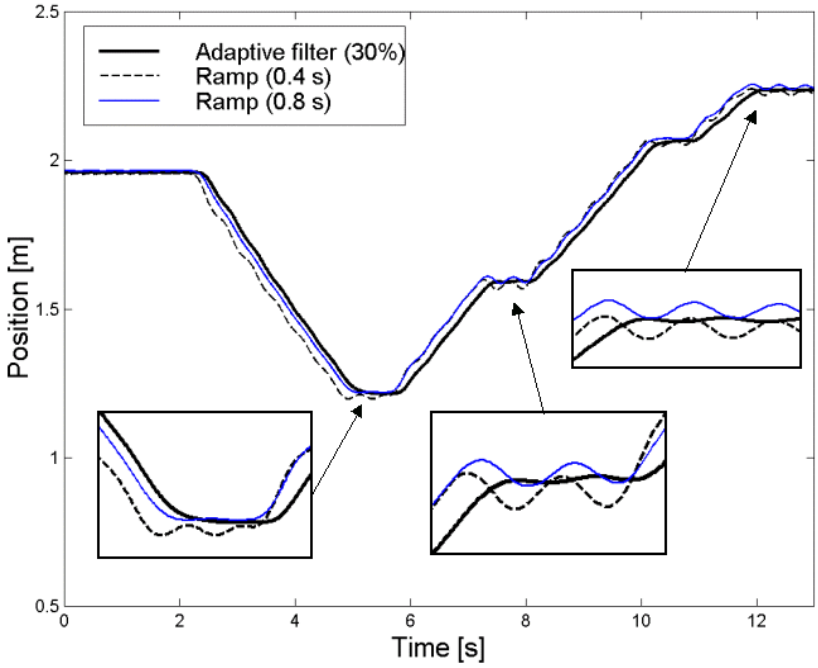

Figure 4.6 The vertical (Y) position of the end tip of the crane

Figure 4.6 shows that the adaptive filter enables smoother decelerations without small vibrations at the end tip. Figure 4.4 and Figure 4.6 reveal that changing the ramp time from normal to slow does not fully eliminate pressure vibration and its effect, the oscillation of the end tip; the explanation for this lies in the discontinuous velocity input and transient peak of the jerk (Figure 4.3). Better deceleration enables better position accuracy for the end tip and improves the working efficiency, because the operator of the log crane can now initiate the next movement faster. The acceleration profile was calculated by differentiating the y-

position curve twice (Figure 4.6). The RMS values of each curve can be seen in Table 4.1.

Table 4.1 The RMS values of the test drive and simulation

	RMS (test-drive)	RMS (simulation)
Adaptive filter (30%)	1.06	1.56
Ramp 0.4 s	2.84	2.34
Ramp 0.8 s	1.68	1.91

By applying the reduction of the proposed adaptive control function in the vibration, the amplitudes in the test simulations and drives were obtained. The adaptive control function reduced the RMS value of the vibration at the end tip of the boom by between 38 % and 63 % (by 18-33% in the simulations) from the values obtained using the conventional ramp functions in the example test drive. The results of the test drives are not fully comparable with the test simulations because of a smaller valve that was installed in the real boom during the test drives, because of a malfunction of the original valve. However, the adaptive control function showed benefits that lea to the interest to patent the method before longer field tests (Pat FI 109349, Pat EP 1174384A1, Pat US 6553278B2).

4.3 Determination of the Payload and Vibration Recognition

The calculation algorithm was tested using old pressure and position data that had been collected during different test-drives of the TJ71F72 crane. When the load mass used was known, the task was to tune the calculation algorithm to the specified mass. In the step response tests, the crane was driven fast up from the ground using the lift cylinder. The stroke of the lift cylinder is shown in Figure 4.7 (a). The crane was not loaded, so the only load came from the gripper, rotator and components such as hoses, tubes and auxiliary parts. The weight of the gripper and the rotator was known to be 225 kilos. The pressure in the chambers of the lift cylinder vibrated a lot after deceleration at 5 seconds, Figure 4.7 (b).

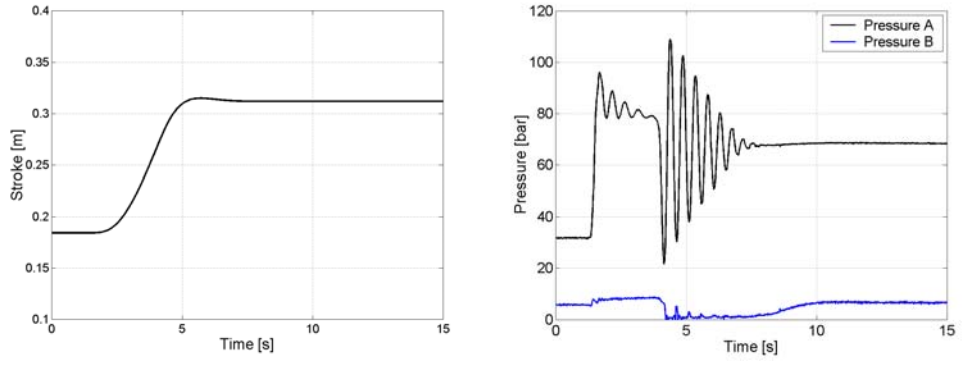

(a) (b)

Figure 4.7 The stroke of the lift cylinder (a) and pressure in the chambers of the lift cylinder (b).

The load was calculated using the equations presented in Chapter 3.2.4. The pressure vibration causes an error in the load calculation algorithm, which can be seen in Figure 4.8 . Otherwise, the load calculated by the algorithm is approximately 75 kilos too heavy. The result was considered to be sufficiently accurate because all the weights were calculated from simplified geometry, and the weights of some components were unknown. The total weight of the moving parts of the crane was about 900 kilos, and if the estimates in Table 3.4 contain an error of, for example, a total of 50 kilos, the remaining error of 25 kilos (3%) can be considered reasonable.

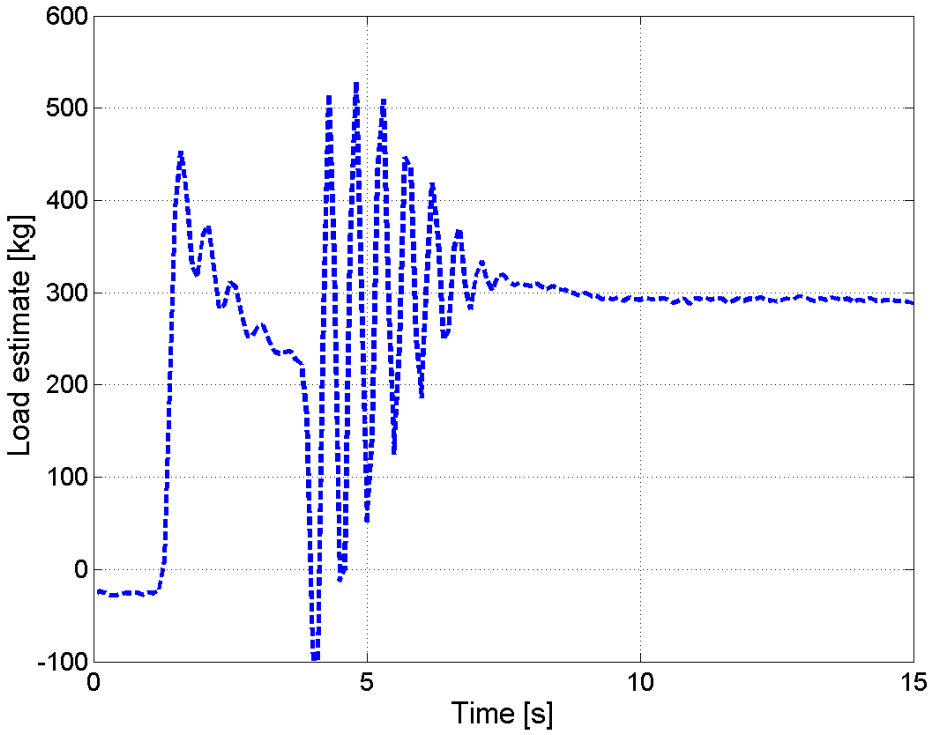

Figure 4.8 The calculated load.

The static error can be calibrated away, but the dynamic error causes bigger problems in the algorithm; most of the time, the pressure oscillates in specific amplitude. Due to the continuous operation of the crane, the calculation algorithm cannot wait for a better signal and the damping of the oscillation. Two solutions were found for this problem: The pressure signal can be low-pass filtered and the oscillation disappears, but the calculation algorithm reacts slowly to changes in the mass load, which restricts the use of the effective low-pass filter. The other option is to accept a larger calculation error and obtain fast reaction to load changes. Calculating the average value of the load instead of using a low-pass filter can reduce the error sensitivity in the faster solution. The average value can be counted over a selected number of samples using a running sum:

$$R_{\text{sum}} = R_{\text{sum}} - m_{\text{avg}} + m_4 \tag{4.1}$$

$$m_{\text{avg}} = \frac{R_{\text{sum}}}{N} \tag{4.2}$$

where R_{sum} is the running sum, m_{avg} the average load value calculated over the last N samples, m_4 the recent load value and N the number of samples selected for calculation.

The reaction times to load changes can be easily tuned by changing the number of samples, N. The calculation of only an average value does not fully eliminate the problem because only the high pressure peaks disappear and the low amplitude vibration remains. This low amplitude pressure vibration leads to a considerable error and cannot be reduced for reasons similar to those in the case of the low pass filter. One solution is to use logical operations in calculation. If vibration exceeds the limit value, the previous load values are used; otherwise new load values are calculated. The flowchart in Figure 4.9 shows a proposal for a solution to the problem of calculating an accurate load mass value in the MATLAB/Simulink interface.

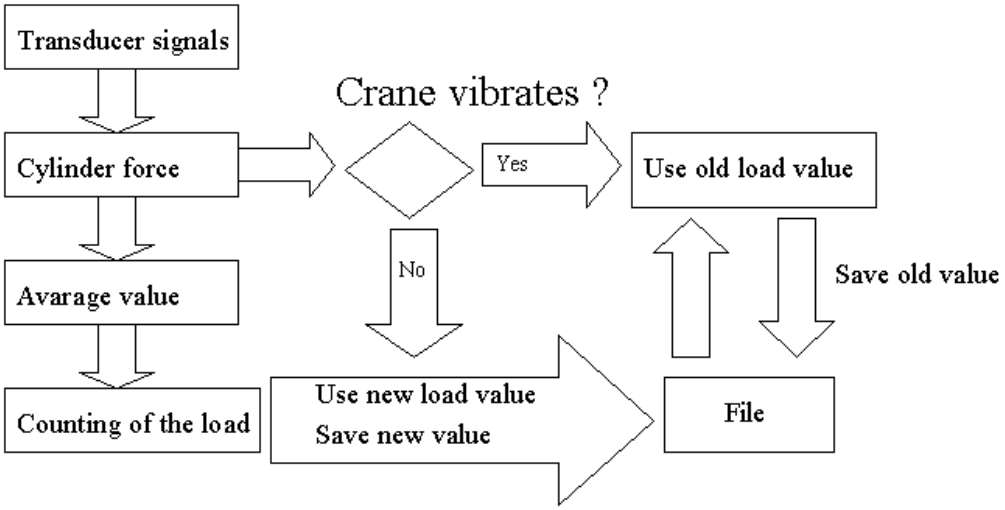

Figure 4.9 The calculation of the load.

The value of the cylinder force was calculated using Equation (3.54) and this value was compared to the set value. The vibration limit value of 20 kN was observed to give the best result. When the cylinder force remains below the limit value, the new value is used as the load value and is saved onto a file. The old values are used for as long as the vibration is suppressed under the limit value, after which new values are enabled. Figure 4.10 a) and b) present a load calculated similarly to that in Figure 4.8 and show effect of using logical operation under different settings.

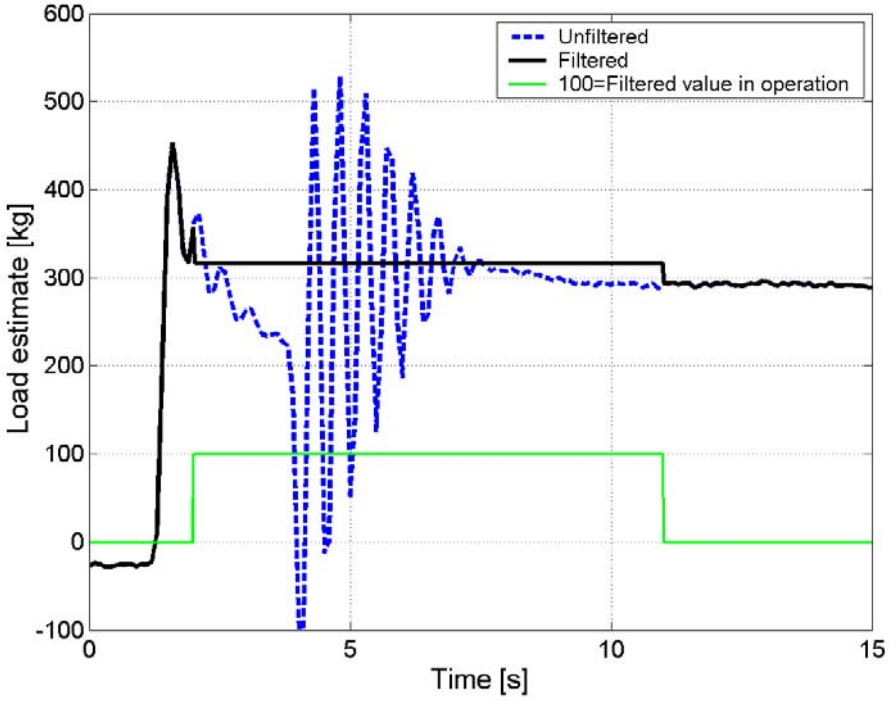

(a)

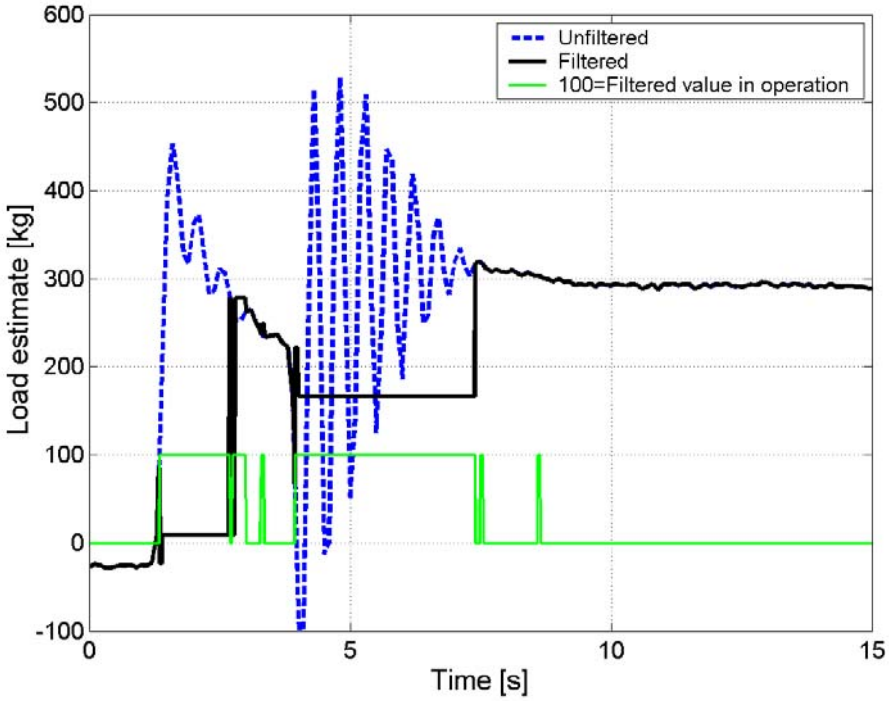

(b)

Figure 4.10 The load estimates for when a filter algorithm is in operation.

In Figure 4.10 a), the average load is calculated in over one second and in (b) over 0.05 second. In both cases, the force vibration limit had been set to 20 kN. There

are many options that could be used to find an optimized solution for the filter parameters, but this thesis uses only a few tunings.

After the successful step response tests, the crane was driven through the whole workspace. Because the test crane was in a laboratory hall, the roof of the hall restricted the operation of the crane. In the example given here, the crane was driven up using the lift cylinder, after which the jib cylinder was extended to its full length to bend the jib boom to almost 180 degrees. The crane lifted a 170-kg mass load that resulted in a total of a 400-kg load at the end tip of the crane. Figure 4.11, Figure 4.12 and Figure 4.13 show the cylinder strokes and pressure changes at the same time as well as the calculated load mass when filtering was in operation.

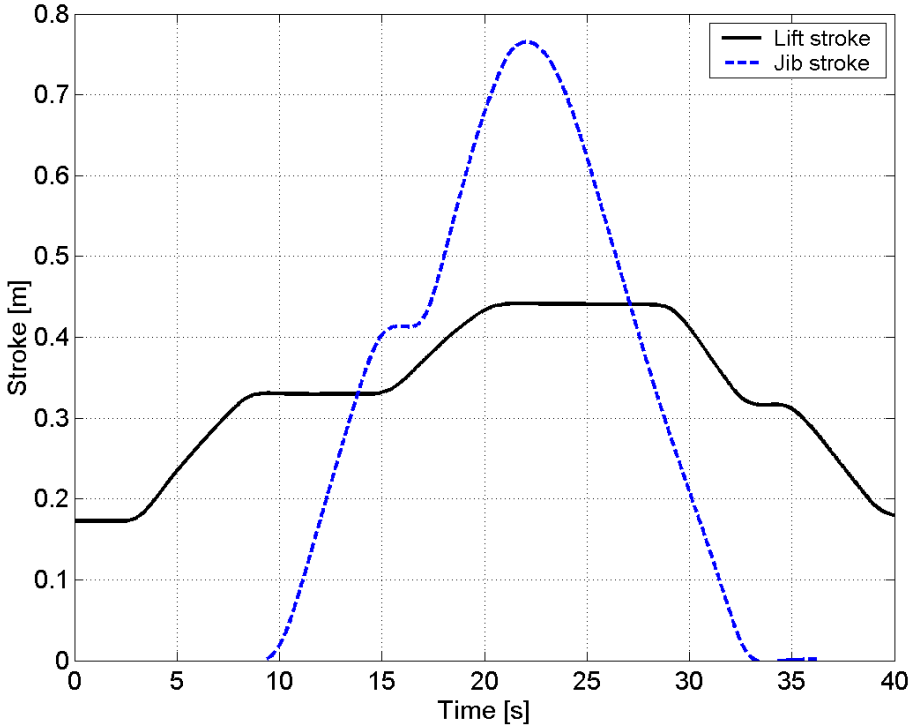

Figure 4.11 The cylinder stroke

The relative angle between the jib boom and lift boom exceeds 90 degrees when the stroke of the jib cylinder is 0.54m (time = 17 s.). At this moment, the pressure of the lift cylinder starts to decrease.

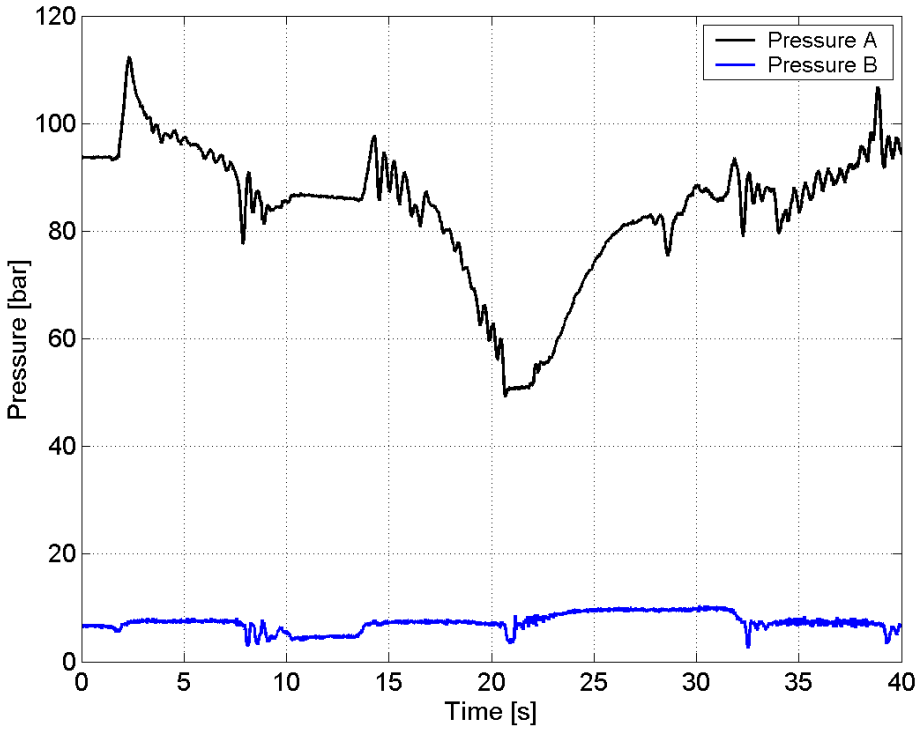

Figure 4.12 The pressure of the lift cylinder

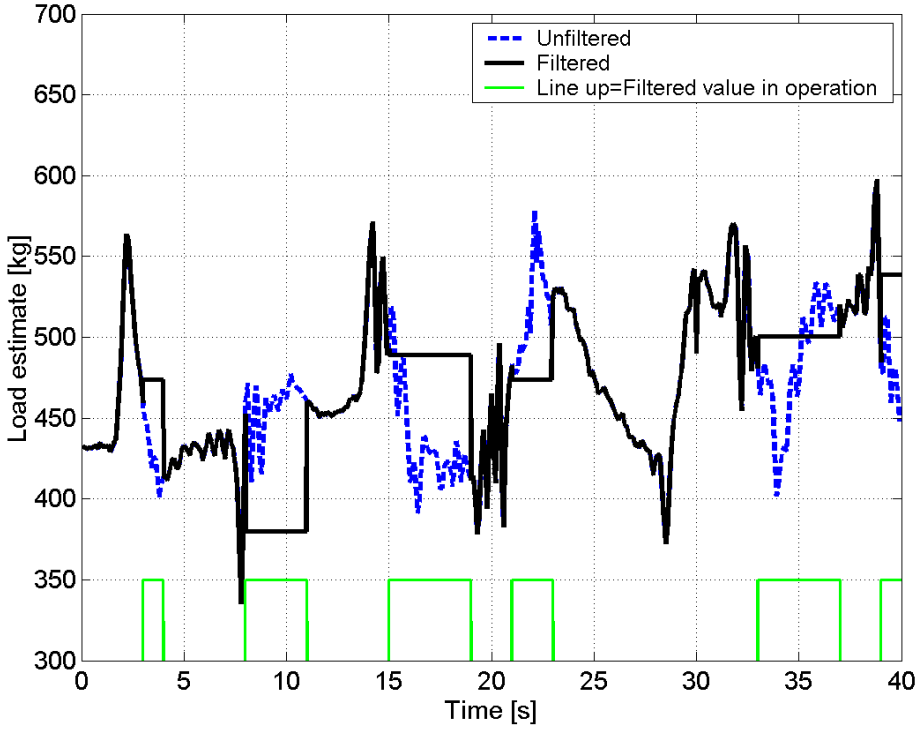

Figure 4.13 The calculated load mass

In order to provide updated load information for the adaptive filter, the calculation algorithm had to detect when the load could be counted from the pressure and

when old load values had to be supplied to the filter algorithm. For this reason, it was necessary to test and tune the vibration recognition module. Wrong load information could lead to an unwanted feedback loop in which an excessively small load value could lead to an overly large filtering frequency as well as to an overly fast valve input and the overly fast movement of the crane and an increase in vibration, which would attenuate the load calculation. On the other hand, the vibration recognition module should be able to detect the release and a picking up of the load fast enough for the filter frequency of the adaptive filter to be correct prior to the lifting of the load.

The vibration recognition capabilities of the algorithm were tested for the picking up and releasing of a 170-kg load mass using the gripper. The crane was kept in the same position and inclination. Figure 4.14 shows the calculated load. The total load at the end tip of the crane is about 400 kg; therefore, the same +70 kg static load error that is present in the step response tests is also present here. The pick-up and release cause large vibrations in amplitude.

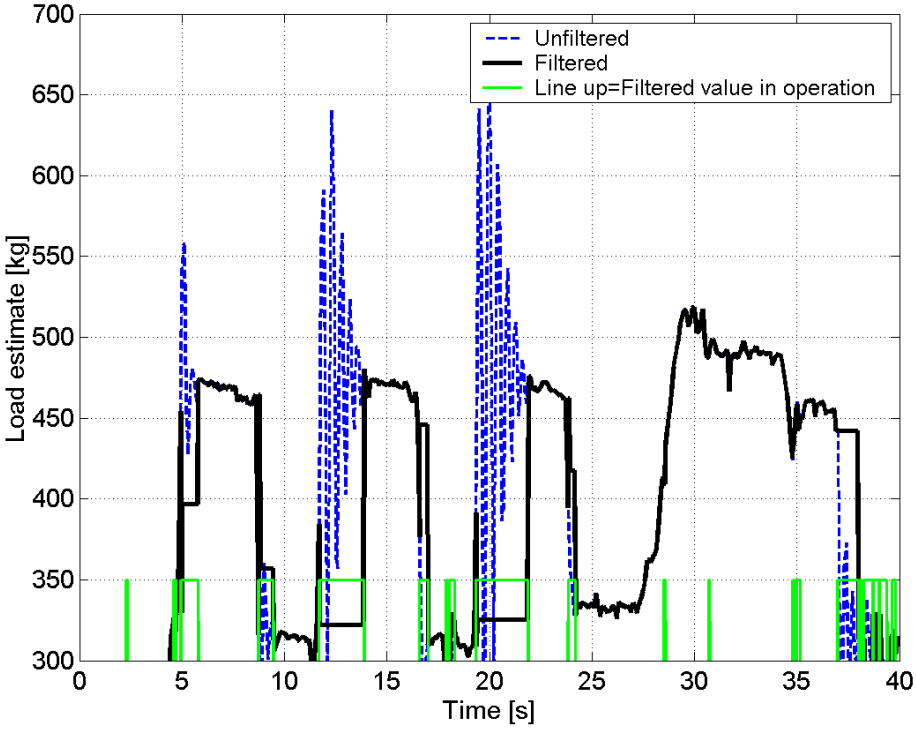

Figure 4.14 The pick-ups and releases of a 170-kg load using the gripper.

Despite the fact that the biggest pressure peaks can be filtered out, the response time to changes in the load increased to between 1 and 2 seconds, which can be considered to be too long. Depending on the working conditions and the log, the operator picks up the log as fast as they can. The normal settings of the gripper control are such that the log is locked in under 0.5 seconds and often, the operator starts lifting the log at the same time. This leads to the requirement to recognize the load immediately, and sufficient low-pass filtering against big pressure peaks cannot be used.

One feasible solution is to raise the vibration limit in the vibration recognition module. Increasing the limit to 50 kN improves the response time as Figure 4.15 shows:

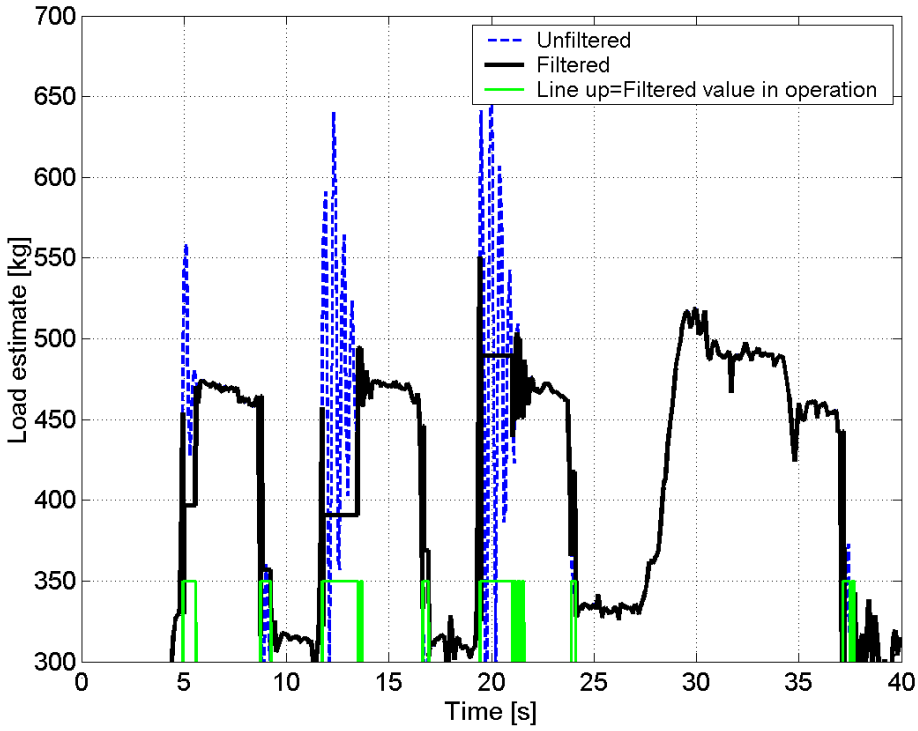

Figure 4.15 The effect of increasing the force vibration limit.

Increasing the force vibration limit to 50 kN influences the calculation of the filter frequency. Using three different settings in load estimation, the natural frequencies are calculated to find the influence of the load value on vibration. First, the load value vector was calculated without filtering, and the thus obtained vector was compared with two different filtered load estimate vectors. The first filter (high) was tuned in order to find the fast changes in the load and the second one reacted more slowly to changes in the load (low). The results are shown in Figure 4.16 . Throughout the work cycle, the lowest natural frequency stays within approximately the 1.4- to 2.0-Hz range. If the frequency is calculated from filtered load value, the range narrows to 1.55-1.95 Hz. The use of a filter in load the calculation algorithm can be justified, because of the narrower load range and more stable load values.

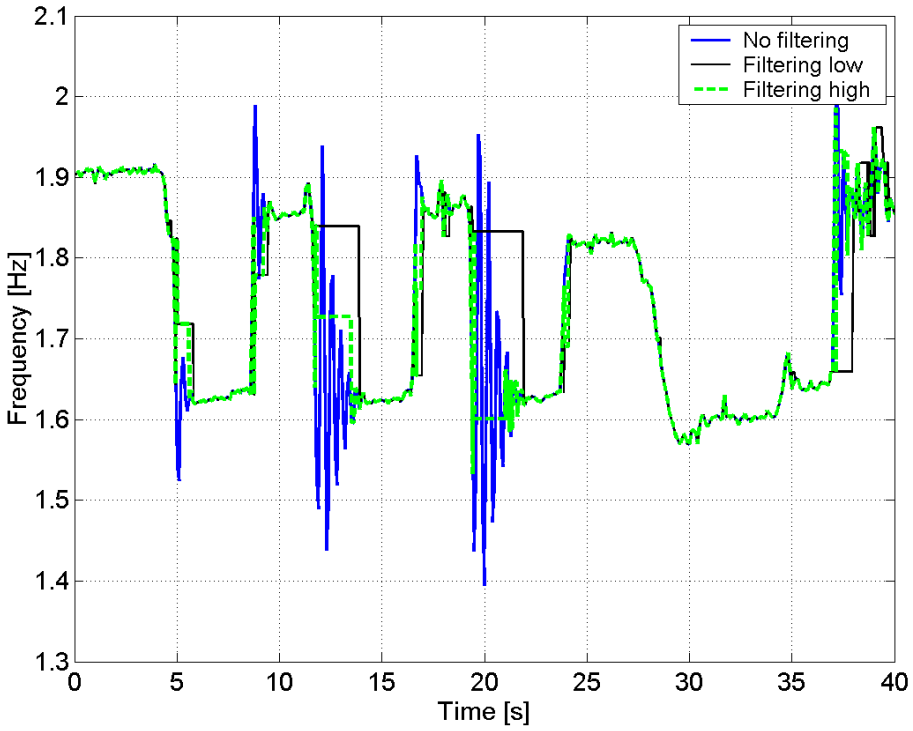

Figure 4.16 The lowest natural frequency range.

4.4 Semi-Active Damping

The testing of semi-active damping was initiated with step response tests that were driven using the laboratory cranes. It is well known that pressure vibration in the chambers of the lift cylinders is similar to the movement of the end tip of the crane. The position of the end tip of the crane was not measured, but an examination of the changes in the pressure and stress data illustrates the behavior of the crane. The manually driven step response tests, see Figures 4.17-4.19, show how active vibration control influences the pressure and stress.

The functioning principle of semi-active damping can be seen in Figure 4.17. The damping signal moves a spool of the control valve, which increases vibration. The phase difference between the control signal and the vibrations is 180°. This phase difference suppresses vibration, first in the lift cylinder, and then leads to the same vibration reduction at the end tip of the boom. Semi-active damping reduces the vibration amplitudes of the pressure and the stress from the second peak onwards, because it cannot predict increases in vibration.

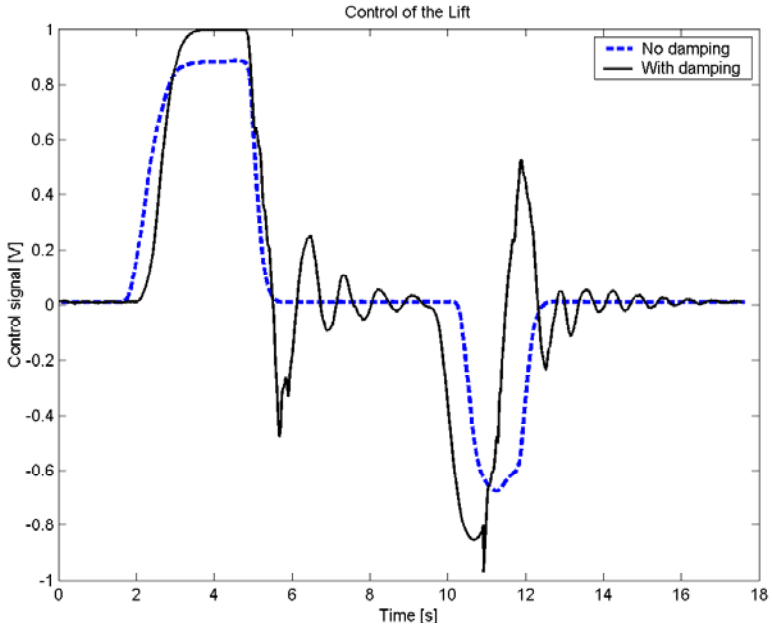

Figure 4.17 A comparison of the control signal, with and without semi-active damping, obtained from manually driven up-and-down step response tests.

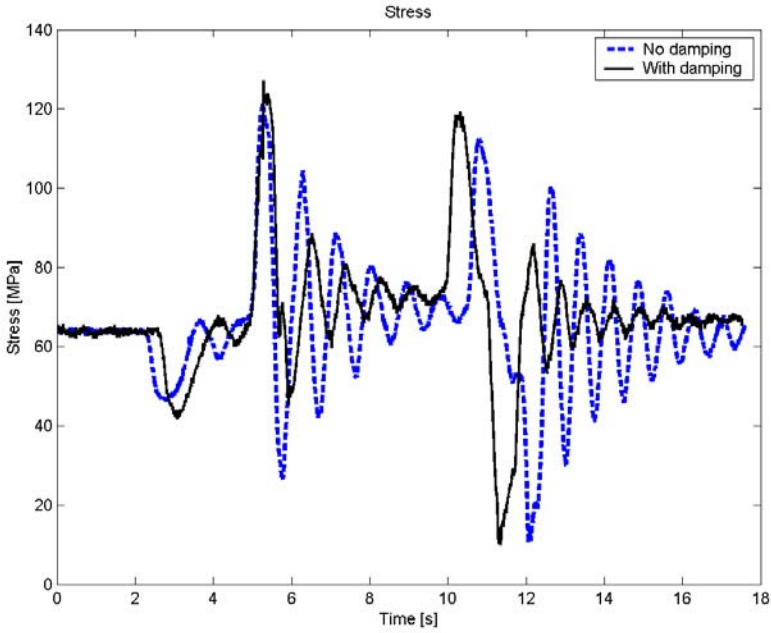

Figure 4.18 A comparison between traditional control and active damping, up-and-down step response. The stress in the lift boom.

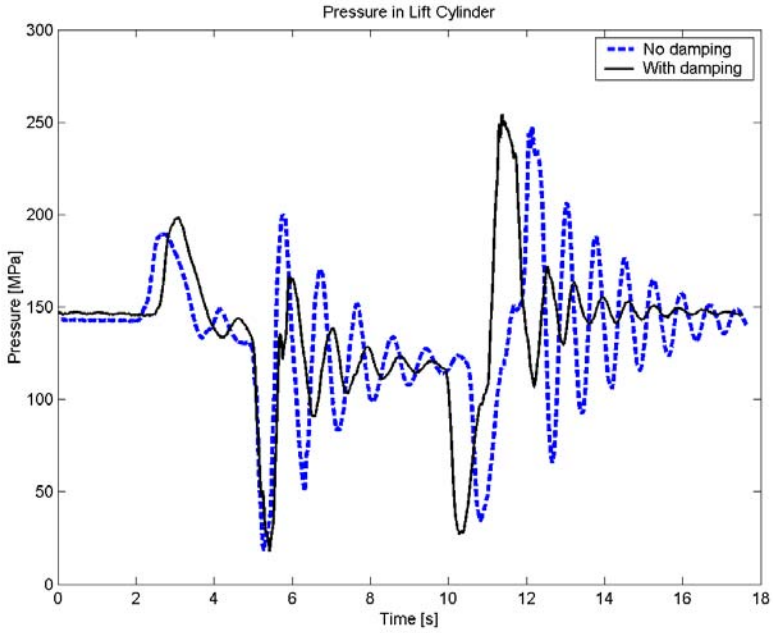

Figure 4.19 A comparison between traditional control and active damping, up-and-down step response. The pressure of the lift cylinder.

The RMS value was calculated from the stress and vibration curves. The active damping method reduces the RMS value of pressure vibration by 21-43% and stress vibration by 8-42% from the levels that correspond to the tests performed without damping in the up-and-down step response.

4.5 Field Tests

4.5.1 Step Response Tests

All the field tests were performed using a TJ71F100 crane. In the step response steps, the lift cylinder was used to move the end tip of the crane up and down. The tests in the field were preformed manually, which means that the control signals were not all exactly the same. At this point, it has to be mentioned that the load on the gripper can also swing randomly, which means that manual control is not a critical error source in the measurements. In different cases, the crane goes through similar movements under manual control, and the initial (theoretical) velocity input to the valve of the lift cylinder is shown in Figure 4.20. The velocity input shown in Figure 4.20 makes the crane move up, stay in the upper position for a while and move back to starting point.

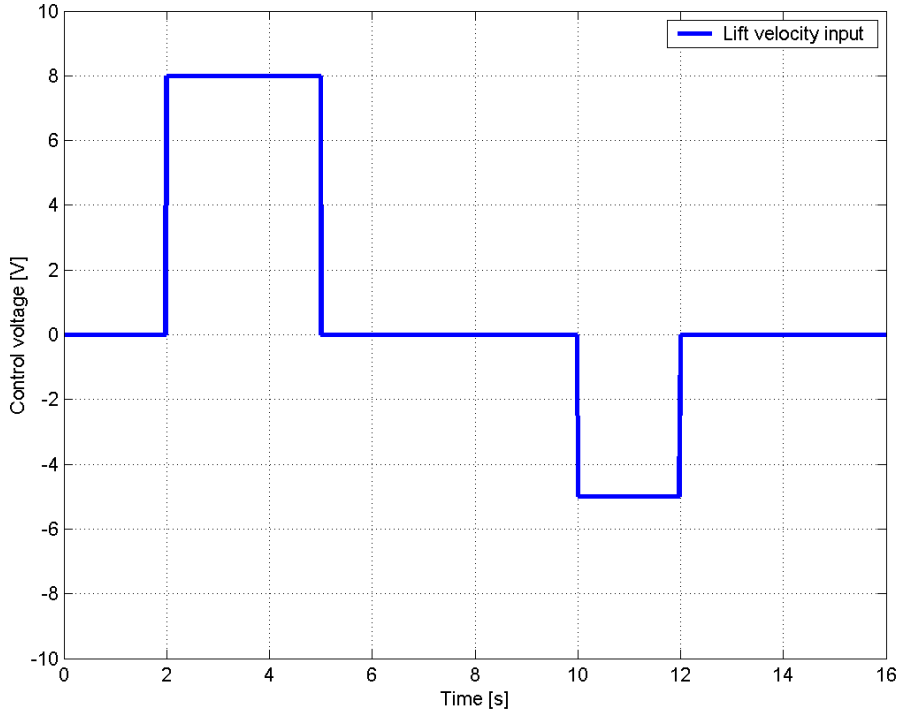

Figure 4.20 Step Response. The velocity input to the valve of the lift cylinder.

The velocity inputs for different controllers in the case of step response were discussed in chapter 3 (see Figure 3.1). Since the field test tests were performed manually, the differences between the inputs are small in comparison compared to theoretically calculated differences. Figure 4.21 shows the effect of an adaptive filter on the movement of the end tip of the crane. The adaptive filter uses 30 % of the lowest natural frequency of the manipulator. The vertical movement of the end tip of the crane is shown respectively in Figure 4.22.

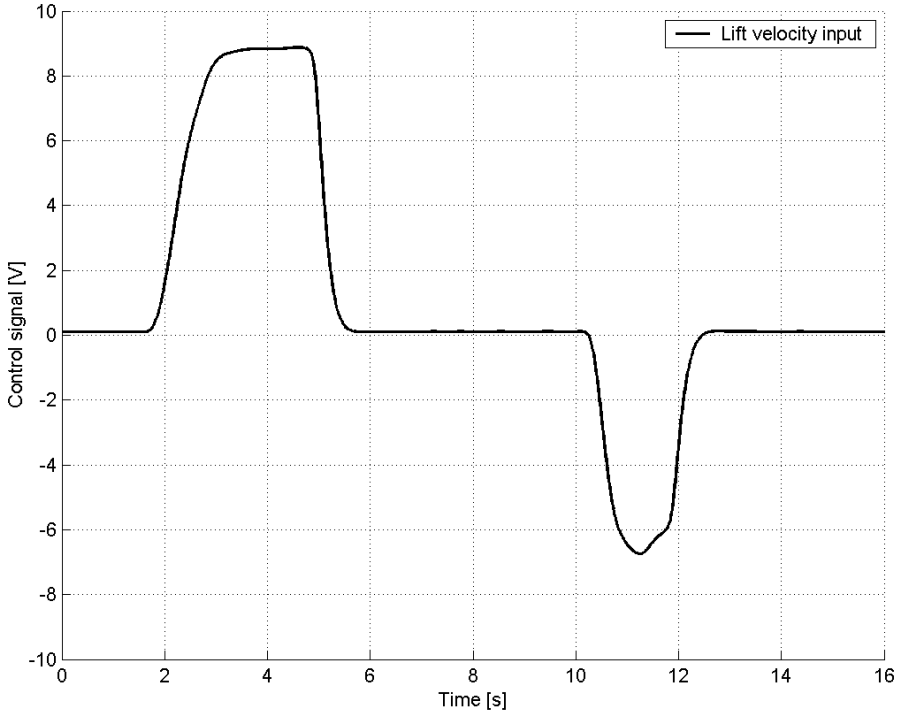

Figure 4.21 The control signal of the lift cylinder, the adaptive filter (30%)

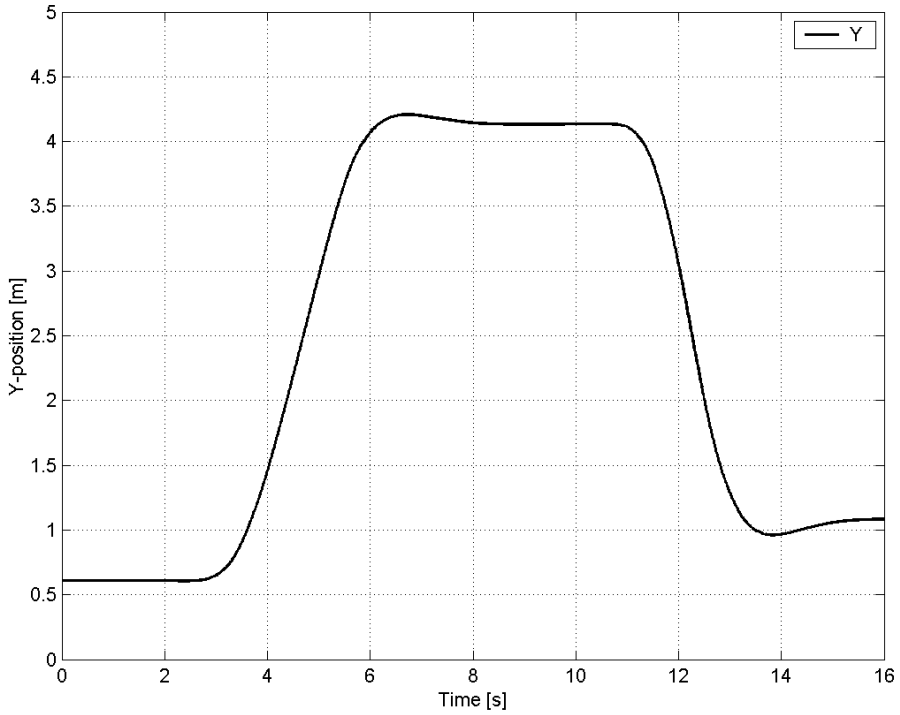

Figure 4.22 The vertical movement of the end tip of the crane.

The step responses were driven with three feasible filter tunings: 20, 25 and 30 % of the lowest natural frequency of the crane. From these settings, the average

value of 25 % was noticed to be most suitable for normal operation. Tuning of 20 % caused the manipulator to react too slowly to the operator's commands and 30 % caused excessive vibrations in stop situations. The results of the step response tests and their comparison with those of ramp control is presented in Table 4.2. The pressure of the lift cylinder and strain gauge measurement data from point three (see Figure 4.1) is used as a measure of vibration. Stress vibration adheres to the above results. The RMS value of the pressure and stress vibration for when the ramp function is in use is given a reference value of 100, to which the results for the different filters are compared. The reference value is the average value of similar test step response tests and is scaled to a value of 100. The semi-active damper was also tested with the adaptive filter, and the corresponding results are shown. The "semi-active" column indicates when the semi-active damping is on (1,2) or off (0). The RMS value defines the average energy content of vibration over a defined sample group. The disadvantage of using the RMS value is that it does not cater for fast transient peaks that may have a significant influence on the fatigue damage of a welded structure.

Table 4.2 The results of the step response test. The "semi-active" column shows the co-coefficients used in the semi active damping.

Filter tuning %	Semi-active	Pressure RMS	Change %	Stress RMS	Change %
RAMP	0	**100**		**100,0**	
20	0	83,0	17,0	79,2	20,8
20	1	59,1	40,9	43,0	57,0
20	2	53,6	46,4	45,8	54,2
25	0	85,8	14,2	78,0	22,0
25	1	79,9	20,1	56,5	43,5
25	2	68,3	31,7	44,7	55,3
30	0	113,3	-13,3	90,6	9,4
30	1	103,0	-3,0	75,6	24,4
30	2	80,1	19,9	63,7	36,3

The results in Table 4.2 show that by using an adaptive filter and a semi-active damper with suitable tunings, the vibrations in the chamber lift cylinder can be reduced. The vibration suppression ranges from 14.2 to 46.4 %. However, an excessive filtering frequency in the adaptive filter can lead to vibration amplification, as was the case when a tuning value of 30 % was used. With 30-% tuning, the vibration increased so severely that even semi-active damping struggled to achieve better result than those of the ramp function. It was only the use of a large co-efficient in pressure feedback (2) that reduced the RMS value of vibration below a comparative number of 100. As mentioned above, the RMS value cannot fully define the influence of the transient peaks, and this is seen in the comparison of the RMS value of pressure with that of stress when 30-% tuning is in use: The RMS value of pressure leads to a negative change, but at the same time, the RMS value of stress leads to positive and promising results. The reason for this was that the structural vibration in the boom was suppressed more quickly than was the pressure vibration. The transient peak in stress is noticeably bigger than in the reference tests performed using the ramp function. These conclusions from the RMS value forced both RMS results to be considered and

the data to be manually analyzed through the compilation of charts from the collected data.

One important result that can be seen in Table 4.2 is that by adding semi-active damping to the control system, vibration suppression reaches results that are 46 % better than those obtained without damping (pressure vibration) and up to 57 % better in the case of stress measurements. Semi-active damping was used with the adaptive filter, and so the obtained improvements are a mixture of the effect of the adaptive filter and the semi-active damper. From Table 4.2, it can be seen that the RMS values decrease when the semi-active damping coefficient has a value of one or two. Unfortunately, semi-active damping could not be tested with the existing control system hardware because the ramp functions were set for the machine's own amplifier cards. The implementation of the damper was not successful with this hardware.

Figure 4.23, Figure 4.24 and Figure 4.25 show the control signal, pressure in the lift cylinder and stress data from strain gauge three (see Figure 4.1). The semi-active damping coefficient has a value of one and the adaptive filter a filter tuning of 25 %.

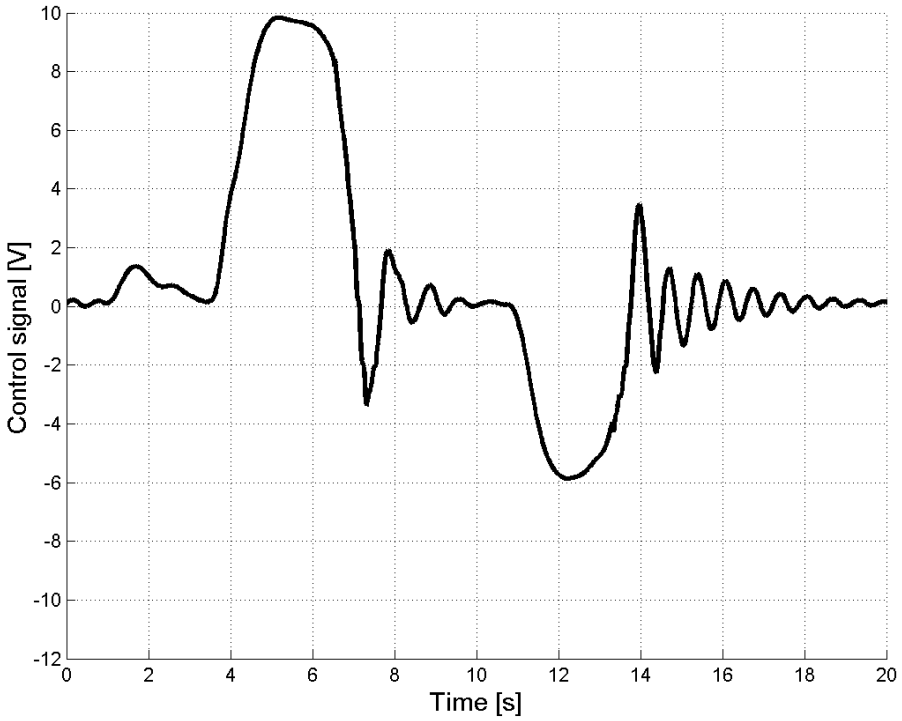

Figure 4.23 The control signal of the lift movement.

Damping suppresses the vibration that originates from the stop movement between approximately 7 to 9 seconds. The same phenomena reoccurs after 14 seconds, but the amplitude of the damping signal is larger because of the greater vibration, see Figure 4.24.

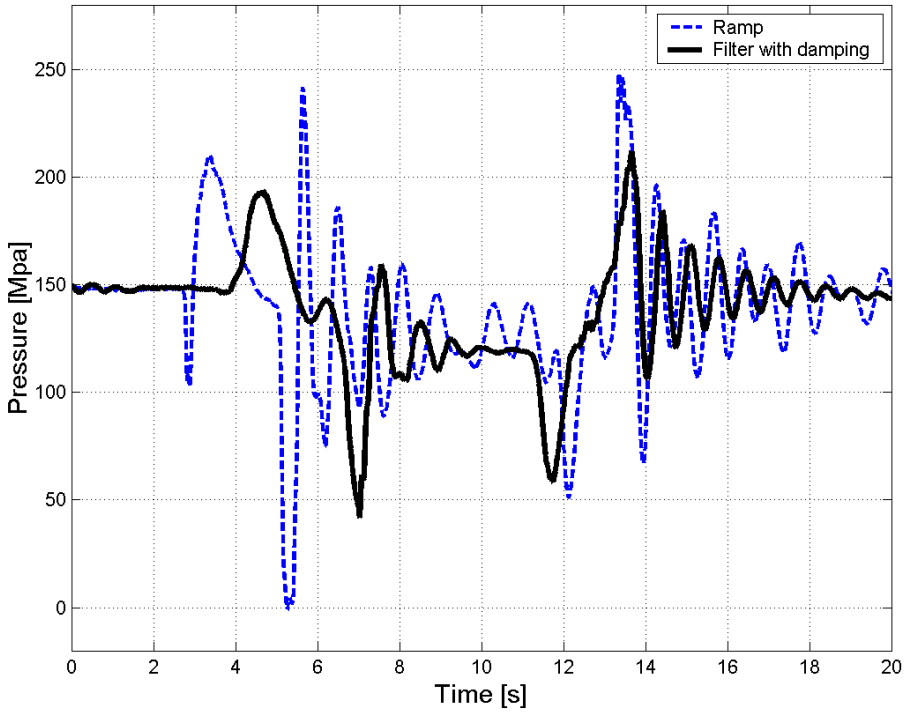

Figure 4.24 The pressure in the lift cylinder

On the first stop, the damper suppresses the pressure effectively. Good vibration suppression is not limited to the presented case only; a general trend that was observed in the test drives was that vibration caused by the stopping of the lift movement was easier to suppress than that of the lowering movement. Similar suppression can be seen from the stress curve in Figure 4.25. The reason for the different stress level at the beginning of the work cycle is that the crane started the movement at a slightly different height and the test cycles were performed at different temperatures.

The daytime temperature changed a lot between the morning and the afternoon. In addition, the machine was operated inside a warehouse between the test drives, and temperature of the strain gauges was subject to significant changes between the different test drive times. However, this static error did not have any effect on the calculation of the RMS value, because this was calculated from high-passed stress values. The effect of the temperature change does not show in the pressure data.

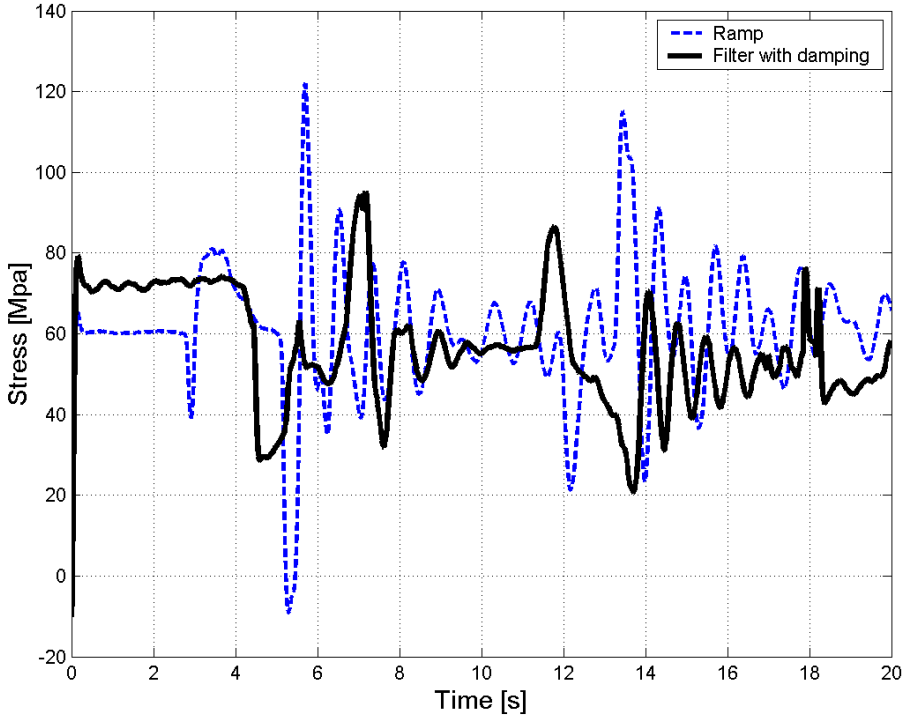

Figure 4.25 The stress in the lift boom.

4.5.2 The Loading of Logs to the Carriage

The loading of the log forwarder is most important function of the crane. The harvester tries to place logs in temporary piles, which eases the work of the operator of the log forwarder. The piles are situated near the driving track in the forest, so most of the logs are picked within a five-meter radius from the log forwarder. In the tests, the logs were positioned on both sides of the circle around the machine and the driver loaded the logs in a similar fashion using different controllers. The lifting distances were slightly larger than in normal operation, but this was also the intention of the tests. After loading, the carriage of the log forwarder was unloaded, and despite the fact that this takes only a small part of total working time, the results were recorded. On average, the loading and unloading work cycles took 3.5 minutes. The long work cycles reduced the influence of random driving errors on the results. By using only the adaptive filter that was tuned to 25 %, pressure vibration was reduced by 8 % and stress by 13 %. The addition of semi-active damping to the control system did not significantly improve the result.

4.6 Notes on the Field Measurements

The age of the log cranes used in the tests implied that the joints had backslashes and there were possible structural deformations in some parts of the booms. These cannot be measured accurately without the disassembly of the crane, but the test driver defined the crane as being too old for professional use (2-3 eight hours work shifts per day). Also, the noise made by the joints was easily recognized. Backslashes caused high frequency structural vibrations in the crane, which semi-active damping could not eliminate before the vibration could be seen from the pressure data. On the other hand, the use of high gain (2) in semi-active damping produces high-frequency vibration. The effect of high gain and backslashes on the pressure and control signal can be seen in Figure 4.26 and Figure 4.27.

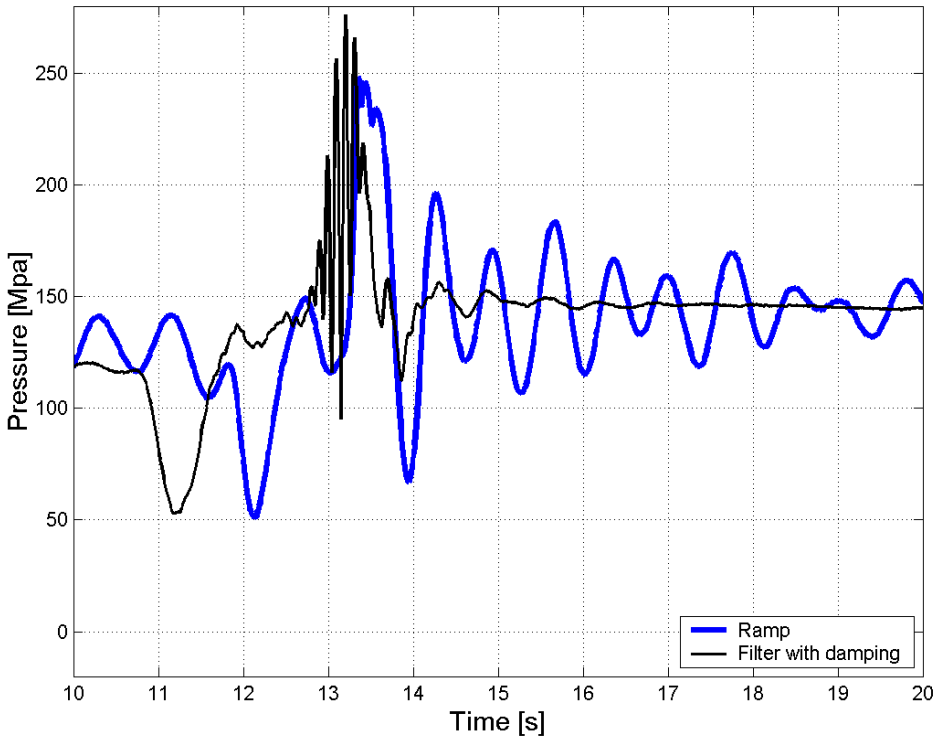

Figure 4.26 The effect of backlashes and high gain on the pressure

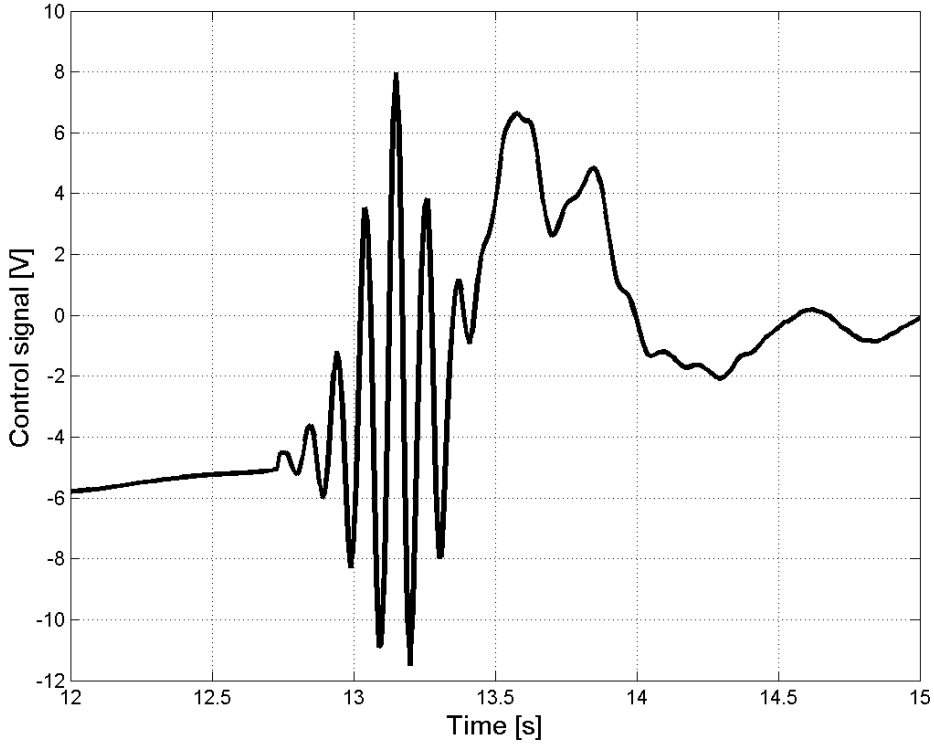

Figure 4.27 The effect of the high frequency vibration of the pressure on the control signal.

Fast Fourier Transform (FFT) analysis gives the frequency content of the control signal. Frequency domain analysis (Figure 4.28) shows more clearly what can be seen in Figure 4.27: the frequencies contained in a control signal that produces vibration (D=2) are higher than those contained in a signal that does not produce vibration (D=1), and the system is fed energy that is concentrated around 10 Hz. It can be concluded that the controller itself can behave in the desired manner, but the mechanism being controlled can exhibit factors that increase vibration through unsuitable controller tunings. Despite the high-frequency content of the control signal, the movement of the end tip of the crane remains smooth and stable. Nevertheless, high-frequency vibration can yield other difficulties as far as the fatigue life of the structure or the comfortable operation of the machine are concerned.

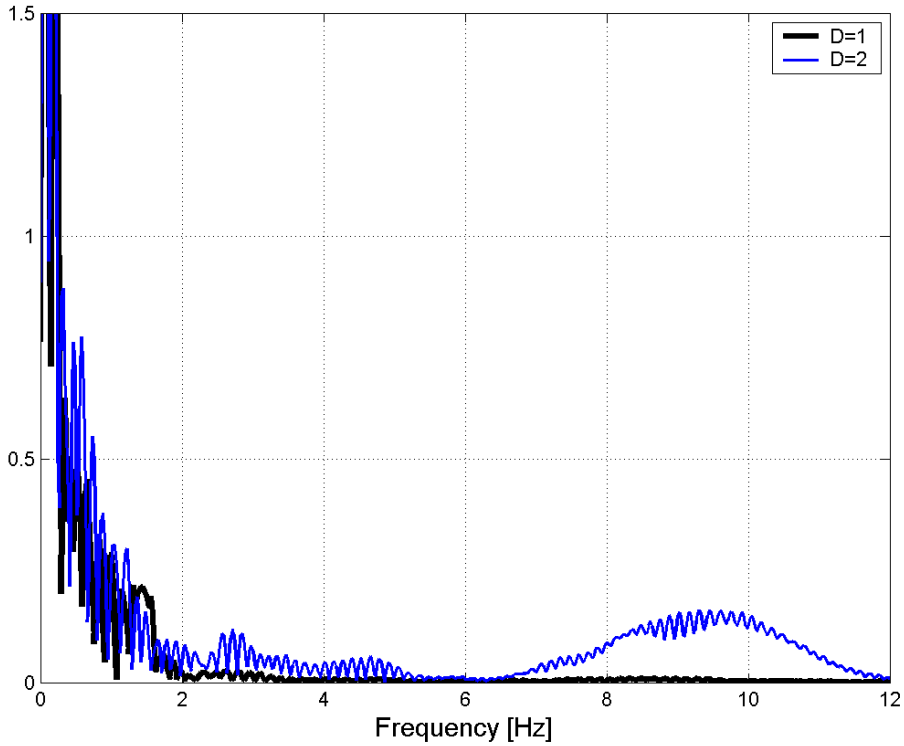

Figure 4.28 The frequency content of the control signal after semi-active damping.

The weather changed a lot during the test drives: in December 2001, the temperature was about –20 degrees on the worst days. In January 2002, some tests were performed at temperatures of almost zero degrees. The effect of the temperature was minimized by the warming of the strain gauge amplifier and by the storage of the log forwarder inside the workshop prior to the tests. Even so, the cold wind rapidly cooled the equipment and machine. The effect of the temperature can be seen mostly in the strain gauge measurements that had to be scaled in the post-processing; otherwise, the effect of the temperature is difficult to estimate. Most of the targets of measurement had large ranges, and so small transducer errors have no real effect to the results. In general, cold weather slightly stiffens the behavior of the log forwarder; the bearing greases are almost solid, the properties of the wheels become stiffer and the engine and hydraulic oils are cold.

Most of the time and effort spent on the tests went into the tuning of the control system and the repair of numerous small components of the electric devices. For this reason, the schedule collapsed and the result database lacks the systematic testing of some of the tunings of the controller. The best performing controller options were tested, and long work cycles were driven in order to obtain an opinion from the test operator. Not all the work cycles were recorded, and the results included some irrelevant movements that made automatic post-processing impossible. Most work cycles were performed by the operator, which means that

the repeatability of the control signal is not comparable to the computer-driven operator.

4.7 Discussion and Future Suggestions

Two vibration suppression methods, adaptive filter and semi-active damping, were presented in this dissertation. The aim of both methods is to improve the dynamic behaviour of commercial log cranes, but their approaches to the problem differ slightly from each other. The adaptive filter cuts off high frequency impulses coming from the operator and, thereby, works against system's inner disturbances. Semi-active damping suppresses the crane's oscillation which is often caused by some external disturbance such as collision with an obstacle. Semi-active damping is also able to suppress vibrations caused excessively rapid control signals given by the operator. The proposed methods, adaptive filtration and semi-active damping, were implemented in a real crane and tests carried out for long durations. The results of the test drives were post-processed and RMS values calculated in order for a traditional method to be compared with the proposed methods. The result of comparison can be summarized as follows:

-in step response tests performed under laboratory conditions, adaptive filter achieved an improvement of 63 % in pressure vibration in comparison to the traditional method . The crane used in these experiments can be classified as being very flexible and gave overly optimistic results. With a rigid crane that was bolted to the rigid floor, the adaptive filter had only a minor influence on the same tunings. In field tests performed on the crane when it was used in a real log forwarder, a correctly tuned (25 % tuning) adaptive filter reduced pressure vibration by 14-17 % and in longer loading work cycles, the reduction was only 8 %. The test operator did not report any major disadvantages that hindered the operation of the crane.

-semi-active damping reduced the RMS value of pressure vibration by 21-43%. The improvement obtained for the best tunings was about 46% when a real log crane was used. In this work cycle, the adaptive filter was used in parallel with semi-active damping.

The benefits obtained depend heavily on the flexibility of the crane: Long and flexible cranes benefit much more from the proposed methods than do rigid cranes. Differences were observed between the results of the laboratory and field measurements, the main reason being the stiffness of the base of the crane: a rigid concrete floor does not have the same damping characteristics as does the chassis and wheels of a log forwarder and the soil under the machine. Also, when the carriage is empty and heavy logs are lifted using the crane, the carriage tends to incline off the soil. This phenomenon effectively eliminates the vibrations of crane, although it was not a specifically intended or designed feature.

For the adaptive filter, the results for longer work cycles were small, only 8 % improvement in pressure vibration. This deviation from the results for step response tests will be explained next. First, the test operator had twenty years experience in operating log forwarders and harvesters. Some test work cycles

were run without any new controller or ramp functions, and the operator was not informed of this. The results were confusing: The operator did not notice any major differences in the operation of the machine other than that the crane was a little too fast for loading. The obvious conclusion is that the experienced operator suppresses the vibration of the crane with his driving touch. Any big control mistakes cannot be observed from these "diversionary" damper tests. Afterwards, the operator mentioned out an uncomfortable driving experience, by which he meant that without any shaping function (ramp, filter), the crane could be driven but demanded extra attention and carefulness.

Another important reason for the minor suppression of vibrations during the long work cycles lay in the characteristics of the crane's movement. During normal operation in a free workspace, the operator keeps the crane in motion for most of the time. Since semi-active damping was tuned to function only during deceleration and stopping (control signal under 2 volts), it had only a small effect if the crane moved faster. In addition, the above-mentioned reason that the operator combined his operation skills with the respective controller weakened the results for the tested controllers. In the step response tests, the operator just tried to repeat similar rough movement, which gave the controllers a good opportunity to demonstrate their performance capabilities.

Although the results for the loading work cycles were below the expected results, their direction was in line with the desired. On the other hand, semi-active damping produced promising results in all the test situations and proved to be an effective vibration suppression method if given the time to work; this means that the operator has to be conscious of the existing damping and let it suppress vibration. Of course, the operator can suppress vibrations by himself, but considering the most suitable work method is outside the scope of this work. These control methods can offer an inexperienced operator more benefits than they can for experts. Many driving mistakes force first-time operators, like this author, to stop the operation of the crane and wait for it to become stable. Semi-active damping suppresses vibration about two times faster when the operator does not participate. Although all new operators have a certain number of operating hours behind them when they start working professionally with forestry machinery, these vibration suppression methods could help them to achieve better usability, avoid collisions with standing trees or the carriage, and thereby, enable the faster, more effective operation of the machine.

One possible area of application for the proposed methods is their use in automatic work cycles. In the field of excavators, automatic depth control systems and digging systems that carry out some simple tasks automatically already exist. One interesting idea would be, for instance, to develop an automatic carriage unloading option for log forwarders. The operator could set different points in the workspace for the control computer that would automatically calculate the trajectories. The implementation of the automatic picking up and releasing of loads is difficult and would require the operator's participation, but between these two operations, there is only point-to-point movement that could be driven by an automatic control system.

Another application in which semi-active damping could provide benefits is the control of the crane's slew cylinder. The crane is very flexible in the horizontal direction which is driven using the slew cylinder. Generally, operators handle deceleration in this horizontal movement carefully, starting deceleration long before the target point. If the crane is loaded at the same time, deceleration in the horizontal direction can easily cause the swinging of the load to increase, which makes the task of controlling the crane more demanding. Semi-active damping was tested quickly in slew control during the test drives, and it was observed to effectively suppress load swinging. The negative aspect was that semi-active damping caused "ghost movement" in the crane, which is generally not permitted by operators. So-called ghost movement occurs after the operator has stopped actively controlling the machine and gives the operator a scary sensation. This problem was not solved, because damping in the horizontal direction was not in the scope of this project.

5 Conclusions

This thesis discusses the vibration problems in the cranes used in commercial forestry machines. In many manipulator applications, it is not possible to attain better dynamics through traditional approaches, such as stiffening the manipulator structure. The improvement of the dynamics of flexible manipulators requires advanced control methods. This thesis concentrates on developing tools and controllers for suppressing vibrations. These tools require auxiliary transducers, installed in specific points in the crane, and electronically controlled directional control valves. The basic difference between the proposed methods and existing control functions and damping systems used in forest machinery is that the former take into account the changing dynamics of the crane and do not require auxiliary actuators.

At first, an adaptive filter was developed. The filtering frequency was defined to be a part of the lowest natural frequency of the crane. The algorithm that calculates this essential parameter of the filter was developed. The natural frequencies of the crane were collected using a dynamic simulation model of a full-scale crane. The model included definitions of the critical flexible components, hydraulic circuits, forces and kinematics of the crane. The nature of the dynamics of the crane with respect to the crane's position, inclination and load mass were defined using a suitable surface fitting procedure that was written in the form of an algorithm. This algorithm uses the cylinder stroke lengths and mass load as its inputs and returns the lowest natural frequency as its output.

The mass load of the crane was not measured using any transducer but was calculated using the kinematics of the crane and the cylinder forces. An analytic model of the crane was built up and used to calculate the torques in the joints. As the torque required to move the lift boom is known and the cylinder force of the lift cylinder can be calculated from the lift cylinder pressure measurements, the load mass can be calculated.

On the basis of references from literature, the semi-active damping method was developed for the crane of a log forwarder. The semi-active damping method is based on pressure feedback. The measured pressure enables the calculation of the cylinder force and the high-passed force provides information on the scale of the pressure vibration amplitude in the lift cylinder. The pressure vibration in the lift cylinder is analogical to the vibration at the end tip of the crane. Force vibration, scaled with suitable gain, can be added to the control signal of the valve of the lift cylinder. There is a phase difference of 180 degrees between this damping signal and the force vibration of the lift cylinder.

A widely used ramp control function was selected to be the reference control method. The result data collected using the ramp function was compared with the results of the proposed methods. The RMS value was selected to be the comparison target. The calculation of the RMS values was performed from the high-passed result data. Different work cycles were driven to in order for the performance of the methods to be observed and for the test operator's opinions to be obtained. In the step tests, the adaptive filter was proved a working vibration

suppression method if the manipulator used has a long reach and the tendency to undergo large deflections when loaded. In longer work cycles, the results of the adaptive filter were at the same level as those achieved by a professional driver with the ramp control; this does not necessary mean that no benefits are obtained using the adaptive filter.

Semi-active pressure feedback performed effective vibration suppression in all the test types. In the step response tests, the fast stopping of the crane excited vibration that normally dies out through structural damping after a varying time. In the loading work cycles, the crane tended to be in motion for most of the time and when semi-active damping was tuned to function only when operator's signal was below a certain value, damping had little effect. In situations, in which the crane collided with something, the damper suppressed the vibration if the operator stopped controlling the machine actively for a while. In deceleration situations, damping worked as it did in the step tests.

The results of the measurements demonstrated the benefits that led to the interest to patent the adaptive filter. Semi-active damping is widely used in different industrial solutions and was not patented, although it offers potential for forest machinery control systems.

REFERENCES

ADAMS online help, ADAMS/Linear with ADAMS/ SOLVER [version 11.0]. 2002. Mechanical Dynamics. Software online help.

Cavallo A. et. al.1999. A Sliding Manifold approach for Vibration Reduction of Flexible Systems. Automatica 35. Elsevier Science Ltd. P. 1689-1696.

Craig J.J. 1986. Introduction to Robotics: Mechanics & Control. Addison-Wesley. USA. 303 p.

Chapnik B.V., et al. 1993. Controlling the Impact Response of a One-Link Flexible Robotic Arm. IEEE Transaction on Robotics and Automation, vol.9, No 3, June 1993. P.346-351.

Deniard J., Faillot, J-L., Swevers J., Torfs D. 1993. Design and Implementation of an Antivibration Robot Control Software, in Vibration Control of Flexible Servo Mechanism, ESPRIT Project 1561: Sacody, Vol. 1. edited by Faillot, J-L. Germany. Springer-Verlag.

Doebelin E.O. 1990. Measurement Systems. 4. edition. McGraw-Hill Publ. Co. USA. 960 p.

dSPACE. 2001. Solution for Control -Catalog 2001. dSPACE Gmbh. Germany. Software and Hardware catalog.

Everett L.J. et al. 1999. Design Flexible Manipulators With the Lowest Natural Frequency Nearly Independent of Position. IEEE Transactions on Robotics and Automation, vol. 15, No. 4, August 1999. P.605-611

Hakala M.K, Kullaa J. et al. 1994. Mekaanisten värähtelyjen hallinta, VTT Tiedotteita. Espoo. 105 p. In Finnish.

Handroos H. 1990. Methods for combining a theoretical and an empirical approach in modelling pressure and flow control valves for CAE-programs for fluid power circuits. Acta Polytechnica Scandinavica. PhD thesis, Tampere University of Technology. 52 p. ISBN 951-666-315-X

Konttinen H., Drushka K. 1997. Metsäkoneiden maailmanhistoria. Otava. Helsinki. 254 p. In Finnish. ISBN 951-1-14744-7.

Kovanen J., Handroos H. 2001 A. Dynamic Behavior Based on Novel Open-Loop Control Method for a Log Crane. Proceeding of SICFP'01 (Seventh Scandinavian International Conference on Fluid Power), May 30-June 1. Linköping, Sweden. ISBN 91-7373-056-4.

Kovanen J., Handroos H. 2001B. Adaptive Open-Loop Control Method for a Hydraulically Driven Flexible Manipulator. Proceeding of AIM'01 (International Conference on Advanced Intelligent Mechatronics), July 8-12. Como, Italy, ISBN 0-7803-6736-7

Kovanen J., Handroos H. 2002. Active Vibration Control Method For a Hydraulically Driven Flexible Manipulator. Proceeding of ICMA'02 (The Fourth International Conference on Machine Automation), Sebtember 11-13, Tampere, Finland. ISBN 952-15-0861-2

Krus P.,Gunnarsson S. 1995. Adaptive Control with Impact Detection of a Hydraulic Actuator Connected to a Flexible Mechanical Structure, Proceeding of The Fourth Scandinavian International Conference on Fluid Power, September 26-29, Tampere, Finland. P. 1104-1115. ISBN 951-722-374-9

Kwon D.S. et al. 1995. Tracking Control of the Hydraulically Actuated Flexible Manipulator, IEEE, ICRA 1995 Proceedings, May 21-27, 1995 Japan. p. 2200-2205. ISSN 0-7803-1965-6.

Käppi T., Ellman A. 1999. Modelling and Simulation of Proportional Mobile Valves. Proceeding of JHPS 1999 International symposium. P. 531-536. ISBN 4-931070-04-3

Linjama M. 1998. The Modelling and Actuator Space Control of Flexible Hydraulic Cranes. Doctoral thesis. Tampere University of Technology, Espoo. 1998. ISBN 952-5148-54-8.

Macfarlane S, Croft E.A. 2001. Design of Jerk Bounded Trajectories for On-line Industrial Robot Applications. Proceeding of IEEE International Conference on Robotics and Automation (ICRA 2001), May 21-26, 2001 Seoul. P.979-984. ISSN 1050-4729.

Masakazu H. et al. 2001. Digging Control System for Hydraulic Excavator, Mechatronics 11/2001. Elsevier Science Ltd. P.665-676

MATLAB Help. 1999. Program manual [electric], version 6.0. Mathworks Inc.

Meckl P.H., Seering W.P. 1985. Minimizing Residual Vibration for Point to Point Motion. Journal of Vibration, Acoustics, Stress, and Reliability in Design, v 107, no 4, October, 1985. P. 378-382

Meckl P.H., Seering W.P. 1988. Shaping Reference Inputs to Reduce Residual Vibration for a Cartesian Robot. ASME. Dynamic Systems and Control Division (Publication) DSC Symposium on Robotics, Nov 27-Dec 2 1988. Chicago, USA.

Merritt H.E. 1967. Hydraulic Control Systems. New York. Wiley & Sons. 358 p. ISBN 0-471-59617-5

Metsälehti 7/2002. 2002. Metsätalouden kehittämiskeskus Tapion julkaisu 7/2002, vol. 69. In Finnish. ISSN 0355-0893.

Mikkola A. 1997. Studies of Fatigue Damage in a Hydraulically Driven Boom System Using Virtual Prototype Simulations. Doctoral thesis, Lappeenranta University of Technology. Lappeenranta, Finland. 61 p. ISBN 951-764-173-7

MTT Vakola (Maataloustegnologian tutkimus). 2003. Maatalous- ja metsäkoneiden myynti vuosina 1999 - 2001 [web document, cited 20 Mars 2003]. Available from World Wide Web: http://www.mtt.fi/mtl. In Finnish.

Määttälä M. 2002. Mäntäpainevaraajan toiminnan vaikutus puutavarakuormaimeen. Master thesis, University of Oulu. 78 p. In Finnish.

Nagai M. 1993. Recent Research on Active Suspension for Ground Vehicles. JSME International Journal Series C, vol. 36, No 2. P.161-170 .

Nohynek P., Lumme V.E., 1996. Kunnonvalvonnan värähtelymittaukset. Kunnossapitoyhdistys ry. 159 p. In Finnish.

Papadopoulos E., Soumen S. 1996. On the Dynamic Modeling of an Articulated electrohydraulic Forestry Machine. Proceeding of the 1996 AIAA Forum on Advanced Developments in Space Robotics, August 1-2.

Pat. EP1174384. 2002. A Method and System for Guiding a Boom. Timberjack Oy (Kovanen J. & Handroos H.). Publ. 23.1.2002, Appl. no. 01660138.7.
Publ. 23.1.2002 , Appl. nr. 01660138.7.

Pat. FI 109349B. 2002. Menetelmä puomin ohjaamiseksi ja puomin ohjausjärjestelmä. Timberjack Oy (Kovanen J. & Handroos H.). Publ. 15.7.2002, Appl. no. 20001682. In Finnish.

Pat. JP5060104. 1993. Vibration Suppressing and Controlling Device of Working Equipment in Hydraulic Working Machine, Hitachi Constr. Mach. Co LTD (Yamagata E.). Publ. 9.3.1993. esp@cenet-free patent information on the internet [online], European Patent Organisation, January 2003, [cited 10 January 2003]. Available from World Wide Web: http://fi.espacenet.com/

Pat. JP5321297. 1993. Vibration Suppressing Control Device For Operation Device of Hydraulic Working Machine, Hitachi Constr. Mach. Co LTD (Yamagata E.). Publ. 7.12.1993. esp@cenet -free patent information on the internet [online], European Patent Organisation, January 2003, [cited 10 January 2003]. Available from World Wide Web: http://fi.espacenet.com/

Pat. JP5157101. 1993. Vibration Suppressing Device for Hydraulic Working Machine, Hitachi Constr. Mach. Co LTD (Yamagata E.). Publ. 22.6.1993. esp@cenet -free patent information on the internet [online], European Patent Organisation, January 2003, [cited 10 January 2003]. Available from World Wide Web: http://fi.espacenet.com/

Pat. JP6185501. 1994. Oscillation Limiter of Hydraulic Working Machine. Hitachi Constr. Mach. Co LTD (Yamagata E.). Publ. 5.7.1994. esp@cenet -free

patent information on the internet [online], European Patent Organisation, January 2003, [cited 10 January 2003]. Available from World Wide Web: http://fi.espacenet.com/

Pat. US 4815614. 1989. Control System for a Crane, Putkonen et al. Publ. 28.3.1989. Appl.No 62 199.

Pat. US 4869474. 1989. Vehicle Engine Suspension Systems. BTR plc (Best A., Bethell D.M, Hoole R.). Publ. 26.9.1989. United States Patent and Trademark Office [online], January 2003, [cited 10 January 2003]. Available from World Wide Web: http://www.uspto.gov/patft/index.html

Pat. US 4916635. 1990. Shaping Command Inputs to Minimize Unwanted Dynamics. Massachusetts Institute of Technology (Singer N. et al.). Publ.10.4.1990, United States Patent and Trademark Office [online], January 2003, [cited 10 January 2003]. Available from World Wide Web: http://www.uspto.gov/patft/index.html

Pat. US 5423523. 1990. Integrated Hydraulic Mount for Active Vibration Control System. Noise Cancellation Technologies, Inc. (GossmanW.E., Burke M.J.). Publ.13.6.1990. United States Patent and Trademark Office [online], January 2003, [cited 10 January 2003]. Available from World Wide Web: http://www.uspto.gov/patft/index.html

Pat. US 5465035. 1995. Band Limited Control of a Flexible Structure Using Piecewise Trigonometric Input Signals. Quantum Corporation (Scaramuzzo J., John A.). Publ. 7.11.1995. United States Patent and Trademark Office [online], January 2003, [cited 10 January 2003]. Available from World Wide Web: http://www.uspto.gov/patft/index.html

Pat. US 5459383. 1995. Robust active damping control system. Quantum Corporation (Sidman M.D., Hvostov H.S.). Publ. 17.10.1995. United States Patent and Trademark Office [online], January 2003, [cited 10 January 2003]. Available from World Wide Web: http://www.uspto.gov/patft/index.html

Pat.US 5638267. 1994. Method and Apparatus for Minimizing Unwanted Dynamics in a Physical System. Convolve, Inc. (Singhose W.E., Singer N.C.). Publ. 10.6.1994. United States Patent and Trademark Office [online], January 2003, [cited 10 January 2003]. Available from World Wide Web: http://www.uspto.gov/patft/index.html

Pat. US 6553278B2. 2003. Method for Guiding a Boom and a System for Guiding a Boom. Timberjack Oy (Kovanen J. & Handroos H.). Publ. 22.4.2003, Appl. No. 09/908,385

Proakis J.G., Manolakis D.G. 1988. Digital Signal Processing. Macmillan Publishing Company. USA. 969 p.

Rao S.S. 1990. Mechanical Vibrations. Second edition. Addison Wesley. USA. 718 p. ISBN 0-201-50156-2

Rouvinen A. 1995. Hydraulijärjestelmän mallintaminen ADAMS– ohjelmistossa. Master thesis. Lappeenranta University of Technology. Lappeenranta. 49 p. In Finnish.

Shabana A.A. 1998. Dynamics of Multibody Systems. Second edition. Cambridge University Press. USA. 372 p.

Singhose W.E. 1997. Command Generation for Flexible Systems. Doctoral thesis. Massachusetts Institute of Technology. USA. 285 p.

Siren M. 1998. Hakkuukonetyö, sen korjuujälki ja puustovaurioiden ennustaminen. Metsäntutkimuslaitoksen tiedonantoja 694. Helsinki. 179 p. In Finnish. ISBN 951-40-1635-1

Sohoni V.N., Whitesell J. 1986. Automatic Linearization of Constrained Dynamical Models. Journal of Mechanisms, Transmissions and Automation in Design, September 1986. ASME. USA. P. 300-304

Appendix A Lowest Natural Frequencies of the Different Cranes

PATU 655

Lift cylinder stroke.
X= [0.03 0.07 0.134 0.20 0.264 0.30 0.40 0.45 0.50]

Jib cylinder stroke.
Y= [0.00001 0.19 0.39 0.59 0.65]'

Mass without the gripper and the rotator.

$\mathbf{f}_1$=[4.01 3.75 3.62 3.46 3.33 3.22 3.10 3.05 3.05
3.96 3.87 3.65 3.45 3.28 3.23 3.12 3.08 2.95
4.17 3.98 3.51 3.54 3.39 3.36 3.17 3.18 3.24
4.53 4.32 4.13 3.97 3.81 3.68 3.56 3.72 3.40
4.72 4.63 4.32 4.12 3.92 3.80 3.61 3.57 3.56]

Mass 200 kg

$\mathbf{f}_2$=[2.33 2.29 2.18 2.13 2.15 2.06 1.95 1.91 1.94
2.36 2.31 2.23 2.18 2.15 2.21 2.05 2.04 2.00
2.38 2.35 2.33 2.30 2.30 2.28 2.26 2.04 2.33
2.74 2.51 2.76 2.61 2.56 2.51 2.57 2.62 2.61
3.01 2.98 2.94 2.90 2.89 2.89 2.86 2.89 2.88]

Mass 400 kg

$\mathbf{f}_3$=[1.81 1.75 1.76 1.85 1.67 1.68 1.54 1.52 1.53
1.84 1.66 1.76 1.65 1.66 1.59 1.46 1.60 1.57
1.87 1.82 1.80 1.78 1.77 1.76 1.82 1.73 1.77
2.14 2.14 2.05 2.07 2.02 2.14 2.00 2.03 2.05
3.00 2.98 2.93 2.91 2.89 2.87 2.83 2.88 2.89]

TJ71F72

Lift cylinder stroke, angle between pillar and the lift boom -25, 0, 25 and 45 degrees.
X= [0.185 0.33 0.49 0.61]

Jib cylinder stroke, angle between the lift and jib boom -15, -45, -60, -90, -120 degrees
Y= [0.134 0.323 0.417 0.59 0.73]

Without gripper and rotator.

$\mathbf{f}_1$= [2.1031 2.4581 2.2641 1.9268
2.1511 2.5191 2.3251 1.9679
2.2206 2.5841 2.3856 2.0159
2.3742 2.7781 2.5617 2.1696
2.6094 3.0467 2.8106 2.3735]

Mass 200 kg

$\mathbf{f}_2$= [1.4980 1.7447 1.6118 1.3999
1.5633 1.8414 1.7106 1.4478
1.6586 1.9152 1.7784 1.5169
1.8505 2.1550 2.0033 1.7056
2.1859 2.5512 2.36765 1.8535]

Mass 400 kg

$\mathbf{f}_3$= [1.2173 1.5082 1.3225 1.1339
1.3770 1.5141 1.4011 1.1957
1.3582 1.5758 1.4745 1.2593
1.5552 1.7772 1.6912 1.4524
1.9055 2.2166 2.0679 1.7713]

Mass 600 kg

$\mathbf{f}_4$= [1.0399 1.2310 1.1485 0.9826
1.1120 1.3149 1.2225 1.0444
1.1775 1.5381 1.2849 1.1014
1.3690 1.6000 1.4880 1.2863
1.7057 1.9779 1.85474 1.6008]

Mass 800 kg

$\mathbf{f}_5$ = [0.9228 1.1047 1.0297 0.8829
0.9603 1.1768 1.0985 0.9408
0.9625 1.0846 1.1601 0.9968
1.2313 1.4455 1.3481 1.1701
1.1619 1.4474 1.3521 1.4719]

TJ72F100

Lift cylinder stroke, angle between pillar and the lift boom -25, 0, 25 and 45 degrees.
X= [0.185 0.33 0.49 0.61]

Jib cylinder stroke, angle between the lift and jib boom -15, -45, -60, -90, -120 degrees.

Y= [0.134 0.323 0.417 0.59 0.73]

Mass 300 kg

$\mathbf{f}_1$=	[1.3471	1.5743	1.4761	1.2540
	1.3911	1.6271	1.5146	1.2971
	1.4185	1.6797	1.5638	1.3402
	1.6040	1.8688	1.7334	1.4869
	1.1910	2.1723	2.0265	1.7347]

Mass 600 kg

$\mathbf{f}_2$=	[1.0631	1.2496	1.1684	1.0042
	1.1124	1.3066	1.2203	1.0488
	1.1460	1.3572	1.2706	1.0928
	1.3189	1.5330	1.4306	1.2386
	1.7241	1.8421	1.7321	1.4945]

Mass 800 kg

$\mathbf{f}_3$=	[0.9434	1.1202	1.0465	0.9026
	0.9966	1.1735	1.0967	0.9475
	1.0294	1.2207	1.1468	0.9896
	1.1958	1.3923	1.3034	1.1305
	1.4601	1.6871	1.5648	1.3828]

Mass 1000 kg

$\mathbf{f}_4$=	[0.7967	1.0201	0.9569	0.8270
	0.9092	1.0750	1.0079	0.8707
	0.9472	1.1210	1.0545	0.9120
	1.1009	1.2803	1.2021	1.0487
	1.3554	1.5643	1.4805	1.2904]

Using extension reduces to the lowest natural frequencies of the TJ71F100 crane according to the Figure A.1-A.3.

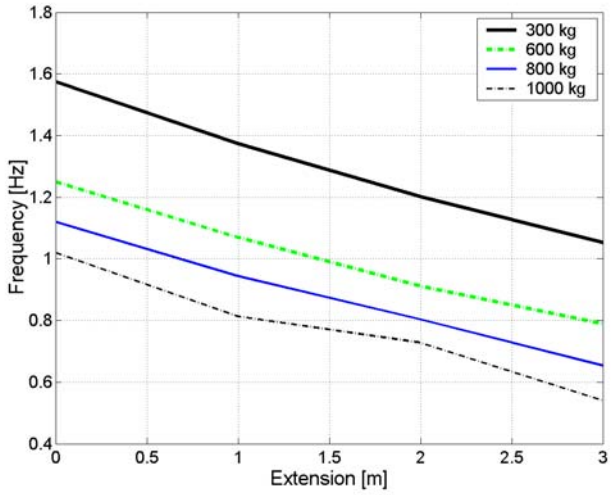

Figure A.1 Effect of the extension. Position: Lift boom 0 degrees, jib boom -15 degrees

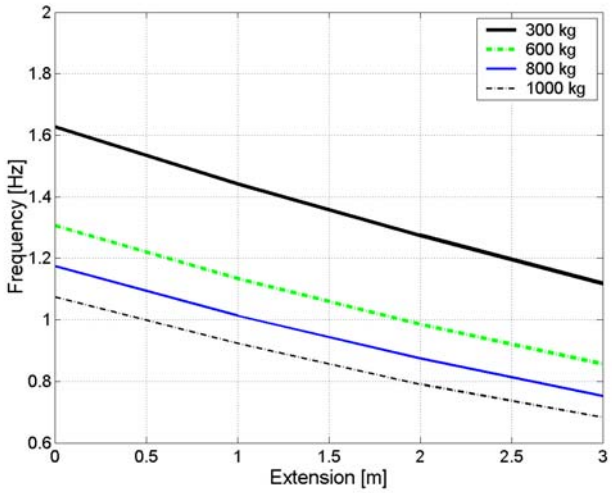

Figure A.2 Effect of the extension. Position: Lift boom 0 degrees, jib boom - 45 degrees

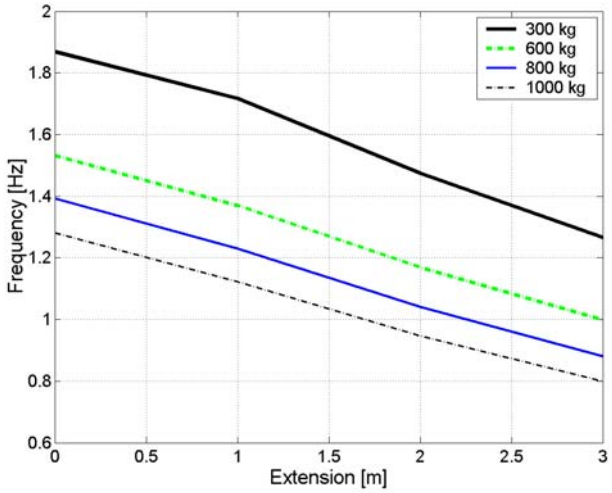

Figure A.3 Effect of the extension. Position: Lift boom 0 degrees, jib boom - 90 degrees

Appendix B Transformation Matrixes

$$\mathbf{T}_{01} = \begin{bmatrix} 1 & 0 & 0 & -0.148 \\ 0 & 1 & 0 & 1.785 \\ 0 & 0 & 1 & 0 \\ 0 & 0 & 0 & 1 \end{bmatrix}$$

$$\mathbf{T}_{17} = \begin{bmatrix} \cos(\theta_1) & -\sin(\theta_1) & 0 & 0.365 \\ \sin(\theta_1) & \cos(\theta_1) & 0 & -0.085 \\ 0 & 0 & 1 & 0 \\ 0 & 0 & 0 & 1 \end{bmatrix}$$

$$\mathbf{T}_{12} = \begin{bmatrix} \cos(\theta_1) & -\sin(\theta_1) & 0 & 3.55 \\ \sin(\theta_1) & \cos(\theta_1) & 0 & 0.20 \\ 0 & 0 & 1 & 0 \\ 0 & 0 & 0 & 1 \end{bmatrix}$$

$$\mathbf{T}_{23} = \begin{bmatrix} \cos(-\theta_2) & -\sin(-\theta_2) & 0 & -0.06 \\ \sin(-\theta_2) & \cos(-\theta_2) & 0 & 0.222 \\ 0 & 0 & 1 & 0 \\ 0 & 0 & 0 & 1 \end{bmatrix}$$

$$\mathbf{T}_{34} = \begin{bmatrix} 1 & 0 & 0 & 2.30 \\ 0 & 1 & 0 & -0.012 \\ 0 & 0 & 1 & 0 \\ 0 & 0 & 0 & 1 \end{bmatrix}$$

$$\mathbf{T}_{45} = \begin{bmatrix} 1 & 0 & 0 & 0.3 + s_3 \\ 0 & 1 & 0 & 0 \\ 0 & 0 & 1 & 0 \\ 0 & 0 & 0 & 1 \end{bmatrix}$$

$$\mathbf{T}_{m1} = \begin{bmatrix} \cos(\theta_1) & -\sin(\theta_1) & 0 & 1.813 \\ \sin(\theta_1) & \cos(\theta_1) & 0 & 0.241 \\ 0 & 0 & 1 & 0 \\ 0 & 0 & 0 & 1 \end{bmatrix}$$

$$\mathbf{T}_{m2} = \begin{bmatrix} 1 & 0 & 0 & 0.805 \\ 0 & 1 & 0 & -0.023 \\ 0 & 0 & 1 & 0 \\ 0 & 0 & 0 & 1 \end{bmatrix}$$

$$\mathbf{T}_{m3} = \begin{bmatrix} 1 & 0 & 0 & 1.436 + s_3 \\ 0 & 1 & 0 & 0.012 \\ 0 & 0 & 1 & 0 \\ 0 & 0 & 0 & 1 \end{bmatrix}$$

$$\mathbf{T}_{m4} = \begin{bmatrix} 1 & 0 & 0 & 0.3 + s_3 \\ 0 & 1 & 0 & 0 \\ 0 & 0 & 1 & 0 \\ 0 & 0 & 0 & 1 \end{bmatrix}$$

Appendix C Four Bar Mechanism

Chapter 4 presents kinematics of the crane. Same figure and table about the naming of the joints and lengths of the links are repeated here.

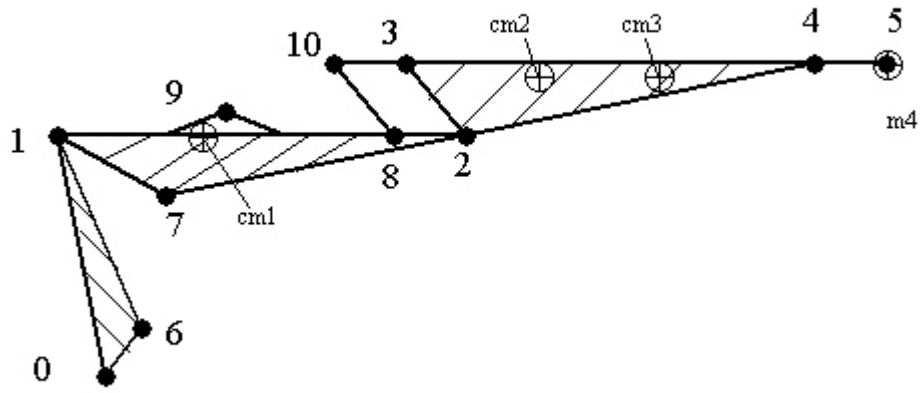

Figure C.1 Numbering of the joints.

Table C.1Vector lengths

Vector	Length [m]	Vector	Length [m]
$0\text{-}1_x$	0.148	$0\text{-}6_x$	0.192
$0\text{-}1_y$	1.785	$0\text{-}6_y$	0.6
$1\text{-}2_x$	3.55	$1\text{-}7_x$	0.365
$1\text{-}2_y$	0.2	$1\text{-}7_y$	-0.085
$2\text{-}3_x$	-0.06	$9\text{-}8_x$	1.558
$2\text{-}3_y$	0.222	$9\text{-}8_y$	-0.245
$3\text{-}4_x$	2.3	$8\text{-}2_x$	0.180
$3\text{-}4_y$	-0.012	$8\text{-}2_y$	-0.005
$4\text{-}5_x$	0.17	8-10	0.515
$4\text{-}5_y$	0.0	10-3	0.550
$1\text{-}6_x$	0.34	3-2	0.23
$1\text{-}6_y$	1.185		

Vectors are named as following example:
L_{16x}=1-6_x
L_{16y}=1-6_y
L_{16}=1-6 (Length)

$$L_{16} = \sqrt{L_{16x}{}^2 + L_{16y}{}^2}$$

$$L_{17} = \sqrt{L_{17x}{}^2 + L_{17y}{}^2}$$

Naming of the angles is presented in Figure C.2.

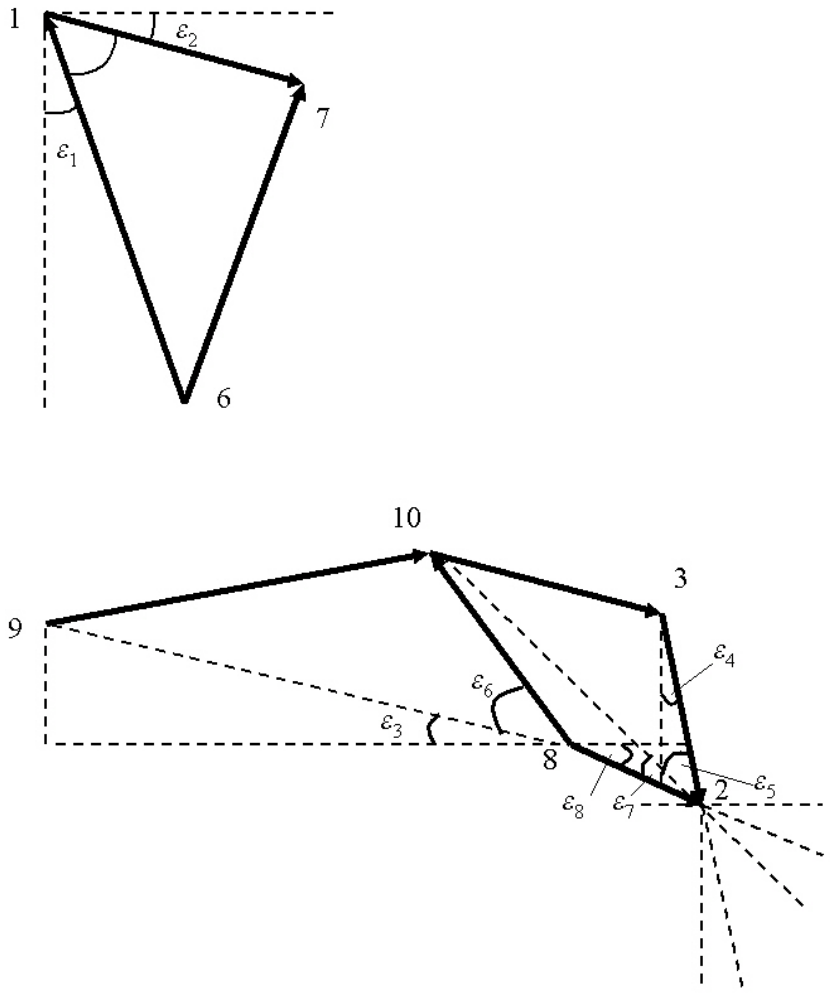

Figure C.2 Names of the angles

$$\varepsilon_1 = a\tan\left(\frac{L_{16x}}{L_{16y}}\right)$$

$$\varepsilon_2 = a\tan\left(\frac{L_{17y}}{L_{17x}}\right)$$

$$L_{98} = \sqrt{{L_{98x}}^2 + {L_{98y}}^2}$$

$$L_{82} = \sqrt{{L_{82x}}^2 + {L_{82y}}^2}$$

$$\varepsilon_3 = a\tan\left(\frac{L_{98y}}{L_{98x}}\right)$$

$$\varepsilon_8 = a\tan\left(\frac{L_{82y}}{L_{82x}}\right)$$

$$\varepsilon_4 = a\tan\left(\frac{L_{23y}}{L_{23x}}\right)$$

$$L_{67} = s_1 + 0.918$$

$$L_{910} = s_2 + 1.134$$

Using law of cosines the angle between pillar and lift boom can be expressed as

$$\alpha_L = a\cos\left(\frac{{L_{67}}^2 - {L_{16}}^2 - {L_{17}}^2}{-2L_{16}L_{17}}\right) + \varepsilon_1 + \varepsilon_2 - \frac{\pi}{2}.$$

Calculation of the angle between the lift and the jib boom requires some extra angles.

$$\varepsilon_6 = a\cos\left(\frac{{L_{910}}^2 - {L_{98}}^2 - {L_{810}}^2}{-2L_{98}L_{810}}\right)$$

$$\varepsilon_9 = \pi - \varepsilon_3 - \varepsilon_6 - \varepsilon_8$$

$$L_{102} = \left({L_{810}}^2 + {L_{82}}^2 - 2L_{810}L_{82}\cos(\varepsilon_9)\right)^{0.5}$$

$$\varepsilon_7 = a\cos\left(\frac{{L_{910}}^2 - {L_{102}}^2 - {L_{98}}^2}{-2L_{102}L_{98}}\right)$$

$$\varepsilon_5 = a\cos\left(\frac{{L_{103}}^2 - {L_{102}}^2 - {L_{32}}^2}{-2L_{102}L_{32}}\right)$$

Finally the jib angle can be expressed as

$$\alpha_J = \left(-\frac{\pi}{2} - \varepsilon_8 + \varepsilon_7 + \varepsilon_5 + \varepsilon_4\right).$$

Appendix D Outward and Inward Iteration

In the presented case, we have a crane with 3 links; therefore, index *i* runs from 0 to 2 in the outward iteration.
The outward iteration for link 1 (i=0) gives

$$\boldsymbol{\omega}_{1,1} = \mathbf{A}_{1,0}\boldsymbol{\omega}_{0,0} + \dot{\theta}_1 \hat{\boldsymbol{Z}}_{1,1} = \begin{bmatrix} 0 & 0 & \dot{\theta}_1 \end{bmatrix}'$$

$$\mathbf{A}_{1,0} = \begin{bmatrix} \cos(\theta_1) & \sin(\theta_1) & 0 \\ -\sin(\theta_1) & \cos(\theta_1) & 0 \\ 0 & 0 & 1 \end{bmatrix}$$

$$\boldsymbol{\omega}_{0,0} = \begin{bmatrix} 0 & 0 & 0 \end{bmatrix}' \text{ (Base is not rotating)}$$

$$\hat{\boldsymbol{Z}}_{1,1} = \begin{bmatrix} 0 & 0 & 1 \end{bmatrix}'$$

$$\dot{\boldsymbol{\omega}}_{1,1} = \mathbf{A}_{1,0}\dot{\boldsymbol{\omega}}_{0,0} + \mathbf{A}_{1,0}\boldsymbol{\omega}_{0,0} \times \dot{\theta}_1 \hat{\boldsymbol{Z}}_{1,1} + \ddot{\theta}_1 \hat{\boldsymbol{Z}}_{1,1} = \ddot{\theta}_1 \hat{\boldsymbol{Z}}_{1,1} = \begin{bmatrix} 0 & 0 & \ddot{\theta}_1 \end{bmatrix}'$$

$$\dot{\boldsymbol{\omega}}_{0,0} = \begin{bmatrix} 0 & 0 & 0 \end{bmatrix}' \text{ (Base is not rotating)}$$

$$\dot{\boldsymbol{v}}_{1,1} = \mathbf{A}_{1,0}\left(\dot{\boldsymbol{\omega}}_{0,0} \times \boldsymbol{P}_{0,1} + \boldsymbol{\omega}_{0,0} \times (\boldsymbol{\omega}_{0,0} \times \boldsymbol{P}_{0,1}) + \dot{\boldsymbol{v}}_{0,0}\right) = \mathbf{A}_{1,0}\dot{\boldsymbol{v}}_{0,0}$$

$$\boldsymbol{P}_{0,1} = \begin{bmatrix} \mathbf{T}_{0,1}(1,4) & \mathbf{T}_{0,1}(2,4) & \mathbf{T}_{0,1}(3,4) \end{bmatrix}'$$

$$\dot{\boldsymbol{v}}_{0,0} = \begin{bmatrix} 0 & 9.81 & 0 \end{bmatrix}' \text{ (Gravity up)}$$

$$\dot{\boldsymbol{v}}_{1,1,cm} = \dot{\boldsymbol{\omega}}_{1,1} \times \boldsymbol{P}_{1,1,cm} + \boldsymbol{\omega}_{1,1} \times (\boldsymbol{\omega}_{1,1} \times \boldsymbol{P}_{1,1,cm}) + \dot{\boldsymbol{v}}_{1,1})$$

$$\mathbf{P}_{1,1,cm} = \begin{bmatrix} \mathbf{T}_{m1}(1,4) & \mathbf{T}_{m1}(2,4) & \mathbf{T}_{m1}(3,4) \end{bmatrix}'$$

$$\boldsymbol{F}_{1,1} = m_1 \dot{\boldsymbol{v}}_{1,1,cm}$$

$$\boldsymbol{N}_{1,1} = \mathbf{I}_1 \dot{\boldsymbol{\omega}}_{1,1} + \boldsymbol{\omega}_{1,1} \times \mathbf{I}_1 \boldsymbol{\omega}_{1,1}$$

Link 2 (*i*=1):

$$\boldsymbol{\omega}_{2,2} = \mathbf{A}_{2,1}\boldsymbol{\omega}_{1,1} + \dot{\theta}_2 \hat{\boldsymbol{Z}}_{2,2}$$

$$\mathbf{A}_{2,1} = \begin{bmatrix} \cos(\theta_2) & \sin(\theta_2) & 0 \\ -\sin(\theta_2) & \cos(\theta_2) & 0 \\ 0 & 0 & 1 \end{bmatrix}$$

$$\hat{\mathbf{Z}}_{2,2} = \begin{bmatrix} 0 & 0 & 1 \end{bmatrix}'$$

$$\dot{\boldsymbol{\omega}}_{2,2} = \mathbf{A}_{2,1}\dot{\boldsymbol{\omega}}_{1,1} + \mathbf{A}_{2,1}\boldsymbol{\omega}_{1,1} \times \dot{\theta}_2 \hat{\boldsymbol{Z}}_{2,2} + \ddot{\theta}_2 \hat{\boldsymbol{Z}}_{2,2}$$

$$\dot{\boldsymbol{v}}_{2,2} = \mathbf{A}_{2,1}\left(\dot{\boldsymbol{\omega}}_{1,1} \times \boldsymbol{P}_{1,2} + \boldsymbol{\omega}_{1,1} \times (\boldsymbol{\omega}_{1,1} \times \boldsymbol{P}_{1,2}) + \dot{\boldsymbol{v}}_{1,1}\right)$$

$$\boldsymbol{P}_{1,2} = \left[\mathbf{T}_{2,3}(1,4) + \mathbf{T}_{3,4}(1,4) \quad \mathbf{T}_{2,3}(2,4) + \mathbf{T}_{3,4}(2,4) \quad \mathbf{T}_{2,3}(3,4) + \mathbf{T}_{3,4}(3,4)\right]'$$

$$\dot{\boldsymbol{v}}_{2,2,cm} = \dot{\boldsymbol{\omega}}_{2,2} \times \boldsymbol{P}_{2,2,cm} + \boldsymbol{\omega}_{2,2} \times (\boldsymbol{\omega}_{2,2} \times \boldsymbol{P}_{2,2,cm}) + \dot{\boldsymbol{v}}_{2,2})$$

$$\boldsymbol{P}_{2,2,cm} = \left[\mathbf{T}_{m2}(1,4) \quad \mathbf{T}_{m2}(2,4) \quad \mathbf{T}_{m2}(3,4)\right]'$$

$$\boldsymbol{F}_{2,2} = m_2 \dot{\boldsymbol{v}}_{2,2,cm}$$

$$\boldsymbol{N}_{2,2} = \mathbf{I}_2 \dot{\boldsymbol{\omega}}_{2,2} + \boldsymbol{\omega}_{2,2} \times \mathbf{I}_2 \boldsymbol{\omega}_{2,2}$$

For link 3 (i=2) equations are:

$$\boldsymbol{\omega}_{3,3} = \mathbf{A}_{3,2}\boldsymbol{\omega}_{2,2} + \dot{\theta}_3 \hat{\boldsymbol{Z}}_{3,3}$$

$$\mathbf{A}_{3,2} = \begin{bmatrix} 1 & 0 & 0 \\ 0 & 1 & 0 \\ 0 & 0 & 1 \end{bmatrix}$$

$\dot{\boldsymbol{\theta}}_3 = 0$ (prismatic joint)

$$\hat{\boldsymbol{Z}}_{2,2} = \begin{bmatrix} 0 & 0 & 1 \end{bmatrix}'$$

$$\dot{\boldsymbol{\omega}}_{3,3} = \mathbf{A}_{3,2}\dot{\boldsymbol{\omega}}_{2,2}$$

$$\dot{\boldsymbol{v}}_{3,3} = \mathbf{A}_{3,2}\left(\dot{\boldsymbol{\omega}}_{2,2} \times \boldsymbol{P}_{2,3} + \boldsymbol{\omega}_{2,2} \times (\boldsymbol{\omega}_{2,2} \times \boldsymbol{P}_{2,3}) + \dot{\boldsymbol{v}}_{2,2}\right)$$

$$\boldsymbol{P}_{2,3} = \left[\mathbf{T}_{4,5}(1,4) \quad \mathbf{T}_{4,5}(2,4) \quad \mathbf{T}_{4,5}(3,4)\right]'$$

$$\dot{\boldsymbol{v}}_{3,3,cm} = \dot{\boldsymbol{\omega}}_{3,3} \times \boldsymbol{P}_{3,3,cm} + \boldsymbol{\omega}_{3,3} \times (\boldsymbol{\omega}_{3,3} \times \boldsymbol{P}_{3,3,cm}) + \dot{\boldsymbol{v}}_{3,3})$$

$$\boldsymbol{P}_{3,3,cm} = \begin{bmatrix} -0.979 + s_3 & -0.012 & 0 \end{bmatrix}'$$

s_3 = cylinder 3 stroke

$$\boldsymbol{F}_{3,3} = m_3 \dot{\boldsymbol{v}}_{3,3,cm}$$

$$\boldsymbol{N}_{3,3} = \mathbf{I}_3 \dot{\boldsymbol{\omega}}_{3,3} + \boldsymbol{\omega}_{3,3} \times \mathbf{I}_3 \boldsymbol{\omega}_{3,3}$$

The inward iteration is performed from link 3 to link 1. Index i runs from 3 to 1.

$$\boldsymbol{f}_{3,3} = \mathbf{A}_{3,4}\boldsymbol{f}_{4,4} + \boldsymbol{F}_{3,3}$$

where $\boldsymbol{f}_{4,4}$ is unknown.

$$\mathbf{A}_{3,4} = \begin{bmatrix} 1 & 0 & 0 \\ 0 & 1 & 0 \\ 0 & 0 & 1 \end{bmatrix}$$

$$\boldsymbol{n}_{3,3} = \boldsymbol{N}_{3,3} + \mathbf{A}_{3,4}\boldsymbol{n}_{4,4} + \boldsymbol{P}_{3,3,cm} \times \boldsymbol{F}_{3,3} + \boldsymbol{P}_{3,4} \times \mathbf{A}_{3,4}\boldsymbol{f}_{4,4}$$

$\boldsymbol{n}_{4,4} = \begin{bmatrix} 0 & 0 & 0 \end{bmatrix}'$ (the moment acting to the load mass)

The last term calculates the torque coming from force vector $\boldsymbol{f}_{4,4}$ about joint 3. Because the force vector from the load mass points down in the y-direction most of the time, the last term in the equation could be simplified to a form in which the force vector is multiplied by the moment arm. However, the equations are kept in the original form until the end of the iteration.

Joint 3 is of the prismatic type, and so the torque is counted as follows:
$\boldsymbol{\tau}_3 = \boldsymbol{f}_{3,3}{}^T \widehat{\mathbf{Z}}_{3,3}$.

For link 2 (i=2):

$$\boldsymbol{f}_{2,2} = \mathbf{A}_{2,3}\boldsymbol{f}_{3,3} + \boldsymbol{F}_{2,2}$$

where $\mathbf{A}_{2,3} = \mathbf{A}_{3,4}$. Substituting $\boldsymbol{f}_{3,3}$ we get

$$\boldsymbol{f}_{2,2} = \mathbf{A}_{2,3}\mathbf{A}_{3,4}\boldsymbol{f}_{4,4} + \mathbf{A}_{2,3}\boldsymbol{F}_{3,3} + \boldsymbol{F}_{2,2} = \boldsymbol{f}_{4,4} + \boldsymbol{F}_{3,3} + \boldsymbol{F}_{2,2}.$$
$$\boldsymbol{n}_{2,2} = \boldsymbol{N}_{2,2} + \mathbf{A}_{2,3}\boldsymbol{n}_{3,3} + \boldsymbol{P}_{2,2,cm} \times \boldsymbol{F}_{2,2} + \boldsymbol{P}_{2,3} \times \mathbf{A}_{2,3}\boldsymbol{f}_{3,3}$$

$$\boldsymbol{n}_{2,2} = \boldsymbol{N}_{2,2} + \mathbf{A}_{2,3}\left(\boldsymbol{N}_{3,3} + \boldsymbol{P}_{3,3,cm} \times \boldsymbol{F}_{3,3} + \boldsymbol{P}_{3,4} \times \mathbf{A}_{3,4}\boldsymbol{f}_{4,4}\right) + \boldsymbol{P}_{2,2,cm} \times \boldsymbol{F}_{2,2}$$
$$+ \boldsymbol{P}_{2,3} \times \mathbf{A}_{2,3}\boldsymbol{f}_{4,4} + \mathbf{P}_{2,3} \times \mathbf{A}_{2,3}\mathbf{F}_{3,3}$$

$$\boldsymbol{\tau}_2 = \boldsymbol{n}_{2,2}{}^T \widehat{\mathbf{Z}}_{2,2}$$

For link 1 (i=1):

$$\boldsymbol{f}_{1,1} = \mathbf{A}_{1,2}\boldsymbol{f}_{2,2} + \boldsymbol{F}_{1,1}$$
$$\boldsymbol{n}_{1,1} = \boldsymbol{N}_{1,1} + \mathbf{A}_{1,2}\boldsymbol{n}_{2,2} + \boldsymbol{P}_{1,1,cm} \times \boldsymbol{F}_{1,1} + \boldsymbol{P}_{1,2} \times \mathbf{A}_{1,2}\boldsymbol{f}_{2,2}$$
$$\boldsymbol{\tau}_1 = \boldsymbol{n}_{1,1}{}^T \widehat{\mathbf{Z}}_{1,1}$$

Substituting $\boldsymbol{n}_{2,2}$ and $\boldsymbol{f}_{2,2}$

$$\begin{aligned}
&\boldsymbol{n}_{1,1} = \boldsymbol{N}_{1,1} + \mathbf{A}_{1,2}\boldsymbol{N}_{2,2} + \mathbf{A}_{1,2}\mathbf{A}_{2,3}\boldsymbol{N}_{3,3} + \mathbf{A}_{1,2}\mathbf{A}_{2,3}\boldsymbol{P}_{3,3,cm} \times \boldsymbol{F}_{3,3} \\
&+ \mathbf{A}_{1,2}\mathbf{A}_{2,3}\left(\boldsymbol{P}_{3,4} \times \mathbf{A}_{3,4}\boldsymbol{f}_{4,4}\right)\boldsymbol{f}_{4,4} + \mathbf{A}_{1,2}\boldsymbol{P}_{2,2,cm} \times \boldsymbol{F}_{2,2} \\
&+ \mathbf{A}_{1,2}\left(\boldsymbol{P}_{2,3} \times \mathbf{A}_{2,3}\right)\boldsymbol{f}_{4,4} + \mathbf{A}_{1,2}\left(\boldsymbol{P}_{2,3} \times \mathbf{A}_{2,3}\boldsymbol{F}_{3,3}\right) + \boldsymbol{P}_{1,1,cm} \times \boldsymbol{F}_{1,1} \\
&+ \left(\mathbf{P}_{1,2} \times \mathbf{A}_{1,2}\right)\boldsymbol{f}_{4,4} + \boldsymbol{P}_{1,2} \times \mathbf{A}_{1,2}\left(\boldsymbol{F}_{3,3} + \boldsymbol{F}_{2,2}\right)
\end{aligned} \tag{D.1}$$

The lift cylinder produces the torque required in the joint 1. Using the measured pressures, the lift cylinder force can be calculated. The moment arm and force transmission angle are calculated using global coordinates from $\mathbf{J}_{p7}$. The negative x-axis value of joint J_{p0} has to be take into account by adding the x-value (0.148) to the x-coordinate value of $\mathbf{J}_{p7}$. Multiplying the moment arm with the cylinder force gives a new form for $\boldsymbol{\tau}_1$.

$$\boldsymbol{\tau}_1 = \left[0 \quad 0 \quad F_c \sin(\beta)\left(\mathbf{J}_{p7}(1,4) + 0.148\right)\right] \tag{D.2}$$

Setting torque equations (D.1) and (D.2) equal and making simplification $\boldsymbol{N}_{tot} = \boldsymbol{N}_{1,1} + \mathbf{A}_{1,2}\boldsymbol{N}_{2,2} + \mathbf{A}_{1,2}\mathbf{A}_{2,3}\boldsymbol{N}_{3,3}$,

$\boldsymbol{n}_{1,1}$ gets form

$$\begin{aligned}
&\left[0 \quad 0 \quad F_c \sin(\beta)\left(\mathbf{J}_{p7}(1,4) + 0.148\right)\right] = \\
&\boldsymbol{N}_{tot} + \mathbf{A}_{1,2}\mathbf{A}_{2,3}\boldsymbol{P}_{3,3,cm} \times \boldsymbol{F}_{3,3} + \mathbf{A}_{1,2}\mathbf{A}_{2,3}\left(\boldsymbol{P}_{3,4} \times \mathbf{A}_{3,4}\boldsymbol{f}_{4,4}\right) \\
&+ \mathbf{A}_{1,2}\boldsymbol{P}_{2,2,cm} \times \boldsymbol{F}_{2,2} + \mathbf{A}_{1,2}\left(\boldsymbol{P}_{2,3} \times \mathbf{A}_{2,3}\boldsymbol{f}_{4,4}\right) + \mathbf{A}_{1,2}\left(\boldsymbol{P}_{2,3} \times \mathbf{A}_{2,3}\boldsymbol{F}_{3,3}\right) \\
&+ \boldsymbol{P}_{1,1,cm} \times \boldsymbol{F}_{1,1} + \left(\boldsymbol{P}_{1,2} \times \mathbf{A}_{1,2}\boldsymbol{f}_{4,4}\right) + \boldsymbol{P}_{1,2} \times \mathbf{A}_{1,2}\left(\boldsymbol{F}_{3,3} + \boldsymbol{F}_{2,2}\right)
\end{aligned}$$

$$\begin{aligned}
&\mathbf{A}_{1,2}\mathbf{A}_{2,3}\left(\boldsymbol{P}_{3,4} \times \mathbf{A}_{3,4}\boldsymbol{f}_{4,4}\right) + \mathbf{A}_{1,2}\left(\boldsymbol{P}_{2,3} \times \mathbf{A}_{2,3}\boldsymbol{f}_{4,4}\right) + \left(\boldsymbol{P}_{1,2} \times \mathbf{A}_{1,2}\boldsymbol{f}_{4,4}\right) = \\
&-\boldsymbol{N}_{tot} - \mathbf{A}_{1,2}\mathbf{A}_{2,3}\boldsymbol{P}_{3,3,cm} \times \boldsymbol{F}_{3,3} - \mathbf{A}_{1,2}\boldsymbol{P}_{2,2,cm} \times \boldsymbol{F}_{2,2} - \mathbf{A}_{1,2}\left(\boldsymbol{P}_{2,3} \times \mathbf{A}_{2,3}\boldsymbol{F}_{3,3}\right) \\
&-\boldsymbol{P}_{1,1,cm} \times \boldsymbol{F}_{1,1} - \boldsymbol{P}_{1,2} \times \mathbf{A}_{1,2}\left(\boldsymbol{F}_{3,3} + \boldsymbol{F}_{2,2}\right) + \left[0 \quad 0 \quad F_c \sin(\beta)\left(\mathbf{J}_{p7}(1,4) + 0.148\right)\right]
\end{aligned}$$

Assuming that

$$\begin{aligned}
&\mathbf{A}_{1,2}\mathbf{A}_{2,3}\left(\boldsymbol{P}_{3,4} \times \mathbf{A}_{3,4}\boldsymbol{f}_{4,4}\right) + \mathbf{A}_{1,2}\left(\boldsymbol{P}_{2,3} \times \mathbf{A}_{2,3}\boldsymbol{f}_{4,4}\right) + \left(\boldsymbol{P}_{1,2} \times \mathbf{A}_{1,2}\boldsymbol{f}_{4,4}\right) \approx \\
&\left(\mathbf{J}_{p4}(1,4) - \mathbf{J}_{p1}(1,4)\right)
\end{aligned}$$

the equation for the load mass, $\boldsymbol{f}_{4,4}$, can be written as

$$\begin{aligned}
&\boldsymbol{f}_{4,4} = \left(\mathbf{J}_{p4}(1,4) - \mathbf{J}_{p1}(1,4)\right)^{-1} \cdot (-1) \cdot \\
&\left(\boldsymbol{N}_{tot} + \mathbf{A}_{1,2}\mathbf{A}_{2,3}\boldsymbol{P}_{3,3,cm} \times \boldsymbol{F}_{3,3} + \mathbf{A}_{1,2}\boldsymbol{P}_{2,2,cm} \times \boldsymbol{F}_{2,2} + \boldsymbol{P}_{1,1,cm} \times \boldsymbol{F}_{1,1}\right. \\
&+ \mathbf{A}_{1,2}\left(\boldsymbol{P}_{2,3} \times \mathbf{A}_{2,3}\boldsymbol{F}_{3,3}\right) + \boldsymbol{P}_{1,2} \times \mathbf{A}_{1,2}\left(\boldsymbol{F}_{3,3} + \boldsymbol{F}_{2,2}\right) \\
&\left.- \left[0 \quad 0 \quad F_c \sin(\beta)\left(\mathbf{J}_{p7}(1,4) + 0.148\right)\right]\right)
\end{aligned}$$

Finally $\boldsymbol{f}_{4,4}$ has to be divided by gravity to get the mass.

$$\begin{aligned}
&\boldsymbol{f}_{4,4} = \left(9.81 * \left(\mathbf{J}_{p4}(1,4) - \mathbf{J}_{p1}(1,4)\right)\right)^{-1} \cdot (-1) \cdot \\
&* \left(\boldsymbol{N}_{tot} + \mathbf{A}_{1,2}\mathbf{A}_{2,3}\boldsymbol{P}_{3,3,cm} \times \boldsymbol{F}_{3,3} + \mathbf{A}_{1,2}\boldsymbol{P}_{2,2,cm} \times \boldsymbol{F}_{2,2} + \boldsymbol{P}_{1,1,cm} \times \boldsymbol{F}_{1,1}\right. \\
&+ \mathbf{A}_{1,2}\left(\boldsymbol{P}_{2,3} \times \mathbf{A}_{2,3}\boldsymbol{F}_{3,3}\right) + \boldsymbol{P}_{1,2} \times \mathbf{A}_{1,2}\left(\boldsymbol{F}_{3,3} + \boldsymbol{F}_{2,2}\right) \\
&\left. - \left[0 \quad 0 \quad F_c \sin(\beta)\left(\mathbf{J}_{p7}(1,4) + 0.148\right)\right]\right)
\end{aligned} \tag{D.3}$$

This equation calculates the load mass of the crane from the position and pressure transducer signals. The equation can be simplified using new variables.

$$\begin{aligned}
\mathbf{G}_1 &= -\left(9.81 \cdot \left(\mathbf{J}_{p4}(1,4) - \mathbf{J}_{p1}(1,4)\right)\right)^{-1} \\
\mathbf{G}_2 &= \mathbf{A}_{1,2}\mathbf{A}_{2,3}\boldsymbol{P}_{3,3,cm} \times \boldsymbol{F}_{3,3} + \mathbf{A}_{1,2}\boldsymbol{P}_{2,2,cm} \times \boldsymbol{F}_{2,2} + \boldsymbol{P}_{1,1,cm} \times \boldsymbol{F}_{1,1} \\
\mathbf{G}_3 &= \mathbf{A}_{1,2}\left(\boldsymbol{P}_{2,3} \times \mathbf{A}_{2,3}\boldsymbol{F}_{3,3}\right) + \boldsymbol{P}_{1,2} \times \mathbf{A}_{1,2}\left(\boldsymbol{F}_{3,3} + \boldsymbol{F}_{2,2}\right)
\end{aligned}$$

$$\boldsymbol{f}_{4,4} = \mathbf{G}_1 \cdot \left(\boldsymbol{N}_{\text{tot}} + \mathbf{G}_2 + \mathbf{G}_3 - \boldsymbol{\tau}_1\right) \tag{D.4}$$